Master's thesis

NTNU
Norwegian University of Science and Technology
Faculty of Natural Sciences
Department of Biotechnology and Food Science

Ingvild Haugnes Aune

Functional Impact of the Autophagy Lysosomal Pathway in Neurodevelopment and Neuroprotection

Master's thesis in Biotechnology
Supervisor: Dr. Mirta Mittelstedt Leal de Sousa
Co-supervisor: Dr. Wei Wang and Prof. Magnar Bjørås
May 2021

NTNU
Norwegian University of
Science and Technology

Ingvild Haugnes Aune

Functional Impact of the Autophagy Lysosomal Pathway in Neurodevelopment and Neuroprotection

Master's thesis in Biotechnology
Supervisor: Dr. Mirta Mittelstedt Leal de Sousa
Co-supervisor: Dr. Wei Wang and Prof. Magnar Bjørås
May 2021

Norwegian University of Science and Technology
Faculty of Natural Sciences
Department of Biotechnology and Food Science

NTNU
Norwegian University of
Science and Technology

Preface

This Master of Science thesis was performed in the master program Biotechnology, Department of Biotechnology and Food Science, and carried out at the Department of Clinical and Molecular Medicine (IKOM) at the Norwegian University of Science and Technology (NTNU), Trondheim Autumn 2020- Spring 2021.

I first want to thank Prof. Magnar Bjørås for accepting me as a master student and giving me the opportunity to take a part of the intriguing world of stem cells and organoids. I have learned so much during this project and for that I am so grateful. I also want to thank my supervisors Dr. Mirta Mittelstedt Leal de Sousa and Dr. Wei Wang for excellent guidance and support during this project. Wei, thank you for the wise words and support when things did not go as planned in the lab. Mirta, thank you for your encouragement in the lab and especially during the writing process of the thesis, it would not be as great without your help.

I also want to thank Vilde, Vanessa, Jørn and Erlend at the lab for the encouraging words and laughs, it has been great having you around this last year. Lastly, I want to thank my lab partner Celine Oanæs. Thank you for being there with me through both achievements and failures during this project. The master's and Trondheim in general would not have been so fun and exciting without you.

Table of Contents

Abstract

Mutations in the ubiquitin C-terminal hydrolase L1 (UCHL1) protein are implicated in human disease, including neurodegenerative disorders. This enzyme is highly expressed in brain, especially in neurons. Although it belongs to a family of enzymes that hydrolyzes ubiquitin, its primary functions are unknown (1). Recently, Bjørås's group identified two mutations in the UCHL1 gene in patients suffering from severe neurological features, including early-onset neurodegeneration with optic atrophy, spasticity paraplegia and ataxia (1). As the autophagy lysosomal pathway (ALP) is dependent on ubiquitin, we hypothesized that UCHL1 dysfunction leads to alterations in ubiquitin processing which would thereby affect the ALP in brain cells (2). In this project, induced pluripotent stem cells (iPSC) derived from fibroblasts of patients harboring mutations in UCHL1, as well as healthy individuals, were used as starting point to generate monolayer forebrain neurons (FB) and cerebral organoids. These 2D and 3D neuronal models were used to investigate the impact of UCHL1 dysfunction on neurodevelopment and neuroprotection via potential alterations in the ALP. We show that iPSCs and neural progenitor cells (NPC) derived from healthy individuals and patients harboring UCHL1 mutations, as well as cerebral organoids derived from healthy individuals were successfully generated and characterized based on morphological features, and expression of specific markers by qPCR and ICC. In addition, analysis of autophagic flux in NPC revealed no dysfunction in ALP in patient- or healthy control-derived cells, at this developmental stage. Preliminary screening of gene expression levels of autophagic markers indicated increased levels of the lysosomal enzyme Cathepsin D in patients-derived NPC, suggesting potential up-regulation of lysosomal function in these cells. This data, however, must be confirmed with several biological replicates and at protein level. Limitations in culturing and differentiating NPC, the intermediate state in the monolayer protocol, hindered further differentiation to FB neurons and the execution of functional assays. Several attempts and different protocols were employed to overcome this difficulty, however, without success. Also, generation of patient-derived cerebral organoids was not feasible and could potentially be a consequence of abnormal neural development due to UCHL1 mutations. Our preliminary data suggest that, if UCHL1 mutations alters ALP function, these effects may be more prominent at later developmental stages, such as at FB or mature motor neurons. Finally, further work is required on the development of more reliable and robust protocols for the generation of NPCs, FB neurons and cerebral organoids.

Abbreviations

Abbreviation	Definition
ALP	Autophagy Lysosomal Pathway
ATG13	Autophagy-related protein 13
BAF1	Bafilomycin A1
BECN1	Beclin 1
BSA	Bovine serum albumin
cDNA	Complementary DNA
CNS	Central Nervous System
CTSD	Cathepsin D
Da	Dalton
DAPI	4,6-diamidino-2-phenylindol
dH_2O	Destilled water
DMEM	Dulbecco's Modified Eagle Medium
DMSO	Dimethyl sulfoxide
DTT	Dithiothreitol
DUB	Deubiquitinating enzymes
EB	Embryoid body
EDTA	Ethylenediaminetetraacetic acid
EGF	Epidermal growth factor
FB	Fore brain
FBS	Fetal Bovine Serum
FGF	Fibroblast growth factor
FIP200	focal adhesion kinase family interacting protein of 200 kD
hiPSC	Human Induced Pluripotent Stem Cells
ICC	Immunocytochemistry
IHC	Immunohistochemistry
iPSC	Induced pluripotent stem cells
LAMP1	Lysosomal associated membrane protein 1
LC3	Light chain 3
LDS	Lithium dodecyl sulfate
mTOR	Mechanistic target of rapamycin
mTOR-C1	Mechanistic target of rapamycin complex 1
mTOR-C2	Mechanistic target of rapamycin complex 2
NPC	Neural progenitor cells
NSC	Neural stem cells
PAGE	Polyacylamid electrophoresis
PBS	Phosphate buffered saline
PBS-T	Phosphate buffered saline with Tween 20
qPCR	Quantitative polymerase chain reaction
RIPA	Radioimmunoprecipitation assay buffer
ROCK	Rho-kinase inhibitors
Rpm	Revolutions per minute
TGF	Transforming growth factor
UCHL1	Ubiquitin C-terminal hydrolase L1
ULK1	Unc51 like autophagy activating kinase 1
UPS	Ubiquitin-Proteasome System
VHC	Vehicle control
WB	Western blot

1.Introduction

This chapter provides an overview on fundamental aspects of the autophagy lysosomal pathway (ALP), the current knowledge on ubiquitin, UCHL1, and the impact of UCHL1 variants in human disease. Further, an outline of the intriguing stem cell technology, including the maintenance of hiPSCs, differentiation to neural progenitor cells (NPCs) and the generation of cerebral organoids is presented.

1.1 Autophagy Lysosomal Pathway (ALP)

Eukaryotic cells employ two major pathways for degradation of dysfunctional proteins and organelles – the ubiquitin-proteasome system (UPS) and the autophagy lysosomal pathway (ALP) (3). While the ubiquitin-proteasome system degrades soluble and small misfolded proteins, the autophagy lysosomal pathway is the major degradative system coordinating the normal turnover of intracellular components such as insoluble proteins, protein aggregates, damaged organelles and macromolecules (4). Autophagy prevents nutritional, metabolic, and infection-mediated stresses and is important in sustaining homeostasis in the cell (4, 5).

There are three types of autophagy in mammalian cells: macroautophagy, chaperone-mediated autophagy (CMA) and microautophagy (5). As ubiquitin is mainly involved in macroautophagy, this system will be further described and referred to as autophagy (3). Autophagy begins with the formation of autophagosomes from the maturation of isolation membranes termed phagophores (4). During the fusion of the phagophore, autophagic receptors recognize and attracts intracellular contents, such as long-lived proteins, aggregated proteins, damaged organelles and intracellular pathogens, to the membrane before the phagophore engulfs it and fuses together to form the autophagosome (5). The autophagosome then fuses with a lysosome to form autolysosomes, in which the lysosomes provide hydrolases that degrade the cargo as well as the inner membrane of the autophagosome (2, 5). The final step involves the transport of the products after the degradation, such as amino acids, back to the cytoplasm for a new round of cellular processes (2). The general scheme of the ALP is illustrated in figure 1.

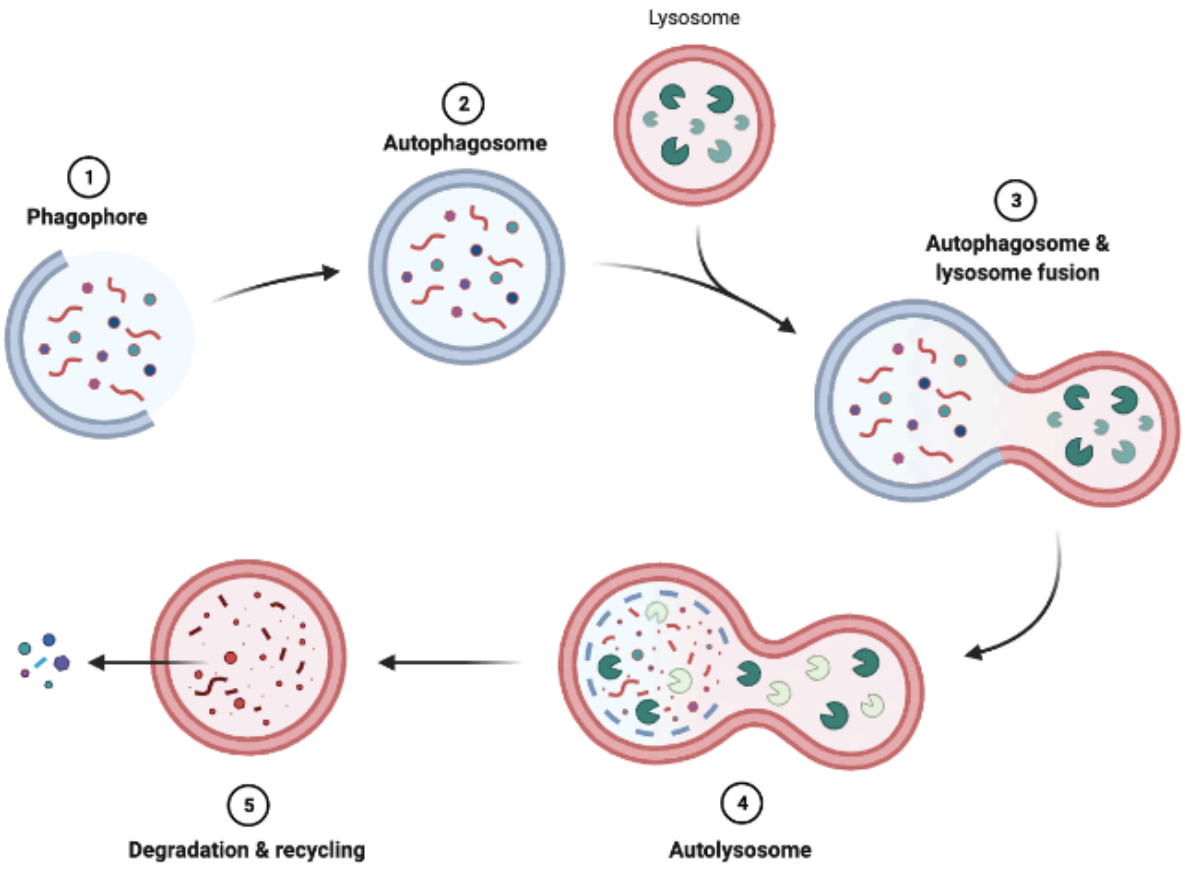

Figure 1: General scheme of the autophagy lysosomal pathway. During autophagy, a phagophore forms and insulates cytoplasmic components before fusion to form an autophagosome (5). The merge between an autophagosome and a lysosome creates the autolysosome leading to cargo degradation by lysosomal hydrolases (5). Figure created using Biorender.com.

Because autophagy is a key mechanism for the energy balance in normal cells, its dysregulation plays a major role in a variety of diseases, including chronic inflammation, cardiomyopathies, cancer and neurodegenerative diseases (5-7). Interestingly, increased autophagic activity can aid the maintenance of homeostasis in cancer cells by improving the removal of damaged cargo (8). This includes oxidized molecules resulting from augmented metabolic stress and accumulated misfolded proteins (8). On the other hand, excessive autophagy has shown to promote programmed cell death (8, 9). Alternatively, a decline in autophagic function has been linked to the accumulation of aggregated misfolded proteins that are hallmarks of neurodegenerative disorders, including Alzheimer's and Parkinson's (2, 6). In addition, since autophagy and lysosomal activities are directly linked, dysfunctional autophagy is commonly found in lysosomal storage diseases (10). There are, therefore, major efforts in understanding the role of the ALP in the accumulation of protein aggregates and its association to the pathogenesis and treatment of human diseases (2, 6, 10, 11).

1.1.1 Autophagy Markers and Modulators

Autophagy is a rather complex system involving many molecular players (7). One of them is the microtubule-associated protein-1 light chain 3 (LC3), a central molecule in the formation of autophagosomes (12). During autophagy, the cytoplasmic LC3-I protein undergoes lipidation forming LC3-II, a component of mammalian autophagosome membranes (3). LC3-II is bound to the autophagosome membrane until its degradation during fusion with the lysosome (13). Based on this, the LC3-II levels are closely related to the number of autophagosomes and serves as a good indicator for autophagic flux (5, 14). The correlation between LC3 and autophagy is illustrated in figure 2.

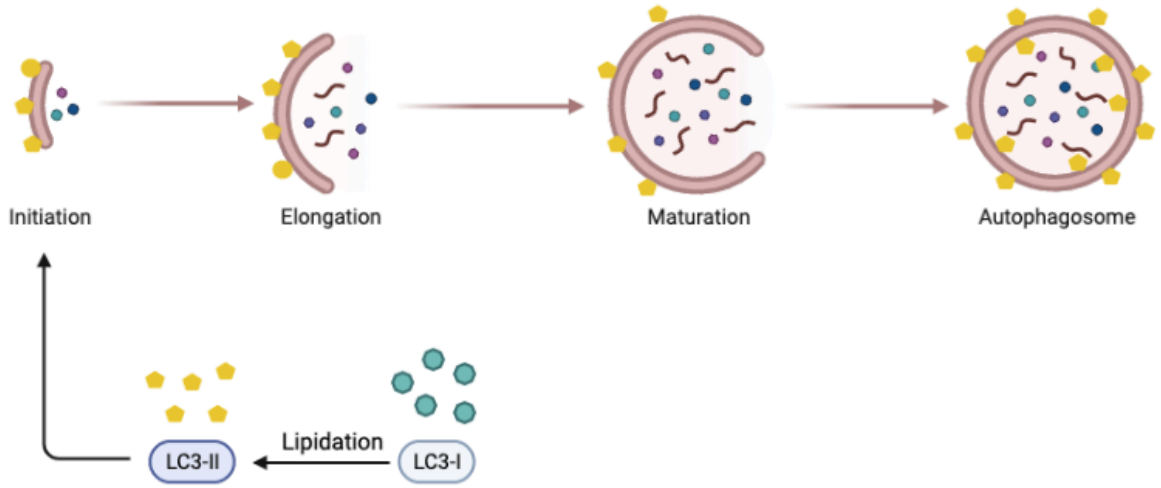

Figure 2: The cytosolic form of LC3 (LC3-I) undergoes C-terminal proteolysis and lipidation which forms LC3-II (12). LC3-II translocates to the autophagosome membrane and is bound until the fusion to a lysosome which degrades it (not shown in figure) (12). Figure created using Biorender.com.

Another common marker for autophagic flux is p62, also termed sequestosome1, a receptor that recognizes toxic cellular waste and binds to LC3-II as well as ubiquitin, thereby promoting the inclusion of ubiquitinated proteins and aggregates into autophagosomes (15). During this process, p62 is also incorporated in the mature autophagosome and degraded in autolysosomes (15). Since autophagy inhibition leads to p62 accumulation and autophagy induction results in decreased p62 levels, p62 has also been used as a marker to study autophagic activity (15, 16). Figure 3 displays p62 in the ALP.

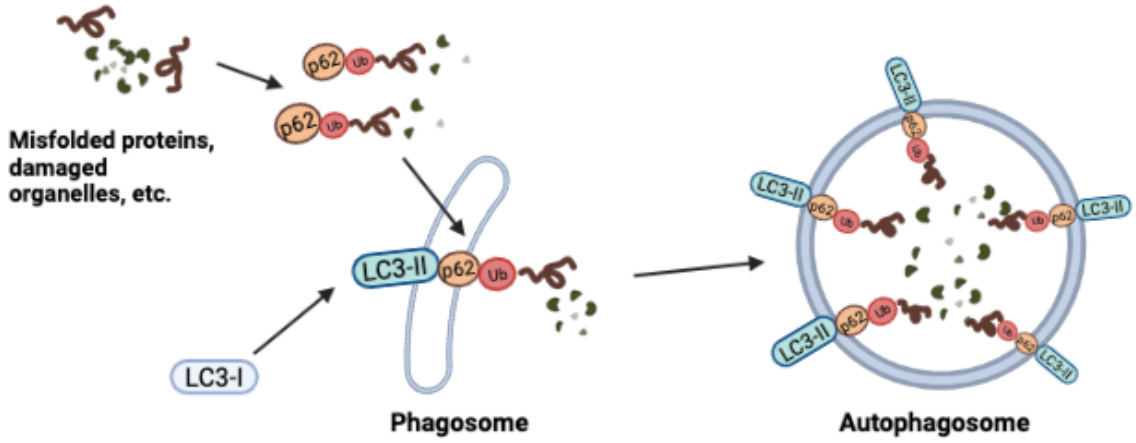

Figure 3: Sequestration of ubiquitinated cargo by p62 followed by its delivery to the autophagosome membrane via p62 binding to LC3-II. Figure created using biorender.com.

The increased levels of LC3-II alone are not adequate as a measurement of autophagic activity as decreased LC3-II degradation in the lysosome due to impaired autophagy flux can also cause its accumulation (17). To determine if increased levels of LC3-II are caused by a true increase in autophagy or a result of an impairment in autophagy, an inhibitor of autophagy can be utilized such as Bafilomycin A1. It inhibits the fusion between the autophagosomes and lysosomes, leading to increased numbers of autophagosomes, thus bound LC3-II and p62 (17). For cells with normal autophagic functions, it is expected an increase in LC3-II and p62 levels after treatment with Bafilomycin A1, as autophagosomes are not formed, consequently blocking LC3-II and p62 degradation. If the levels of LC3-II and p62 do not increase after Bafilomycin A1 treatment, it is most likely that the cells harbor a deficiency in the autophagic activity, such as an inhibition of the autophagosome-lysosome formation (12). Figure 4 illustrates the step of autophagy in which Bafilomycin A1 blocks the formation of the autolysosome.

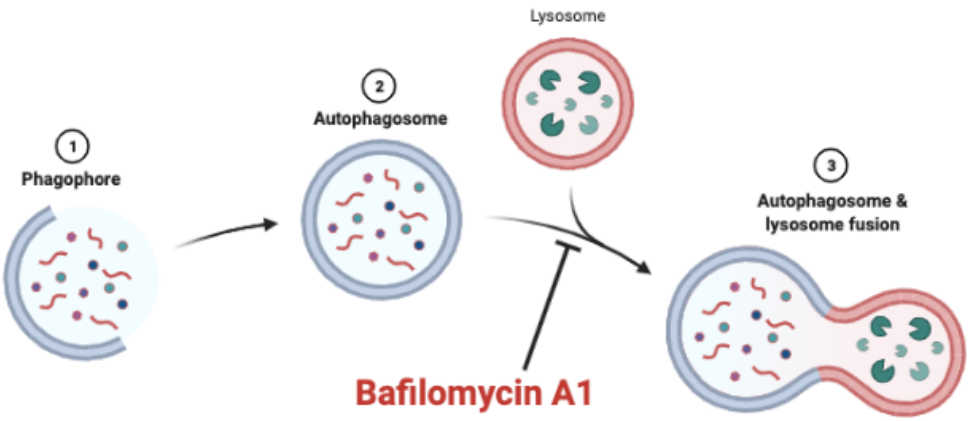

Figure 4: Schematic representation of the formation of the autolysosome and the inhibition caused by Bafilomycin A1. Bafilomycin inhibits the fusion between the autophagosome and the lysosome (18). Figure created using Biorender.com.

Like Bafilomycin, several other compounds can inhibit the ALP. Conversely, many agents, including proteasome inhibitors, can induce ALP. As proteasome inhibitors hamper protein degradation via the ubiquitin proteasomal system (UPS), autophagy is then upregulated to cope with the rapid accumulation of cargo, which is toxic to the cells (19). In this study, three of the most commonly used proteasome inhibitors were used to evaluate biological functions: MG132, Bortezomib and Epoxomicin (20). Their mechanisms of action and specificities are described in table 1.

Table 1: Characteristics of commonly used proteasome inhibitors (20).

Proteasome inhibitor	**Mechanism**	**Function**
MG132	Reversible	Inhibits the 26S proteasome subunit
Bortezomib	Reversible	Inhibits the 20S proteasome subunit
Epoxomicin	Irreversible	Covalently binds to several catalytic subunits (LMP7, MECL1, X and Z)

In the autophagy context, UPS inhibition by MG132 results in upregulation of Beclin1 and LC3, which in turn stimulates autophagy activity (19, 21). Bortezomib triggers an increase in the expression of autophagy genes ATG5 and ATG7 (19) while Epoxomicin was shown to block the AKT-mTOR pathway, thereby inducing autophagy (19).

1.1.2 Ubiquitin and Autophagy

Another key molecule involved in autophagy is ubiquitin (Ub) (22). Ubiquitin is a 76-amino-acid long protein that binds to lysine residues on protein targets (23). It can bind to a substrate as a single molecule, or it can form polyubiquitin chains through a sequential mechanism performed by specialized enzymes (22, 24). Polyubiquitination occurs via conjugation of secondary ubiquitin molecules to a lysine (K6, K11, K27, K29, K33, K48 and K63) or to the N-terminal methionine of the previous ubiquitin molecule (23). While monoubiquitination has been shown to regulate receptor endocytosis and histone modification, polyubiquitination plays diverse functions that are dependent on the type of Ub chain linkages (23). Like other post-translational modifications, ubiquitination is reversible due to the action of deubiquitinating enzymes (DUBs) (22, 24).

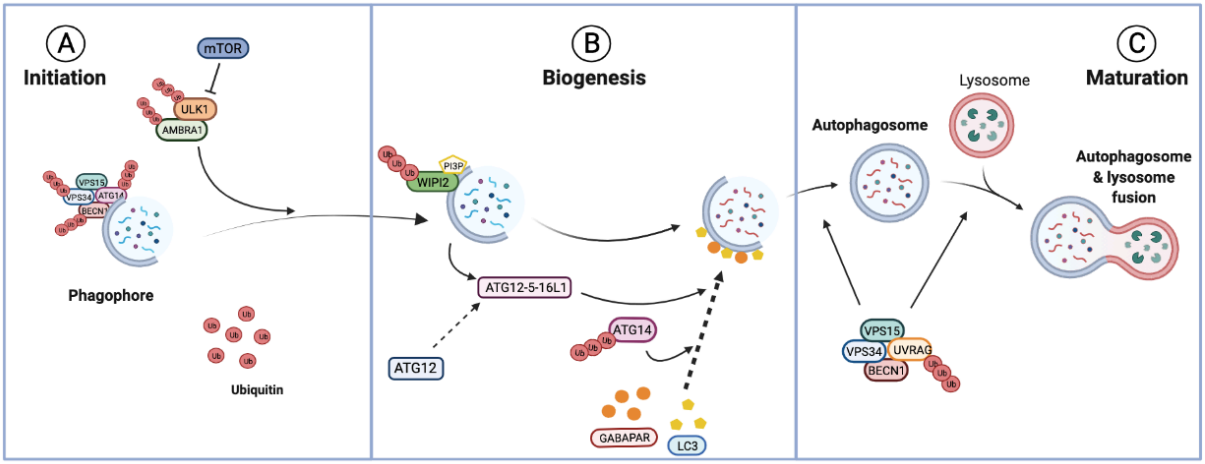

Figure 5: Functional roles of ubiquitin in the regulation of autophagy. (A) Initiation of the formation of the autophagosome. (B) Biogenesis of the autophagosome. (C) Maturation of the autophagosome and the formation of an autolysosome. The autophagosome is subjected to several ubiquitination steps by E3 ligases during autolysosome formation (3). Dashed arrows indicate processes involving multiple steps. Ubiquitin is represented as red beads. Figure created using biorender.com.

During autophagy, p62 recognizes and binds ubiquitinated cargo and delivers it to the autophagosome via simultaneous interaction with the Ub-cargo and LC3 (figure 3) (25). Moreover, ubiquitin affects initiation, biogenesis and maturation of the autophagosome (figure 5) demonstrating its importance and the complexity of its functions in multiple stages of ALP. Indeed, ubiquitination of core autophagy induction factors is one of the most common activities regulating autophagy (3). For instance, ubiquitination of the Beclin1 protein promotes pro-autophagic activity by inducing the assembly of the autophagosome (26). It also acts as a hub for DUB-mediated regulation, where DUBs can regulate the initiation of autophagy (23).

1.2 The deubiquitinating enzyme UCHL1: Ubiquitin C-terminal Hydrolase-1

DUBs are enzymes that remove ubiquitin groups from substrate proteins by hydrolyzing the isopeptide bond between the ubiquitin C-terminus and the substrate, as well as ubiquitin-ubiquitin covalent bonds (22, 24). Approximately 100 human deubiquitinases has been described. Among them is the enzyme Ubiquitin C-terminal hydrolase L1 (UCH-L1) which belongs to the Ub C-terminal hydrolases (UCHs) sub-family of DUBs. Notably, UCHL1 is one of the most abundant proteins in the brain, comprising up to 2% of total neuronal protein (1, 27). Despite its high levels in neurons, the precise roles of the protein remain largely unknown (22, 24). Nevertheless, potential functions have been suggested for the enzyme. UCHL1 activities in both UPS and autophagy have been proposed (28). The protein is believed to have a protective function where it cleaves short peptides to stabilize monomeric ubiquitin in the

UPS (29). UCHL1 cleaves ubiquitin when co-transfected with a plasmid expressing a polyubiquitin gene, where it may act co-translationally on polyubiquitin gene products (29).

Recent studies have suggested roles for UCHL1 in cellular homeostasis by stabilizing ubiquitin monomers or as a neural antioxidant, reacting with and chelating free radicals during acute damage, thereby protecting cells from extensive damage (24). However, few functionally verified interaction partners of UCHL1 in the brain have yet been identified (1). UCHL1 may also influence autophagy through its binding to the lysosome-associated membrane protein 2 (LAMP2), which promotes the fusion and maturation of autophagosomes (22). Moreover, inhibition of UCHL1 induced by protein kinase C (cPKC) y activation, may be involved in downregulation of autophagy, alleviating injuries after middle cerebral artery occlusion in mice (30-33). Importantly, UCHL1 seems to decrease the levels of phosphorylated tau and aggregation of tau protein in mouse neuroblastoma cells (34). Accumulation of Tau proteins is a central event in the pathophysiology of Alzheimer's disease and the clearance of Tau aggregates is directly linked to autophagy (33).

1.2.1 UCHL1 Variants and Human Disease

The importance of UCHL1 becomes evident by its impact in neurodegenerative disorders. Its dysfunction has been associated with Parkinson's and Alzheimer's diseases and recent reports show that UCHL1 is directly implicated with severe clinical features, including early-onset neurodegeneration with optic atrophy, spasticity paraplegia and ataxia (1, 27, 35).

In 2013, Bilguvar *et al.* reported a family of 3 siblings of Turkish origin with a homozygous UCHL1 variant showing childhood-onset neurodegeneration (27). In 2016, a second family of Norwegian origin was reported with UCHL1 mutations displaying similar neurodegeneration (1). Two of the three siblings affected in the Norwegian family are monozygotic twins which developed optical atrophy at an early age, which progressed to ataxia and spasticity paraplegia as they became older (1). Clinical features of the family were dated back to 1972 and it is reported that the twins developed neurological symptoms with progressive visual loss from 10 years of age and stiffness in the legs after 15 years of age (1). At 55 years of age, they were wheelchair dependent (1). Interestingly, the results from several neurophysiological evaluations revealed memory functions that exceed the average (1). iPSCs from these monozygotic twins were provided at the start of the project to investigate the molecular mechanisms behind this neurodegenerative disorder.

Whole exome sequencing of the siblings indicated compound heterozygous variants in UCHL1; c.533G>A (p.Arg178Gln) and c.647C>A (p.Ala216Asp). All three siblings were reported to be heterozygous for both missense variants. The Arg178Gln (R178Q) mutation led to increased enzymatic activity, while Ala216Asp (A216D) mutation led to loss of function of the UCHL1, compared to the wild type (1). The enzymatic activity of Arg178Gln compared to WT is presented in figure 6.

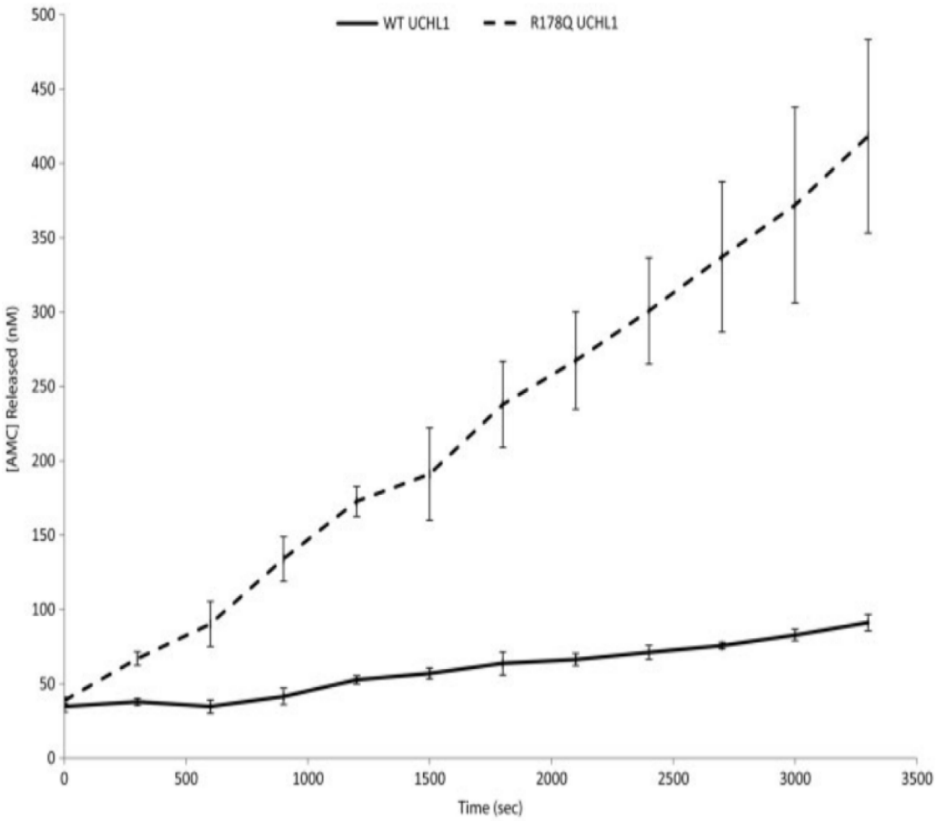

Figure 6: *In vitro* activity assay reveals a 4-fold increased ubiquitin hydrolytic activity of the Arg178Gln (R178Q) mutant compared to WT, reported by Rydning et al. (1). WT UCHL1 (black line) and R178Q UCHL1 (dashed line).

These studies underscore the complexity of the different roles of UCHL1 and its impact on human disease. Therefore, elucidation of UCHL1 functions is of outmost importance for the development of clinically useful therapies, not only for patients harboring mutations on the UCHL1 gene, but for individuals suffering from common neurological disorders associated with defects in ubiquitin processing, namely Alzheimer's and Parkinson' diseases.

1.3 Stem Cell Technology

The research on diseases of the nervous system has been considerably difficult as the nature of most neurological disorders are complex and sporadic (36). Using animal models have shown to be inefficient, as drugs that have displayed efficiency and safety in rodents do not transfer their success in human clinical trials (37). This is mostly due to differences between species, since some biological pathways present in humans are absent or only partially represented in animal models (36, 38). Recently, the success in reprogramming adult cells into iPSCs, and the ability to directly differentiate iPSCs into distinct neuronal subtypes has enabled a whole new world of applications with great potential to overcome limitations imposed by the inaccessibility of neurological tissues and cell types (37, 39-41). The stem cell technology also allows the study of disease mechanisms in the context of each patient's own unique genetic pattern (36). Notably, iPSCs can be differentiated to generate organoids, *i.e.,* three-dimensional (3D) self-organizing structures composed of organ-specific cell types that resemble the architecture and function of innate organs (42).

1.3.1 Induced Pluripotent Stem Cells

Induced Pluripotent Stem Cells (iPSCs) are stem cells obtained by reprogramming differentiated adult cells (43). They are similar to embryonic stem cells (ESCs) which are pluripotent stem cells that arise from the inner cell mass of the blastocyst, however, the iPSCs come with great advantages compared to ESCs (43). Firstly, the iPSCs do not arise from an embryo, but rather from the reprogramming of somatic cells, thereby bypassing the need to destroy embryos (43). This excludes the ethical considerations involved in generating stem cells. Secondly, researchers are able to generate the iPSCs in a patient-specific manner, allowing the generation of autologous transplants without the risk of immune rejection (43).

The generation of iPSCs was initiated by Shinya Yamanaka and his colleagues in 2006 when they successfully managed to reprogram fibroblasts into iPSCs in mice (43). They used retroviral gene transfer and introduced cDNAs that encoded the transcription factors Oct4 (*octamer-binding transcription factor 4*), Sox2 (*sex-determining region Y (SRY) box 2*), Klf4 (*Krüppel-like factor)* and c-Myc (*c-myelocytomatosis oncogene*), into terminally differentiated fibroblasts (43). The success of the reprogramming was confirmed, as the generated cells (iPSC) displayed self-renew capabilities and pluripotency, i.e., were able to differentiate into each of the three germ layers and express the pluripotency markers Oct4, Sox2 and Nanog (43).

Ocer the years, the efficiency in reprogramming fibroblasts into iPSCs has greatly improved and iPSCs have also been generated from several cell types such as liver, skin, blood, prostate and urinary tract cells (43).

During the cultivation of iPSC, it is important that the cells remain in an undifferentiated state. To check and evaluate the condition of the iPSC, one can study the morphology of the cells using a microscope. iPSC have characteristic morphology with a round shape, a large nucleus and a small cytoplasm (37). The cells form compact colonies with clear borders and definite edges (44). If the morphology abbreviates from the normal, it is a sign of differentiation. The detection of specific markers is another method used to identify the presence of iPSC. Transcription factors associated with pluripotency are commonly used for this purpose, such as Nanog and Oct4 (45). Nanog contributes to the cells pluripotency by suppressing the cell determination factors, while Oct4 provides the cells with the ability to self-renew (45, 46).

1.3.2 Generation of Neural Progenitor Cells from Induced Pluripotent Stem Cells

Neural progenitor cells are known as the progenitor cells found in the central nervous system (CNS) (47). These cells are able to differentiate into a number of neuronal and glial cell types such as neurons, astrocytes and oligodendrocytes (47). The characterization of the NPCs depends on their location in the brain, morphology, gene expression profile, temporal distribution and function (47). The generation of NPCs is achieved by plating iPSCs onto a defined matrix, and expose the cells to inductive factors (48). The neural induction principle starts with removing components in the medium that promote self-renewal. This will in turn trigger differentiation towards all the three embryonic germ layers; mesoderm, endoderm and ectoderm (49). The cells are grown as adherent cultures in a serum-free medium supplemented with EGF and other early patterning molecules (50). This will allow the iPSC to differentiate towards the neural lineage and promote the survival of the NPCs (49-51).

An outline of the procedure used to generate patient-specific iPSC, NPC and forebrain (FB) neurons from skin biopsies are presented in figure 7. NPC and FB neurons were chosen as 2D cell culture models to determine cell proliferation and cell survival in response to agents that modulate autophagic and lysosomal activities, as well as determining the levels of ALP markers, as further described.

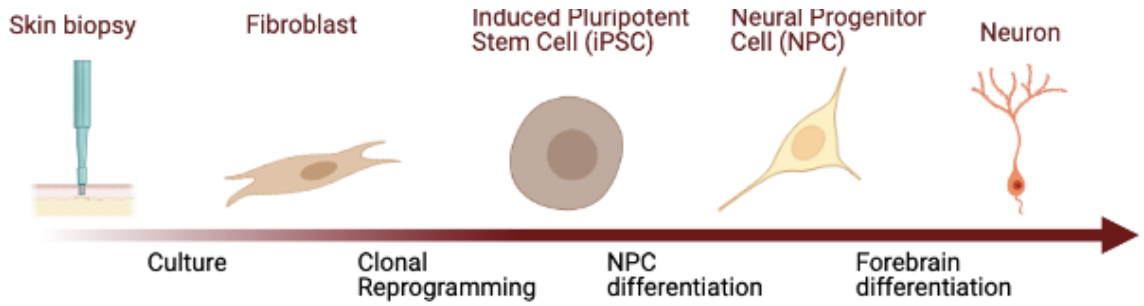

Figure 7: Outline of procedure for generating patient-specific iPSC, NPC and Neurons from skin biopsies. A skin sample is taken from a patient and cultured to fibroblasts. Clonal reprogramming and editing are performed to reprogram the fibroblasts to iPSCs. The iPSCs can be differentiated to NPCs and neurons to make models for neuronal development or drug screening (52) . Figure created using Biorender.com.

Several markers can be used to identify and confirm the generation of NPCs. In this thesis Musashi-1 (MSI-1), Nestin and Sox2 were used for the immunocytochemical staining to detect NPC cells. Musashi-1 and Nestin is expressed in neural progenitor cells as well as neural stem cells (53). Nestin is used as a neuronal marker as it identifies the primitive neuroepithelium (54). Sox2 is a gene that encodes one of the members in the SOX family of transcription factors involved in the determination of cell fate and regulation of embryonic development (55). Proliferative NPCs are characterized by the expression of Sox2 (55).

1.3.3 Generation of Forebrain Neurons from Neural Progenitor Cells

As the patients harboring the mutations in the UCLH1 suffer from sensorimotor neuropathy of axonal type, the study was guided towards the generation of forebrain neurons. The forebrain is the largest region of the brain and includes the entire cerebrum as well as small structures called the diencephalon, which both are included in the regulation of motor functions (56). Dysfunctions in FB neurons are directly linked to severe neurological disorders, including Alzheimer's disease (57), Schizophrenia (58) and Huntington's disease (59).

The generation of FB neurons can be achieved via monolayer or embryoid body (EB) protocols (60). In monolayer protocols, iPSCs are differentiated to neural progenitor cells (NPCS) which then are cultured in a neuronal induction media to produce mature FB neurons. Alternatively, iPSC can be dissociated and cultivated in suspension with neural induction media to promote the formation of embryoid bodies (EBs) (56). Well-known FB specific markers are the transcription factor FOXG1 (Forkhead Box G1) and the forebrain surface antigen FORSE-1 (forebrain-surface-embryonic) (56, 61).

1.3.4 Generation of Cerebral Organoids from Induced Pluripotent Stem Cells

The generation of cerebral organoids from patient-derived iPSCs is an intriguing new technology with the potential to significantly improve studies of neurodegenerative disorders. Cerebral organoids are complex three-dimensional structures which can mimic the composition and tissue organization of the embryonic brain (62). Notably, organoids display semi-physiologic properties maintaining unique and dynamic features, and therefore, can be used as models to display a particular neurological disorder in a more complex manner compared to monolayer cell cultures. The patient-derived iPSC can be differentiated into disease-relevant cell types carrying the genetic background of the donor, thus enabling *de novo* generation of human models of complex disorders (63, 64). They can also be used as drug screening platforms and for personalized medicine, aiming at the development of patient-specific therapies (43). Organoids have been proven to provide access to early stages of human brain development in a way that no mouse models have provided before (65).

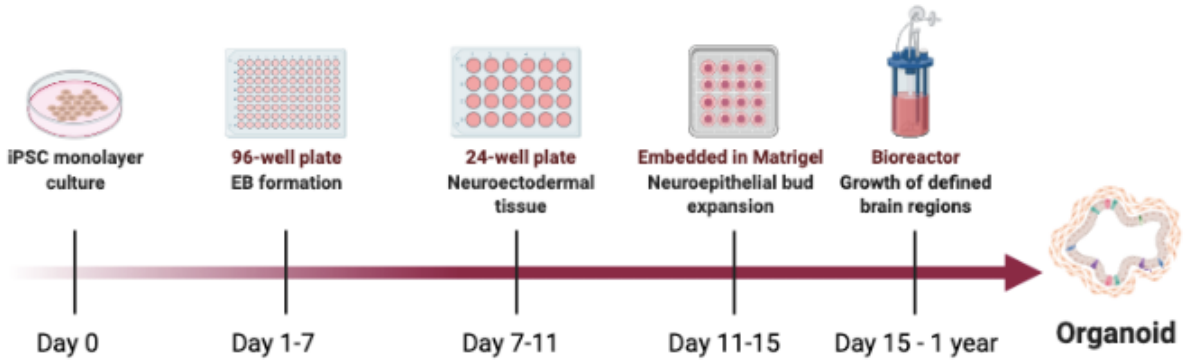

Figure 8: Timeline for the generation of cerebral organoids based on the protocol described by Lancaster *et al.* (66). iPSCs cultured as a monolayer is passaged onto 96-well plate for aggregation and generation of EBs. The EBs are replated to 24-well plates to develop neuroectodermal tissue before being embedded in Matrigel® for neuroepithelial bud expansion. The tissues are then transferred to a bioreactor for growth of defined brain regions (66). Figure created using Biorender.com.

The generation of cerebral organoids involves the induction of neural identity from hiPSCs reprogrammed from fibroblasts (66). By culturing the hiPSCs in media containing specific nutrients and growth factors, the *in vitro* environment has the ability to imitate the *in vivo* cellular environment of the brain (66). As presented in figure 8, the first step of the protocol is to culture the iPSCs in low attachment wells, which will in turn form aggregates of iPSCs, also called embryoid bodies (EBs) (66, 67). Within these embryoid bodies the hiPSCs are stimulated to produce ectoderm with the help of basic fibroblast growth factor (bFGF) and high-dose rho-associated protein kinase (ROCK) inhibitor which limits cell death (68, 69). The EBs are subjected to a minimal medium in a suspension which leads to the formation of neuroectoderm only on the outer surface of the EBs. By the use of an extracellular matrix that supports the 3D

structure, the cells are able to self-organize and form large buds of continuous neuroepithelium protruding from the embryoid bodies. The last part of the protocol is to apply agitation. By the use of a spinning bioreactor or an orbital shaker, the organoids are provided with the nutrients and oxygen required for further growth and development of defined brain regions (66).

The newly formed organoids can be maintained for months under the correct environmental conditions with the correct nutrients (66). This long-term conservation of the organoids enables the study for long term effects or toxicity of certain treatment modalities for the human brain (64, 70).

2. Aims and Hypothesis

UCHL1 is one of the most abundant proteins in the brain, however, its function is largely unknown (1). Patients descending from Norway harboring mutations in the UCHL1 gene displayed severe neurodevelopmental complications, including early-onset neurodegeneration with optic atrophy, spasticity paraplegia and ataxia. We hypothesize that UCHL1 deficiency affects ubiquitin processing, which alters the ALP activities in the brain, leading to neurodegeneration. Accordingly, the major aim of this project is to explore the impact of UCHL1 in neurodevelopment and neuroprotection by studying its potential impact in the autophagy lysosomal pathway, which is regulated by ubiquitin.

To achieve this goal, the project was divided into four major tasks:

i. generation and characterization of NPC, FB neurons and cerebral organoids derived from healthy controls and patients harboring mutations in the UCHL1 gene.
ii. investigation of NPC and FB neurons responses to drugs that modulate autophagy and lysosomal degradation.
iii. evaluation of autophagic flux in NPC and FB neurons.
iv. determination of the levels of autophagic markers in NPC, FB neurons and cerebral organoids at different stages of neural differentiation.

3. Methods

3.1 Coating of Cultureware

Cell lines that do not easily attach to the well plate require coating using biological extracellular matrices (71). The coatings used in this project are Geltrex™ for iPSC culture, Matrigel® for the culture of iPSCs during germ layer differentiation and Poly-L-Ornithine/Laminin for NPC culture. Cultureware and volumes used for coating are listed in table 2, appendix 1.1.

3.1.1 Geltrex™ and Matrigel ®

Geltrex™ and Matrigel® aliquots were thawed on ice and diluted (1:100 dilution for Geltrex™,1:50 for Matrigel®) in DMEM/F12 medium. Geltrex™ and Matrigel® were coated onto each well using volumes according to table 2, appendix 1.1. The coated plates were incubated at 37°C for 1-2 hours prior to use. The plates were stored at 4°C and used within one week. Reagents are listed in table 3, appendix 1.1.

3.1.3 Poly-L-Ornithine/Laminin

Poly-L-Ornithine diluted in PBS with a final concentration of 15 µg/mL was coated onto the plates with volumes following table 2, appendix 1.1. The plates were either incubated at room temperature for two hours, or overnight at 4°C. The 6-plate wells were washed twice with 1 mL PBS and once with 1 mL DMEM/F12 before laminin diluted in a 1:200 dilution in DMEM/F12 were coated onto the plates using volumes according to table 2, appendix 1.1. The plates were incubated either for 2 hours at room temperature, or overnight at 4°C prior to use. The coated plates were stored at 4°C and used within two weeks. Reagents are listed in table 4, appendix 1.1.

3.2 Cell Culture and Passage of iPSCs

Five clones of iPSC were reprogrammed from fibroblasts in Bjørås' lab prior to the project. Two healthy control clones: AGc1 and AGc6, and three clones Bc4, Bc9 and Tc3 from patients III-5 (patient B) and III-6 (patient T) harboring the R178Q and A216D mutations in the UCHL1 gene, reported by Rydning *et al.* (1). Bc4 and Bc9 were reprogrammed from fibroblasts deriving from patient B while Tc3 derived from patient T. In a second attempt to further generate NPC, new lines of iPSC clones were used: AGc1, ATc2, Bc4, Bc6, Tc3 and Tc18. AGc1 and ATc2 were reprogrammed from healthy control fibroblasts, while Bc4 and Bc6 were reprogrammed

from patient B derived fibroblasts, and Tc3 and Tc18 from patient T. None of the iPSCs were cultured for longer than passage number 60.

The iPSCs were cultured on Geltrex™ coated 6-well plates (see section 3.1.1) in a partly self-made medium, designated E8 (+) medium in the incubator (37°C, 5% CO_2). The procedure and reagents for this medium are presented in table 5 and 6, appendix 1.2. The cells were passaged when they exhibited a confluency of 70-80%, usually after 4-5 days of culture. This was performed by washing each well with 1,5 mL of D-PBS before adding 1 mL of EDTA followed by incubation at room temperature for 3,5 minutes. The cells were split in a 1:3 ratio using 1,5 mL E8 (+) medium per well. On day one after passage, the cells were washed with 1,5 mL of D-PBS before adding 1,5 mL of fresh E8 (+) medium. On day two and three, the old medium was replaced by 1,5 mL of new E8 (+) medium. The old medium was replaced with 2 mL of medium the following days. Reagents used for iPSC culture and passage are listed in table 7, appendix 1.2.

3.2.1 Storing iPSCs

For qPCR and karyotyping, iPSCs were stored as pellets. To collect the pellets, cells at 70-80% confluency were washed once with 1,5 mL D-PBS before adding 1 mL PBS and scraping them using a cell scraper. Cells were transferred into Eppendorf tubes and centrifuged at 8000 rpm for 3,5 minutes. The supernatant was aspirated, and the cell pellet stored at -80°C. Reagents used for storage of iPSCs are listed in table 8, appendix 1.2.

3.3 Differentiation to Neural Progenitor Cells

Three different protocols were used for the differentiation of iPSC to NPC as an attempt to overcome the poor survival of NPC, which hindered further differentiation to FB neurons. The iPSCs were ensured to be of a high standard and spontaneously differentiated cells were removed prior to NPC differentiation.

3.3.1 Protocol 1: Monolayer Culture Protocol

The first protocol was a modification of the protocol published by Li *et al (72),* illustrated in figure 9. Upon differentiation to neural stem cells (NSC), iPSC was plated as single cells onto 6-well Geltrex™ coated plates (see section 3.1.1 for coating protocol). The reagents used for the passage and culture of NPCs are listed in table 9, appendix 1.2. The cells were washed

using 1,5 mL D-PBS before adding 1 mL of Accutase followed by incubation for 5-8 minutes for single-cell dissociation. The cells were transferred to 15 mL falcon tubes pre-filled with 5-6 mL of DMEM/F12 before centrifugation for 5 minutes at 1,000 rpm. The supernatant was aspirated, and the cells were resuspended in 1-3 mL of the neural stem cell medium (NSC) containing 10 µM Rock inhibitor (first 24 hours) according to the size of the pellet. A list of reagents used for the NSC medium is listed in table 10, appendix 1.2. A 1:1 dilution of cells and Trypan blue staining were prepared before cell counting performed by Countess II (Thermo Fisher Scientific). 500 000 cells in 2 mL medium were seeded to each well. The cells were cultured in the incubator at 37°C.

Full medium change was performed daily for 6-9 days, according to cell density and morphology. After 6-9 days the NSCs were passaged and seeded using 1-1,5 x 10^5 cells/cm^2, onto Poly-L-Ornithine/Laminin coated plates (see section 3.1.3 for coating protocol) according to the same procedure described in the paragraph above. Full medium change was performed daily using the neural progenitor medium (NEM). Reagents and volumes used for the NEM medium are listed in table 11, appendix 1.2. This medium was used for the rest of the differentiation of NPCs. The NPCs were passaged every 4-5 days and cultured until passage 4-5 using this protocol.

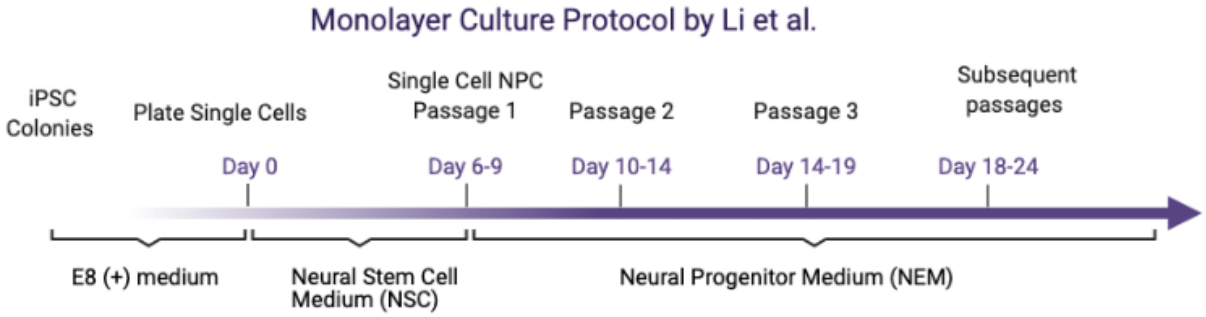

Figure 9: Timeline of monolayer culture protocol by Li et al. Single cell iPSCs are seeded onto Geltrex™ coated plates in NSC medium. After 6-9 days of culture, single cell NPCs are passaged onto Poly-L-Ornithine/Laminin plates and cultured in NEM medium. The cells are passaged every 4-5 days in NEM medium. Figure created using biorender.com.

3.3.2 Protocol 2: Monolayer Culture Protocol

The second protocol used for NPC differentiation was a monolayer culture protocol developed by Stemcell Technologies. Upon NPC differentiation, single-cell iPSCs were passaged onto Poly-L-Ornithine/Laminin coated plates (see section 3.1.3 for coating protocol). The same procedure described in section 3.3.1 was performed, however, using STEMdiff™ Neural

Induction Medium + SMADi with 10 µM Rock inhibitor (first 24 hours) as culture medium, with plating densities of 2,0-2,5 x 10^5 cells/cm^2. Cells were cultured for 7 days for passage 0. The plan was then to passage them every 4-5 days for the following passages. Full medium change was performed daily. The timeline for the protocol is presented in figure 10. The cells did not reach further than passage 1 due to cell death. Specific reagents used for this protocol are listed in table 12, appendix 1.2.

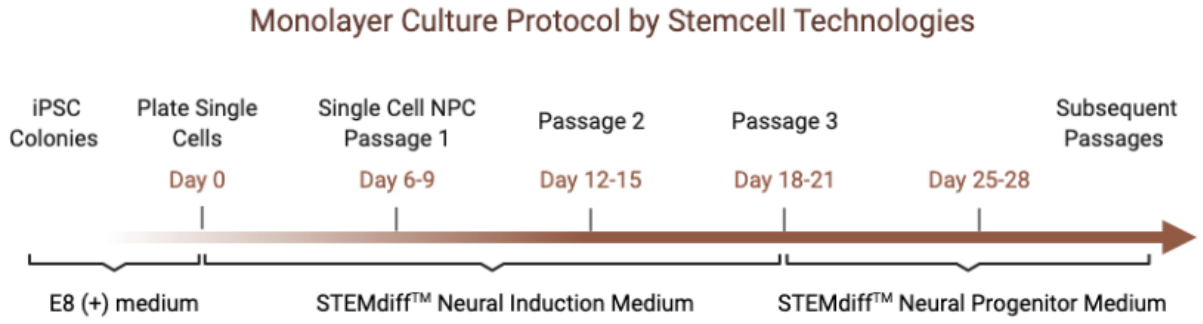

Figure 10: Timeline of the monolayer culture protocol developed by Stemcell Technologies. Single cell iPSCs are seeded onto 6-well plates and grown in STEMdiff™ Neural Induction Medium for 6-9 days. After passage 1, the cells are cultured in the STEMdiff™ Neural Induction medium until passage 3. After passage 3, the NPCs are grown in STEMdiff™ Neural Progenitor Medium for the following subsequent passages. Figure created using Biorender.com based on Stemcell Technologies monolayer protocol.

3.3.3 Protocol 3: Embryoid Body Protocol

For the third NPC differentiation protocol, the EB procedure provided by Stemcell Technologies was used. This protocol uses Aggrewell™800 24-well plates to aggregate the iPSCs to form embryoid bodies which are the starting point for the NPC differentiation. The timeline of the protocol is presented in figure 11.

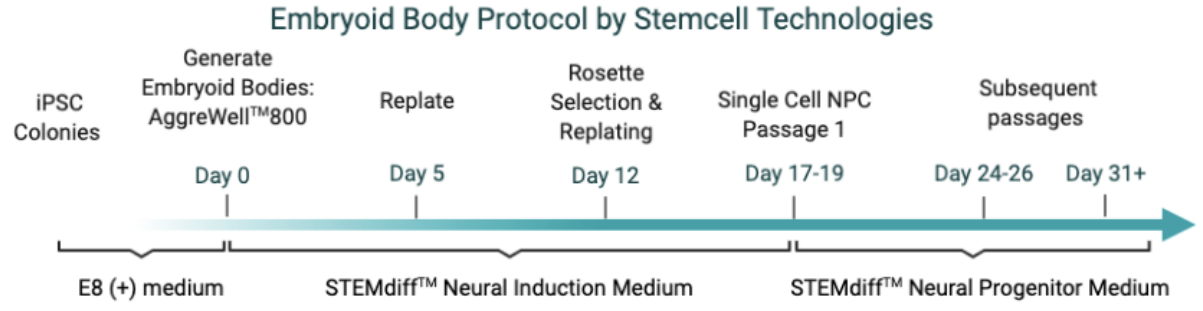

Figure 11: Timeline of Embryoid Body Protocol developed by Stemcell Technologies. Single cell iPSCs are seeded onto Aggrewell™800 and cultured in STEMdiff™ Neural Induction Medium for 5 days. The EBs are replated onto 6-well plates and after 7 additional days rosette selection is executed using the STEMdiff™ Neural Rosette Selection Reagent. After the rosette selection single cell NPCs should start to appear leading to following passages of NPCs. Figure created using biorender.com based on Stemcell Technologies EB protocol.

The Aggrewell™800 was prepared by adding 500 µL Anti-Adherence Rinsing Solution to each well. The plate was centrifuged at 1300 x g for 5 minutes before being observed under a microscope to ensure that the microwells had no bubbles. The anti-adherence rinsing solution was replaced with 1 mL pre-warmed (37°C) STEMdiff™ Neural Induction Medium + SMADi with 10 µM Rock inhibitor.

iPSCs were passaged to the Aggrewell™800 according to section X using STEMdiff™ Neural Induction Medium + SMADi with 10 µM Rock inhibitor (first 24 hours) as culture medium. 3 x 10^6 cells (2 mL) were passaged onto each well of the Aggrewell™800 resulting in 10 000 cells in each microwell. The Aggrewell™800 were centrifuged at 100 x g for 3 minutes to capture the cells in the microwells before examination under the microscope to ensure even distribution. The wells were placed in the incubator (37°C, CO_2 5%). On day 1-4, a partial medium change of 1,5 mL (3/4) was executed using pre-warmed (37°C) STEMdiff™ Neural Induction Medium + SMADi. This was done carefully against the wall to not disrupt the newly formed EBs.

On day 5, the EBs were replated onto Poly-L-Ornithine/Laminin coated 6-well plates (for coating see section 3.1.3). For preparation, a 40 µm reversible strainer rinsed with DMEM/F12 was placed on a 50 mL conical tube. The medium was removed from the Aggrewell™800 and expelled onto the plate to dislodge the EBs before transferring them to the cell strainer using a wide-bore pipette. This step was repeated using 1 mL of DMEM/F12 until all EBs were removed from the Aggrewell™800. The cell strainer was then inverted onto a new 50 mL conical tube and 2 mL pre-warmed (37°C) STEMdiff™ Neural Induction Medium + SMADi was added to the cell strainer to collect the EBs into the tube. The cells were transferred to the wells using a wide-bore pipette. The plates were set in the incubator (37°C).

On day 6 to 11, a daily full-medium change was performed using 2 mL pre-warmed (37°C) STEMdiff™ Neural Induction Medium + SMADi. On day 8, the neural induction was determined using the following formula:

$$\%\, neural\ induction = \frac{\#\ of\ EBs\ with\ \geq 50\%\ neural\ rosettes}{Total\ \#\ of\ EBs}\, x\ 100$$

On day 12, the neural rosette selection was performed. The wells were washed with 1 mL DMEM/F12 before detaching the rosettes by incubation of 1 mL STEMdiff™ Neural Rosette Selection Reagent for 1,5 hours in 37ºC. The Rosette Selection Reagent was aspirated carefully before expelling 1 mL of DMEM/F12 onto the wells to dislodge the neural rosettes. This was repeated until all the neural rosettes were dislodged before collection to 15 mL falcon tubes. The tubes were centrifuged at 350 x g for 5 minutes before aspirating the supernatant and the addition of 2 mL STEMdiff™ Neural Induction Medium + SMADi. The neural rosettes were carefully resuspended before adding them onto new Poly-L-Ornithine/Laminin coated wells. The neural rosettes were evenly distributed and placed in the incubator (37ºC).

On day 13-17, a full medium change of 2 mL was performed using STEMdiff™ Neural Induction Medium + SMADi. As the cells did not form sufficient monolayers of NPCs, the protocol was not further used. Specific reagents used for this protocol are listed in table 13, appendix 1.2.

3.3.4 Storing NPCs

2.3.4.1 Storing Live NPCs

Live cell stocks were prepared and used at later timepoints to resume cell culture. During each passage, after cell counting (see section 3.3.1), 4-6 million cells were transferred to 15 mL falcon tubes and centrifuged at 1000 rpm for 5 minutes. After removing the supernatant, cells were resuspended in the appropriate NPC medium with 10% DMSO. The resuspension was then transferred into Cryo tubes and stored in liquid nitrogen. Reagents are listed in table 14, appendix 1.2.

3.3.4.2 Storing NPC pellets

Cell pellets were also stored for experimental procedures such as qPCR and western blot. During the passage, after the cell count (see section 3.3.1) 2 million cells were transferred into Eppendorf tubes and centrifuged at 8000 rpm for 3,5 minutes. The supernatant was aspirated, and cells were washed with PBS twice before storing the cell pellet at -80ºC. Reagents used are listed in table 15, appendix 1.2.

3.3.5 Thawing NPCs

Cell stocks were thawed in a 37ºC water bath before transferring the cells to a pre-filled 15 mL falcon tube with 5 mL DMEM/F12 and centrifuged at 1000 rpm for 5 minutes. The supernatant was removed, and the appropriate growth medium with 10 µM ROCK inhibitor (first 24 hours) was added. The cells were counted according to section 3.3.1 before seeding onto Poly-L-Ornithine/Laminin coated 6-well plates (section 3.1.3). The cells were then cultured according to section 3.3.1. Reagents used are listed in table 9, appendix 1.2.

3.4 Characterization of iPSC and NPCs

To confirm the successful generation of iPSC and NPCs, in addition to morphological examinations, two fundamental characterization methods were employed. Evaluating the gene expression levels by qPCR and protein levels by immunocytochemistry (ICC). This is done to confirm the successful generation of the different cell types, as well as evaluating the efficiency of differentiation established by the protocols used. For the iPSCs, two additional methods were employed to check the conditions of the cells: germ layer differentiation and karyotyping. Germ layer differentiation was proceeded to confirm their pluripotency by looking at their abilities to differentiate into the three germ layers: mesoderm, endoderm and ectoderm. Karyotyping was performed to check the quality of the iPSCs by testing the cells for recurring karyotypic abnormalities in hPSCs.

3.4.1 qPCR

qPCR is used to measure the gene expression or mRNA synthesis of specific proteins in the cells (73). By isolating RNA from the cells, using reverse transcriptase to create complementary cDNA and performing a qPCR using the cDNA, the gene expression patterns of the specific cell type can be detected (73). These steps are further described in the following subsections.

3.4.1.1 RNA Isolation

Cells have been collected in the form of pellets and stored at -80 ºC, following the method described in section 3.2.1 for iPSCs and 3.3.4.2 for NPCs. The first step of the procedure is to isolate the RNA from these pellets. The RNA isolation was performed using the RNeasy Mini Kit (Qiagen). Reagents used are listed in table 16, appendix 1.3.

The cell pellets were loosened by tapping followed by the addition of a mix of 300 µL RTL buffer and 6 µL b-ME to each tube to dissolve the pellets completely. 300 µL 70% EtOH was added and mixed well before the solution was transferred to spin columns and centrifuged. 350 µL RW1 was added and centrifuged before adding 40 µL of DNase mix containing 5 µL DNase and 35 µL ROD buffer. This was incubated at room temperature for 15 minutes. 350 µL RW1 was added and centrifuged before the addition of 500 µL RPE buffer twice with centrifugation. 60 µL nuclease free H_2O was then added in the middle of the membrane and the RNA was eluted. The flow-through was collected and the amount of isolated RNA was measured using NanoDrop One^C (Thermo Fisher Scientific). The amounts of RNA obtained of iPSC and NPC are listed in table 17 for iPSCs and table 18 for NPCs, appendix 1.3.

3.4.1.2 cDNA Synthesis

The cDNA synthesis was performed using the High-Capacity cDNA Reverse Transcription Kit (Thermo Fisher Scientific). Reagents used are listed in table 19, appendix 1.3. The DNase mastermix was prepared according to table 20, appendix 1.3. RNA, H_2O and 10 µL of the mastermix was added to multiply tubes, to reach a final RNA concentration of 50 ng/ µL. Volumes of sample and H_2O are described in table 17 for iPSCs and table 18 for NPCs, appendix 1.3. The tubes were mixed using a vortex and spun down before being loaded into a thermal cycler (Bio-Rad T100 Thermal Cycler). The program used for the DNA synthesis is listed in table 21, appendix 1.3. The tubes containing cDNA were stored at 4°C after cDNA synthesis.

3.4.1.3 qPCR Set-Up

The experimental design used for the qPCR is described in figure 33, appendix 2.1. Reagents used are listed in table 22, appendix 1.3. A qPCR reaction master mix was prepared according to table 23, appendix 1.3. 3 µL of cDNA (1 ng/ µL) and 17 µL master mix were added to each well. The plate was sealed and mixed using a vortex before being spun down using the mini plate spinner from Labnet. Measurements were performed in a StepOnePlus Real-Time PCR System (Applied Biosystems) and data analyzed using the StepOne Software (Applied Biosystems). Primers used for the iPSC and NPC characterization is listed in table 24, appendix 1.3. Primers used for the detection of autophagic markers are listed in table 25, appendix 1.3.

3.4.2 Cell Imaging and Immunocytochemistry

Immunocytochemistry (ICC) is a technique used to confirm the location and expression of target proteins in a cell using specific antibodies (74). In principle, a primary antibody binds to the specific target protein on the cell, followed by binding of a secondary antibody tagged with a fluorescent dye, which recognizes and binds the primary antibody. If the antibodies recognize their respective targets, the fluorescent dye is activated, and the signal can be visualized under the microscope. Hence, proteins that are characteristic to specific cell types, and therefore named markers, are used to detect the generated cells (74). Reagents used are listed in table 26, appendix 1.4.

The cells were passaged onto Geltrex™ coated 48-well plates and cultured for 48 hours (see section 3.2. for iPSC passage). The medium was replaced with 200 µL of fresh 4% paraformaldehyde (PFA) in PBS and incubated at room temperature for 10 minutes. The PFA was aspirated, and the fixed cells were in 1 mL of PBS until staining was performed.
The cells were permeabilized with 200 µL 0,5% Triton-X/1X PBS for 15 minutes, followed by blocking using 150 µL of 5% BSA, 5% goat serum, 0,1% Triton-X/1X PBS for 30-45 minutes at room temperature. Primary antibodies diluted in blocking buffer according to manufacturer's instructions were added and incubated at room temperature for three hours, or overnight on a shaker at 4ºC. A list of primary antibodies used for iPSC and NPC immunocytochemistry is provided in table 27 for iPSC and table 28 for NPC, appendix 1.4.

Cells were washed three times using 500 µL PBS and a dilution of secondary antibodies diluted in PBS (300 µL) were added to the cells and incubated for 60 minutes at room temperature, protected from light. The cells were washed three times with PBS before incubation with 150 µL 4′,6-diamidino-2-phenylindole (DAPI) diluted in PBS for 10 minutes. Secondary antibodies and their dilutions used for iPSC and NPC immunocytochemistry is listed in table 29, appendix 1.4. The cells were washed three times with PBS and 500 µL of PBS were added to the cells upon visualization under an EVOS FL Auto microscope (Thermo Fisher Scientific). The obtained pictures were edited using "levels" in photoshop for better visualization.

3.4.3 Germ Layer Differentiation

A germ layer differentiation assay validates the pluripotency of iPSCs reprogrammed from fibroblasts by showing that the cell line can generate cell types of all three germ layers: mesoderm, endoderm and ectoderm. The results from the assay can also confirm the efficacy of the protocol in generating high-quality iPSCs. Reagents used for the germ layer differentiation are presented in table 30, appendix 1.5.

The STEMdiff™ Trilineage Differentiation Kit was used for germ layer differentiation. In addition, immunocytochemistry was performed using antibodies specific to the lineages to confirm pluripotency, as well as antibodies specific to one of the other lineages. Briefly, single-cell iPSCs were passaged to 24-well plates according to section 3.2, using cell densities listed in table 31, appendix 1.5. The 24-well plates were previously coated with Matrigel® (coating procedure section 3.1.2). The iPSCs were passaged in E8 (+) medium and cultured for 24 hours in the incubator (37°C). On day one, the E8 (+) was replaced by 1,5 mL STEMdiff™ Trilineage media for the different lineages. Full medium change was performed daily until day 5 for mesoderm and endoderm and day 7 for the ectoderm lineage. On day 5 and day 7, the cells were fixed and stained according to section 3.4.2. The primary antibodies used for the immunocytochemistry are listed in table 32 secondary in table 33, appendix 1.5.

3.4.4 Karyotyping

hiPSCs have the ability to acquire genetic irregularities during prolonged culture which can alter their behavior (75). The cells harboring these genetic irregularities can develop a selective advantage over cells with normal genetics and therefore lead to erroneous conclusions (76). To check for common genetic irregularities, the Genetic Analysis Kit by Stemcell Technologies were used. This kit contains nine primer-probe mixes that detects the majority of recurrent karyotypic abnormalities previously reported in cultured hPSCs. This kit is qPCR based and detect the copy number of the minimal critical regions of commonly mutated genetic loci through the use of double-quenched probes.

3.4.4.1 DNA Isolation

DNA from iPSC stored in the form of pellets at -80ºC was isolated using the DNeasy® Blood and Tissue kit by Qiagen. Reagents used for the karyotyping are listed in table 34, appendix 1.6. Cell pellets were thawed on ice and loosened by resuspension in 200 µL PBS. When the pellets were dissolved, 20 µL of proteinase K were added to digest the protein and inactivate proteins that might degrade the DNA (77). 200 µL of Buffer AL were added, and the tubes were vortexed and incubated at 56ºC for 10 minutes. After incubation, 200 µL of EtOH were added and the tubes were vortexed. The samples were then added to the spin column and centrifuged before adding 500 µL of buffer AW1 and 500 µL of buffer AW2 with centrifugation in between. The DNA was eluted by adding 200 µL Buffer AE and incubated for 1 minute. The column was centrifuged before repeating the same step again to ensure that all of the RNA is rinsed out of the membrane. The amount of isolated DNA was measured using NanoDrop One^{C} (Thermo Fisher Scientific). The amounts of DNA obtained from each sample are listed in table 35, appendix 1.6.

3.4.4.2 qPCR Preparation

Following the manufacturer's instructions, the qPCR master mix and Rox reference dye were prepared along with the genomic DNA control and primer-probe mixes. Eight clones were tested in triplicates for each of the 9 genes provided in the kit. For the samples, the calculated volumes equivalent to 300 ng of DNA was added to the tubes together with nuclease-free water to reach a final volume of 90 µL. A list of volumes used is found in table 35, appendix 1.6. The master mix and dye were then vortexed and 150 µL was added to each DNA sample and mixed by pipetting. According to the number of samples, the volume of primer-probes and nuclease-free water were calculated. Calculations are found in appendix 1.6.

Once all of the reagents were prepared, the layout of the qPCR plate was planned. The layout is provided in figure 34, appendix 2.2. 8 µL of each sample was loaded onto the qPCR plate before loading 2 µL of the primer-probe mix. The plate was read using StepOnePlus Real-Time PCR System (Applied Biosystems). The data was obtained using the StepOne Software (Applied Biosystems). For the data analysis, the Genetic Analysis app provided by Stemcell technologies were used following the instructions provided.
Link: https://stemcell.shinyapps.io/psc_genetic_analysis_app/.

3.5 Cell Viability Assay and Proliferation Assay

Cell viability and proliferation assays were performed to measure the proportion of live cells within a population after treatment of the UPS inhibitors MG132, Bortezomib and Expoxomicin. Based on the viability after treatment, a proliferation assay will be performed to assess the cell survival by providing a readout on the number of actively dividing cells. Both viability and proliferation will be measured using the PrestoBlue™ principle in which the active ingredient resazurin is reduced to resorufin. Resazurin is a cell-permeable compound that is blue in color and non-fluorescent. When the compound enters the live cells, the cellular environment reduces the resazurin to the highly fluorescent red compound resorufin. This results in a color change that can be detected using absorbance-based plate readers (78).

Several viability assays were first performed to delineate the optimal drug concentrations for a time-course experiment (proliferation assay). At this stage, cells were platted and incubated overnight prior to exposure with different drug concentrations for 24 hours. For the proliferation assay, the cell survival was measured after 0 hours, 24 hours, 48 hours and 72 hours using specific drug concentrations based on the viability assays. The set-up for the viability assay is presented in figure 35, appendix 2.3; proliferation assay figure 36, appendix 2.4.

5000 NPCs at passage 3 or 4 (generated using protocol 1) were passaged to each well of the 96-well plate, following the protocol described in section 3.3.1. The cells were cultured in NPC medium for 24 hours before the addition of drugs. The vehicle controls were treated with DMSO using the highest drug concentration. PrestoBlue™ cell viability reagent was added to the wells according to the different time points and incubated at 37°C for 30 minutes. FLUOstar Omega microplate reader (BMG Labtech) was used to measure cell death and data was analyzed by the MARS Data Analysis Software (BMG Labtech). Reagents used for the viability assays are listed in table 36, appendix 1.7.

3.6 Evaluation of Autophagic flux by Western Blot

Autophagic activity will be measured by detecting the levels of LC3 and p62 in NPCs with and without a treatment using the autophagic inhibitor Bafilomycin A1. Bafilomycin A1 inhibits the formation of the autolysosome and thereby inhibits the degradation of LC3 and p62 bound to the autophagosome membrane (12).

3.6.1 Bafilomycin Treatment and Cell Collection

NPCs at passage 2 (generated using protocol 1) were passaged onto 6-well plates with a cell density of 1,0-1,5 x 10^6 cells/cm^2 and incubated for 1 day following section 3.3.1. On day 3, the cells were treated with 100 nM Bafilomycin A1, and the vehicle controls with 100 nM ethanol. The cells were collected after 6 hours of incubation (37°C) by washing with 1 mL PBS before dissociation using 1 mL Accutase for 5 minutes at 37°C, and subsequent collection to a 15 mL tube containing 5 mL DMEM/F12 and centrifuged at 1500 rpm for 5 minutes. Cells were washed twice with 5 mL PBS and transferred to an Eppendorf tube and centrifuged before removing the supernatant and freezing them at -80°C. Reagents used for the treatment and collection of cells are listed in table 37, appendix 1.8.

3.6.2 Protein Extraction and Measurement

A master mix containing several protease inhibitors, phosphatase inhibitors, DNases and RNases was made using the reagents and volumes listed in table 38, appendix 1.8. The cell pellets were thawed on ice and a volume of the master mix was added to each cell pellet depending on the size. As a reference, 60 µL of the master mix was used for 1 000 000 cells. After cell resuspension by pipetting with lysis buffer, the tubes were placed on a roller at 4°C for 1 hour for lysis and nucleic acid degradation. Protein concentration was measured in triplicates using the BioRad protein assay reagent, according to manufactures instructions and absorbance was measured at 595 nm in a spectrophotometer (Shimadzu). Protein concentrations obtained are listed in table 39, appendix 1.8.

3.6.3 Western Blotting

50 µg of protein in LDS NuPAGE sample buffer (Invitrogen) and 100 µM DTT were heated at 70°C for 10 minutes before loading into a pre-cast NuPAGE 4-12% Bis-Tris gel with 10 wells. MES-SDS buffer was used to resolve the low molecular weight proteins, such as LC3-I/II. The run was set for 45 minutes at 200 V. Proteins were then transferred onto a Trans-blot mini PVDF membrane using the Trans-Blot Turbo Transfer System. After blotting, the membrane was incubated in a blocking buffer containing 5% fat-free milk in PBS-T for 1 hour and incubated overnight in the primary antibodies in 5% milk in PBS-T at 4°C on a shaker. The membrane was then washed three times with PBS-T, 10 minutes each, on a shaker and incubated with the secondary antibodies for 1 hour, protected from light. The membrane was then washed three times in PBS-T for 10 minutes each on a shaker before rinsing with PBS and

drying it. The images were acquired using the Odyssey Imaging System (LiCOR Biosciences). Chemicals, primary and secondary antibodies and respective dilutions are described in table 40, 41 and 42, appendix 1.8.

3.7 Cerebral Organoids

3.7.1 Generating Cerebral Organoids

Cerebral organoids were generated following protocols developed by Lancaster *et al.* (66) and Mariani J *et al* with minor modifications (79). A timeline of the generation is presented in figure 12.

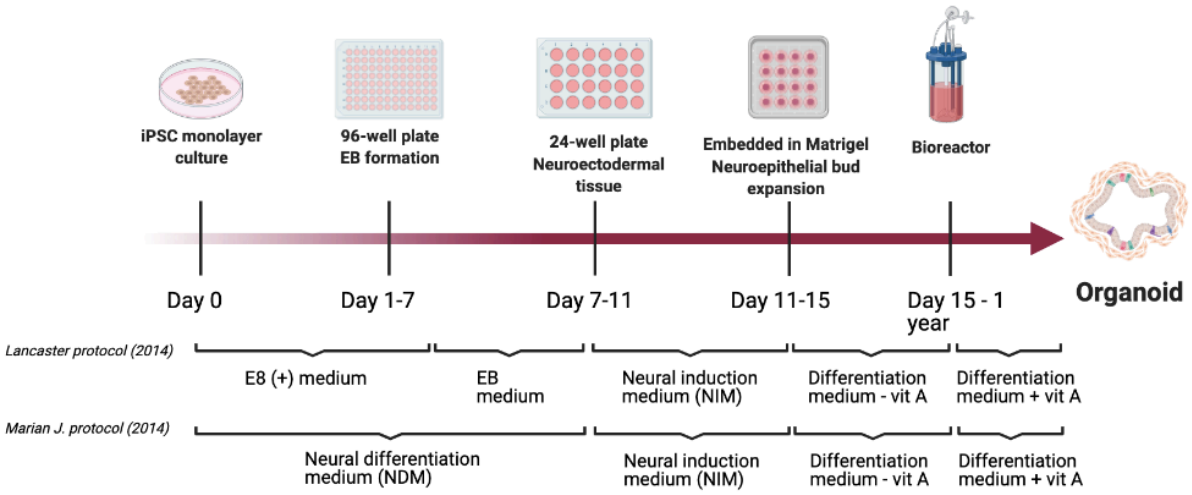

Figure 12: A timeline on the generation of cerebral organoids based on Lancaster et al. (66) and Mariani J. et al (79). Mediums used are shown for each timepoint of the generation. Figure created using Biorender.com.

hiPSCs are first passaged as single cells to ultra-low attachment 96-well plates (Costar) to allow reaggregation of the cells to embryoid bodies (66). 9000 cells were seeded in each of the wells with 150 µL medium following section 3.3.1. The 96-well plates were then centrifuged at 100 x g for 5 minutes before placing them in the incubator (37ºC). Two different approaches were used to grow the EBs. In the first approach, E8 (+) medium with 10 µM Rock inhibitor was used to culture the cells for the first 24 hours. On day 1, the medium was replaced with EB medium which is developed by Lancaster *et al* (66). Reagents and volumes for the EB medium are listed in table 43, appendix 1.9. The medium was changed every other day from day 2 to 7. The second approach was using the neural differentiation medium (NDM) developed by Mariani J. *et al.* directly from the start during the passage of iPSCs and to day 7 of EB culture (79). Full medium change was performed every other day. Reagents and volumes used for the NDM medium are presented in table 44, appendix 1.9.

After 7 days of culture in the 96-well plates, when the EBs were about 500-600 µm in diameter with smooth edges, cells were transferred to ultra-low attachment 24-well plates (Corning). Here, the newly formed EBs are subjected to a neural induction medium (NIM), a medium that only supports the growth neuroectoderm (66). The reagents and volumes used to prepare the NIM are listed in table 45, appendix 1.9. Six EBs were gently transferred into one well with 500 µL NIM medium by using a wide-bore pipette, and cultured for 4-5 days. The EBs were fed with an additional 500 µL of NIM after 48 hours.

The neuroectodermal tissues were transferred to Matrigel® to promote the outgrowth of neuroepithelial buds (66). This is done when the EBs have a bright outer edge. Two different approaches were used for this step of the generation. One approach was to follow Lancaster's protocol where one Matrigel® droplet was reserved for one EB (66). This was done for the biggest EBs that were generated. Parafilm was layered on an empty tip tray and pressed down to make dimples in the parafilm and placed into a 100 mm tissue culture dish. One EB was transferred onto each of the dimples of the parafilm. The medium was aspirated and 35 µL of Matrigel® was placed onto the tissues to cover them before incubation (37º) for 20-30 minutes. When the Matrigel® solidified, the embedded EBs were separated from the parafilm by flushing the differentiation medium vigorously onto the parafilm. 10 mL of differentiation medium without vitamin A was added to each 100 mm culture dish and set in the incubator (37º). Reagents and volumes used to make the differentiation medium are listed in table 46, appendix 1.9. The tissues were incubated for 4 days, where medium change was performed every other day.

The second approach for embedding the EBs in the Matrigel® was based on Qian *et al.* (80). The EBs were transferred from the 24-well plate into a 15 mL falcon tube using a 5 mL pipette. After the EBs settled at the bottom, the excess media was aspirated and 1 mL of differentiation medium without vitamin A was added. 100 µL of Matrigel® was transferred to an Eppendorf tube before taking 66,7 µL of the differentiation medium with approximately 20-30 EBs and transferring it to the Matrigel®. The EBs, medium and Matrigel® were mixed by pipetting gently and transferred to a low-attachment 6-well plate (Sarstedt & Co). The plate was incubated (37ºC) for 30 minutes to solidify the Matrigel®. 3 mL medium was added to the wells followed by incubation for 4 days, and a full medium change was performed every other day.

In the final step of the protocol, neuroectodermal tissues are transferred to a spinning bioreactor or an orbital shaking plate. This step promotes nutrient and oxygen exchange which will allow further growth and development into defined brain regions (66). The embedded tissues were transferred using a cut 5 mL pipette into 15 mL tubes. Then the tissues were pipetted up and down to try to break the Matrigel® before adding them into either a bioreactor or orbital shaker pre-filled with differentiation medium containing vitamin A. Reagents and volumes used to make the differentiation medium with vitamin A is listed in table 46, appendix 1.9. The medium was changed every 7 days in the bioreactor and every 3-4 days in the orbital shaker.

3.7.2 Preparation of Cerebral Organoids for Cryosectioning and Immunohistochemistry

To visualize the morphology and characterize the cerebral organoids, immunohistochemistry with the markers Sox2, Tuj1, Nestin and Pax6 was performed. First, the organoids must be prepared by embedding in a matrix and cryosectioned onto glass slides to successfully visualize the tissue. Thus, organoids were collected in Eppendorf tubes and washed twice with PBS before being fixed by adding 4% paraformaldehyde in PBS containing 1% sucrose and left to incubate at 4°C overnight. Then, organoids were washed with PBS and incubated overnight at 4°C in 15% sucrose in PBS.

Embedding was performed by first covering the bottom of small plastic chambers with OCT compound and setting them in the -80°C freezer to solidify. Meanwhile, the organoids were transferred to 24-well plates and 700 µL Erythrosine dye were added to each well and left for a few seconds to stain the organoids before removal. The organoids were then washed twice using PBS and placed onto the OCT covered the bottom of the chambers before being covered with more OCT compound and stored in the -80 °C freezer, ready for cryosectioning. Reagents used for the preparation is listed in table 47, appendix 1.9.

3.7.3 Cryosectioning and Immunohistochemistry of Cerebral Organoids

The embedded cerebral organoids were cryosectioned using a Leica cryostate. The organoids were sectioned using a thickness between 14 and 20 µm before being placed on SuperFrost Ultra Plus™ Adhesion Slides (Thermo Fisher Scientific). Organoids were grown for 2 weeks, 1 month and 2 months in the bioreactor were used for the immunohistochemistry. The glass slides were stored at -20ºC.

Upon immunostaining, the slides were dried at room temperature for about 5 minutes before drawing circles around the sections using a hydrophobic Dako pen (Dako Denmark). This is done to create a hydrophobic barrier around the sections. PBS-T was applied for 10 minutes before blocking using 100 µL blocking buffer consisting of 5% BSA, 5% goat gut serum, 0,1% Triton-X/1X PBS for 1 hour. The slides were then exposed to the primary antibodies diluted in 100 µL blocking buffer consisting of 0.5% BSA, 0.5% goat gut serum, 0.1% Triton-X/1X PBS overnight at 4ºC.

The next day, the slides were washed 3 times using PBS. The slides were then exposed to the secondary antibodies for 1 hour at room temperature. After incubation, the sections were washed three times using PBS-T for 10 minutes and once using PBS for 10 minutes. The slides were then rinsed using ultra-pure water before drying the slides at room temperature. One drop of ProLong Gold antifade reagent with DAPI was applied to each section before applying a cover glass on top. The organoids were visualized using EVOS FL Auto microscope. Reagents used are listed in table 48, appendix 1.9. A list of primary and secondary antibodies used for the immunohistochemistry is found in table 49 and 50, appendix 1.9.

4. Results and Discussion

4.1 Characterization of iPSC

The goal of the first part of the project was to culture, characterize and evaluate the quality of the given iPSCs clones prior to differentiation to NPCs, FB neurons and cerebral organoids. The iPSC characterization was performed using four methodologies: (i) qPCR for detection of gene expression of pluripotent genes; (ii) ICC for detection of pluripotent markers at protein level; (iii) germ layer differentiation to evaluate the cells abilities to differentiate into the three lineages, and (iv) karyotyping to test the cells for recurring karyotypic abnormalities. The following sections present the results from the characterization and quality control of iPSCs using the methods mentioned above.

4.1.1 Cell Morphology of iPSC

iPSCs quality was first evaluated by examining their morphology. As expected, all iPSC clones displayed morphological features similar to embryonic stem cells, i.e., round shape, large nucleus and small cytoplasm. Figure 13 shows tightly packed, compact iPSCs colonies with distinct borders and well-defined edges both for control and patient cells, with no signs of differentiation. All clones showed similar morphology, so control AGc1 and patient Tc3 cells were chosen to represent iPSC morphological features figure 13.

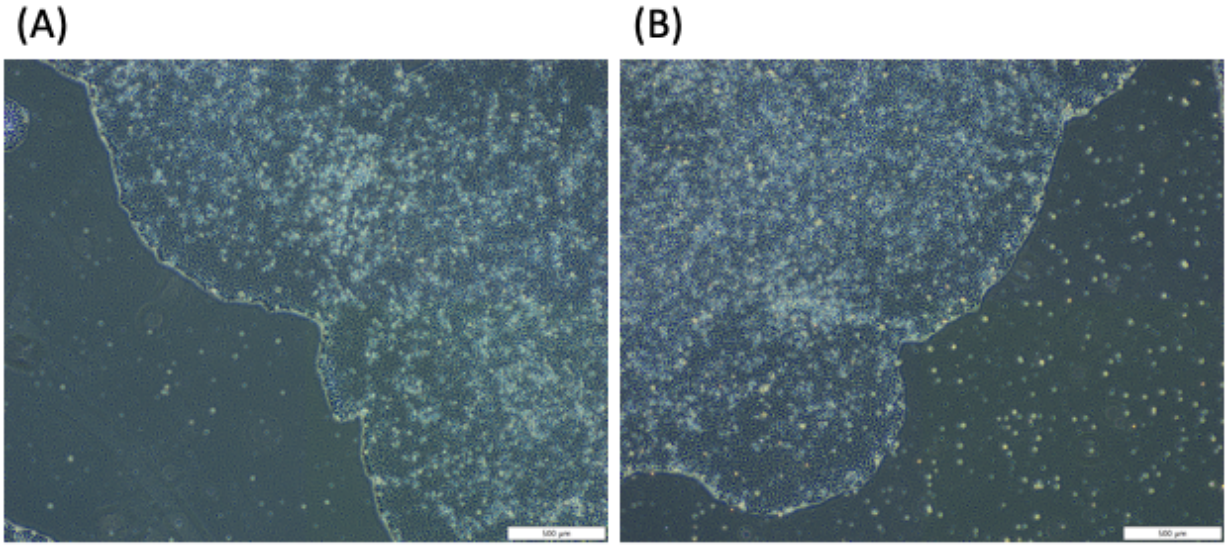

Figure 13: Phase-contrast microscopic pictures of cultured iPSC ready for passage on day 5. Scale bar: 500 µm. (A) Control AGc1. (B) Patient Tc3.

4.1.2 qPCR of Pluripotent Gene Expression of iPSC

To further confirm the pluripotency of iPSC, a qPCR experiment was conducted to evaluate the expression levels of pluripotent markers Nanog, Oct4 and Sox2.

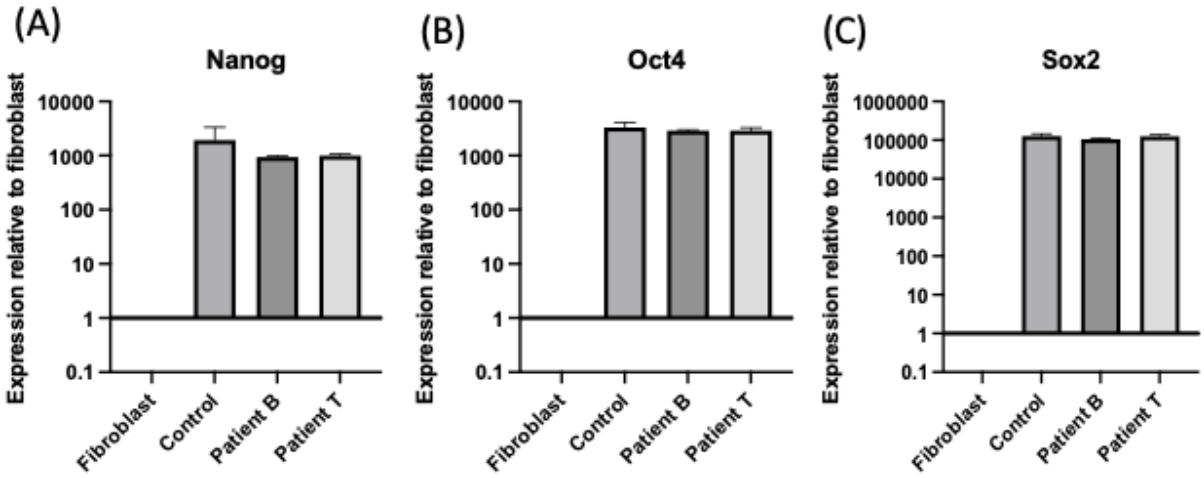

Figure 14: Expression levels of pluripotent marker genes (A) Nanog (B) Oct4 (C) Sox2 relative to fibroblast. Error bars represent the standard deviation of at least 2 independent assays, each with 3 technical replicates.

According to figure 14, higher expression (1000-to-100 000-fold) of all the pluripotent genes was detected in iPSCs compared to parental fibroblast, indicating that each fibroblasts clone has successfully been reprogrammed to iPSCs.

4.1.3 Immunocytochemical staining of iPSC

To evaluate the expression of the pluripotency markers at a protein level, ICC was conducted for Nanog, SSEA4 and Oct4. Not surprisingly, the ICC data confirm the expression of the three pluripotent markers in the iPSCs samples (figure 15). Similar results were obtained for all the other clones, therefore, only control AGc1 and Patient Bc9 are shown for simplicity.

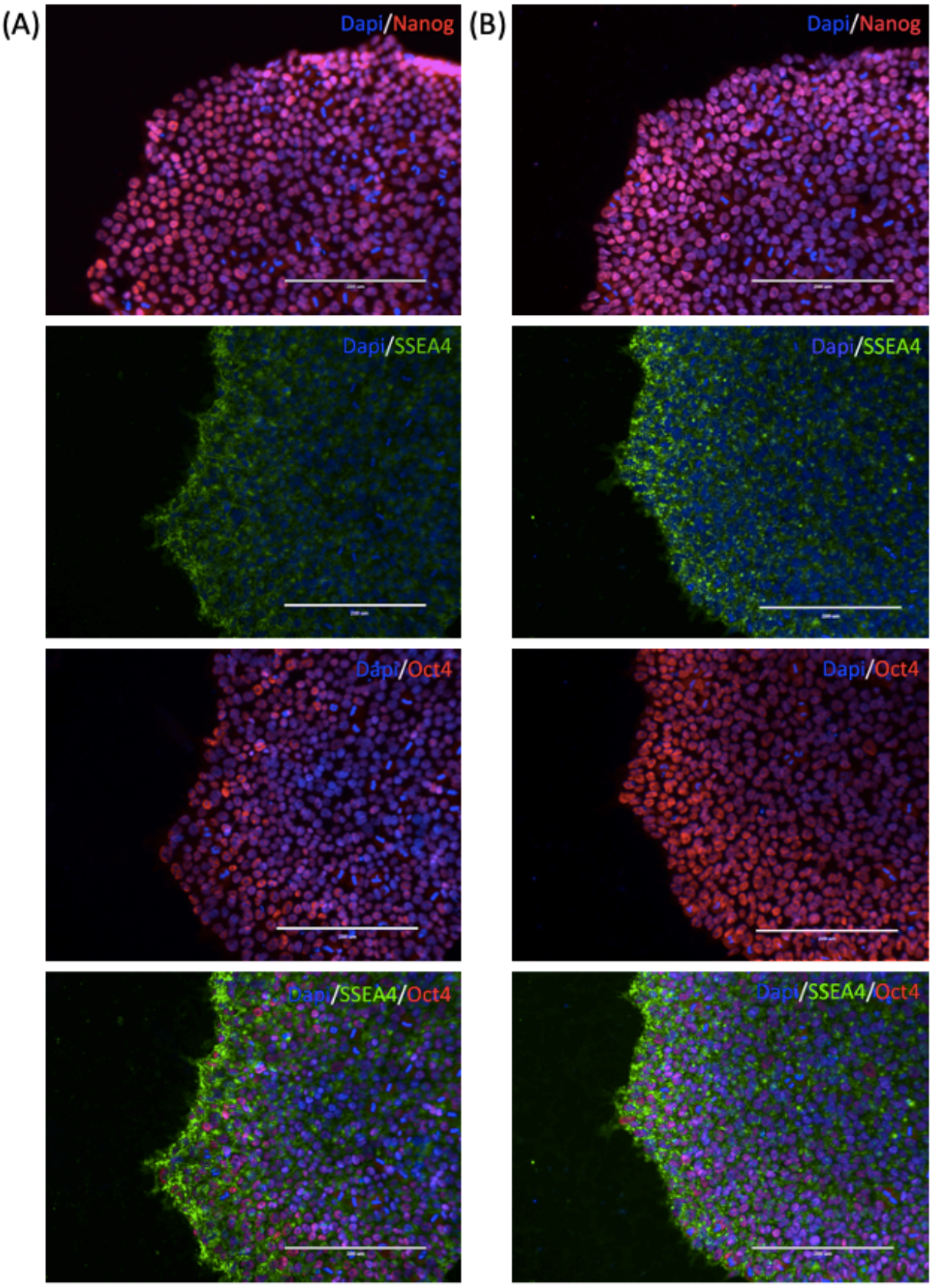

Figure 15: Characterization of the iPSC pluripotency markers Nanog, SSEA4 and Oct4. In all pictures cell nuclei were stained by DAPI (blue). Scale bar: 200 µm. (A) Control AGc1. (B) Patient Bc9. First row: visualization of Nanog (red). Second row: visualization of SSEA4 (green). Third row: visualization of Oct4 (red). Fourth row: double staining of SSEA4 (green) and Oct4 (red).

4.1.4 Germ Layer Differentiation

In addition to ICC of standard pluripotent markers, ICC staining of markers for early differentiation of each germ layer (mesoderm, ectoderm and endoderm) was performed to evaluate whether iPSCs could successfully differentiate to the three germ layers.

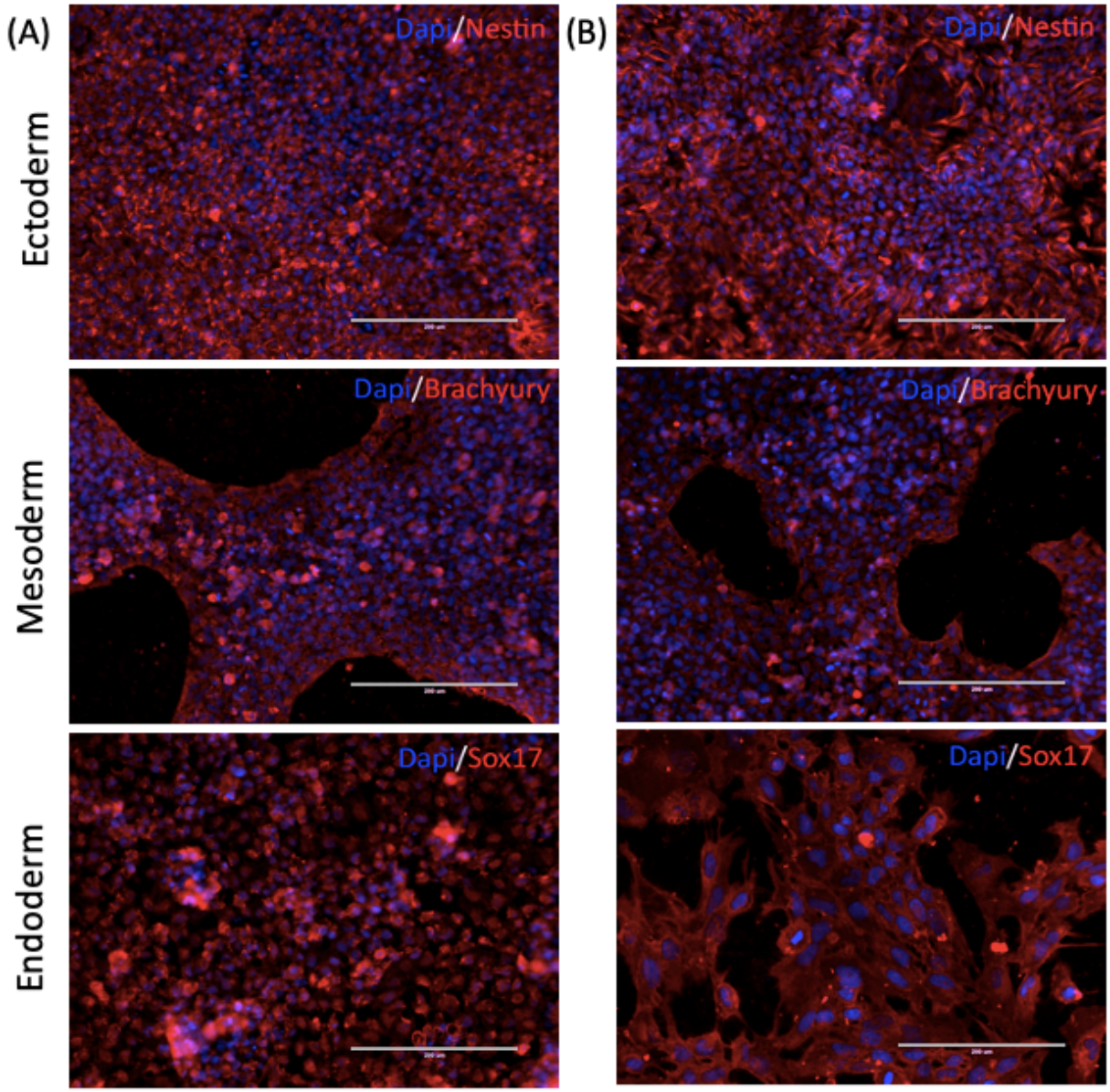

Figure 16: Characterization of germ layer differentiation from iPSC by ICC using specific markers. Cell nuclei were stained with DAPI (blue). Scale bar: 200 µm. (A) Control AGc1. (B) Patient Bc4. First row: Ectodermal cells expressing Nestin. Second row: Mesodermal cells expressing Brachyury. Third row: Endodermal cells expressing Sox17.

As shown in figure 16 (A and B), iPSC directed to ectodermal differentiation expressed the early ectodermal marker Nestin. Similarly, figure 16 (C and D) shows cells expressing the mesodermal marker Brachyury, indicating successful differentiation of IPSC into mesodermal cells. Finally, figure 16 (E and F) shows an expression of the endodermal marker Sox17,

indicating successful differentiation of iPSC into endoderm. Altogether, these data confirm the ability of iPSC in differentiating cells from all three germ layers. As all clones demonstrated similar expression profiles, cells from one control and one patient were selected for illustrative purposes.

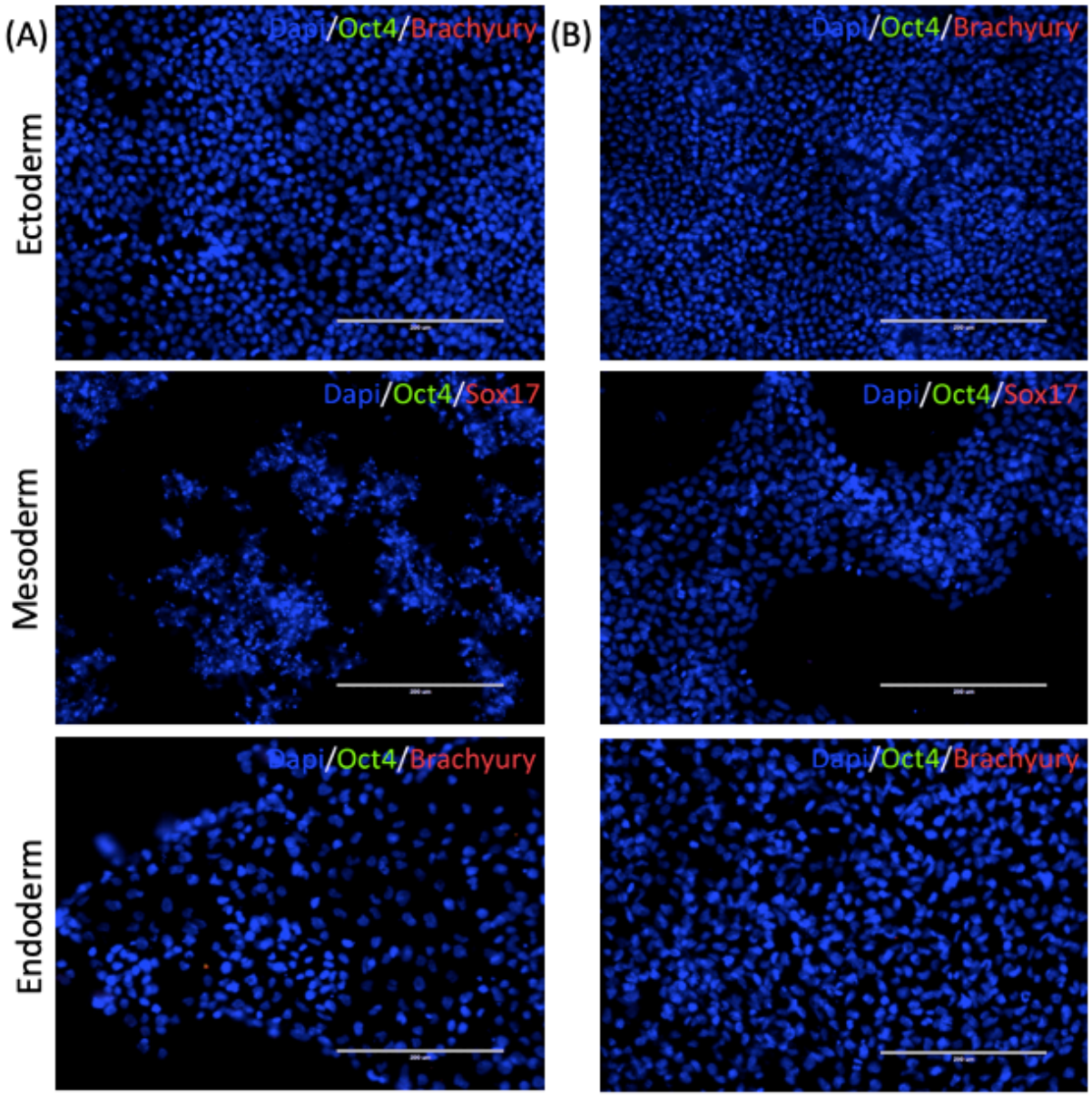

Figure 17: Quality control of germ layer differentiation by ICC. All cells were counterstained with DAPI (blue) for nuclei visualization. Scale bar: 200 µm. (A) Control AGc1. (B) Patient Bc4. First row: Ectodermal cells exposed to the pluripotent marker Oct4 and the mesodermal marker Brachyury. Second row: Mesodermal cells exposed to the pluripotent marker Oct4 and the endodermal marker Sox17. Third row: Endodermal cells exposed to the pluripotent marker Oct4 and the endodermal marker Sox17.

To further confirm that cells have successfully differentiated from the pluripotent state, each germ layer was exposed to the pluripotent marker Oct4. Each germ layer was also exposed to an antibody specific for another germ layer to ensure that the cells have not differentiated into any of the other lineages.

Notably, the pluripotent marker Oct4 was not detected in the generated mesoderm, endoderm and ectoderm cells (figure 17), indicating that these cells are no longer iPSC. Moreover, the ectodermal cells did not express the mesodermal marker Brachyury. The mesodermal cells did not express the endodermal marker Sox17, and the endodermal cells did not express the mesodermal marker Brachyury. This confirms that iPSC differentiation was successful and specific for each of the three germ layers.

4.1.5 Karyotyping

The goal of this experiment was to evaluate the quality of the iPSC by screening for the most common karyotypic abnormalities reported in the long-term culturing of hiPSCs. Figure 18 displays bar plots for each locus tested. According to the instructions of Stemcell Technologies, karyotypic abnormalities are detected when 20-30% of the culture harbor the genetic abnormality. The karyotyping analysis did not reveal any significant change in the copy number, therefore no abnormalities, in the tested gene loci.

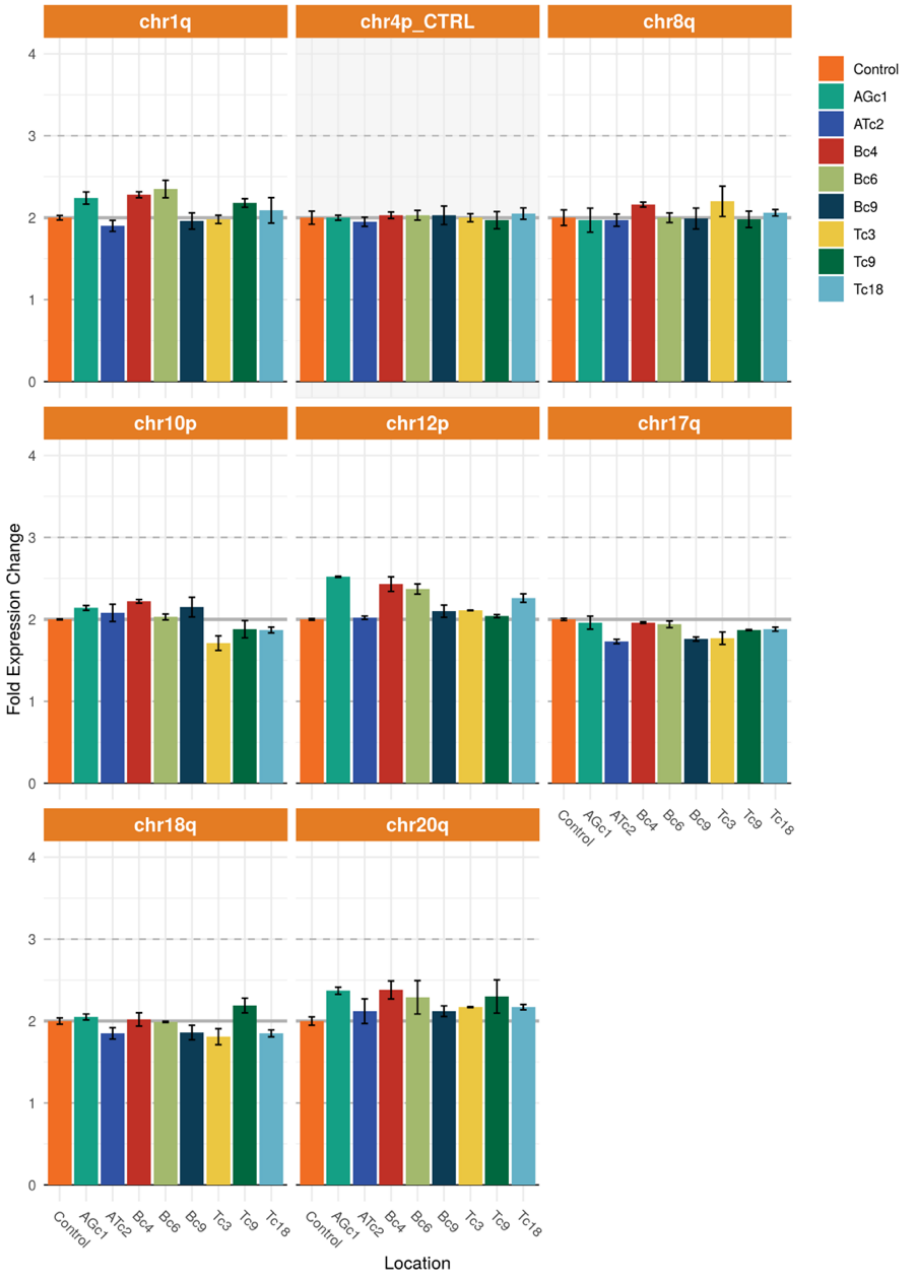

Figure 18: Karyotyping analysis of iPSC clones used in this study. Each plot represents one locus where the y-axis represents the copy number and the x-axis each sample. The control locus chr4 is shaded for quick identification. Data was obtained using the Genetic Analysis App from Stemcell Technologies.

Taken together, these experiments revealed that the cells generated by reprogramming of fibroblasts derived from healthy control and patients carrying UCHL1-mutations are indeed pure iPSC populations, demonstrating the typical morphological and molecular features extensively reported for this cell type. Furthermore, karyotyping analysis, performed as a quality control test to investigate potential alterations in chromosomal copy number, indicate that the generated iPSC displays normal karyotyping. Importantly, the morphology of the iPSCs was strictly controlled throughout the project and differentiated cells (normally less than 10%) were removed by scraping before passaging the iPSCs further.

4.2 Characterization of NPC

In order to study the impact of UCHL1 dysfunction in neurodevelopment and neuroprotection via alterations in the ALP, the iPSCs were further differentiated to the neural lineage. The generated NPCs were characterized based on morphology, qPCR evaluation of gene expression of neural progenitor markers, followed by an analysis of protein expression levels of neural progenitor markers by ICC.

4.2.1 Cell Morphology of NPC

Initially, NPCs were generated using a procedure described by Li *et al* (72), with minor modifications (figure 9). This procedure generated healthy NPCs, which grew as expected until passage 4. Figure 19 (A and B) displays a confluent layer of NPCs with a low amount of cell death. Around passage 4-5, however, a progressive increase in the number of dead cells was repeatedly observed. This occurred for all clones, both during cell culture and after thawing cells at passage 4 to resume cell culture. None of the clones survived further than passage 5, and some died at earlier time points. Normally, NPCs reach a passage number of at least 10 before accumulating any karyotypic abnormalities (81).

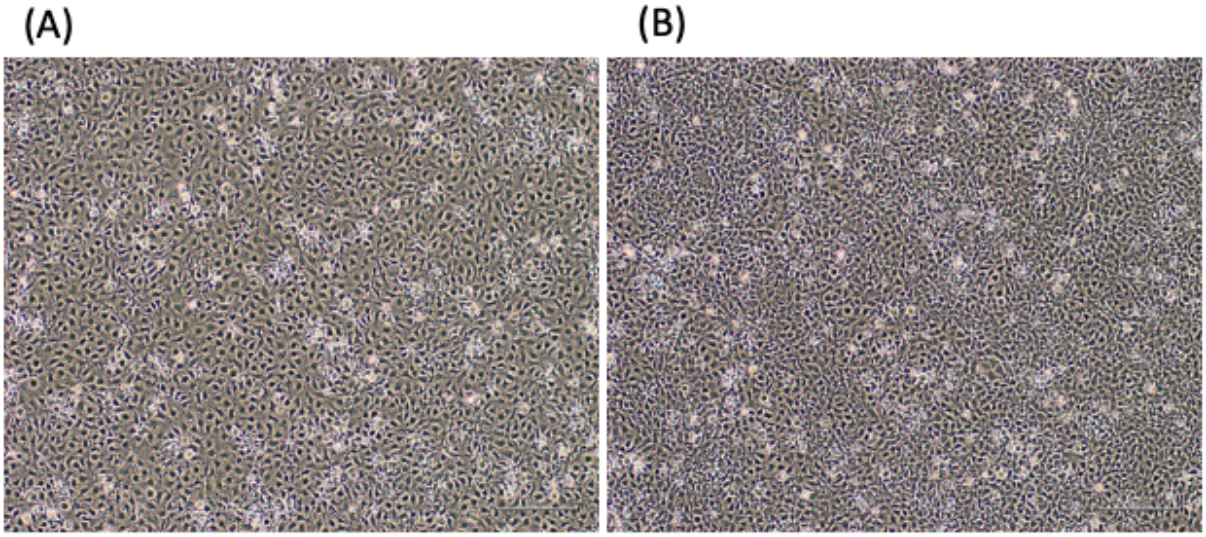

Figure 19: Morphology of healthy NPC cells obtained from culture using the monolayer culture protocol modified from Li et al. (protocol 1, see also figure 9). Scale bar: 200 µm. (A) Control AGc1 at passage 4, day 5. (B) Patient Bc4 at passage 4, day 5.

Notably, as cell death was initially observed from the middle of the wells, suggesting that high cell density could be a major cause, several attempts in culturing cells at different densities were performed. However, cell death also occurred when culturing NPC with lower cell numbers. Both Geltrex™ and Poly-L-Ornithine/Laminin coatings were used for the culture without any significant changes in cell survival.

In an attempt to produce healthy and long-lasting NPCs, which could be further differentiated to FB neurons, a second protocol was employed. A commercial, NPC monolayer protocol developed by Stemcell Technologies was employed, along with their commercial medium (figure 10). In addition, instead of using the clones described when executing Protocol 1 (control clones: AGc1 and AGc6; patient clones Bc4, Bc9 and Tc3), new iPSC lines were added from control (AGc1, ATc2) and patients (Bc4, Bc6, Tc3 and Tc18) fibroblasts. This was performed to exclude potential clonal differences that could be related to poor cell survival. Indeed, variations in clonal properties, such as inherent or acquired genetic differences, could influence iPSC differentiation or survival of NPC.

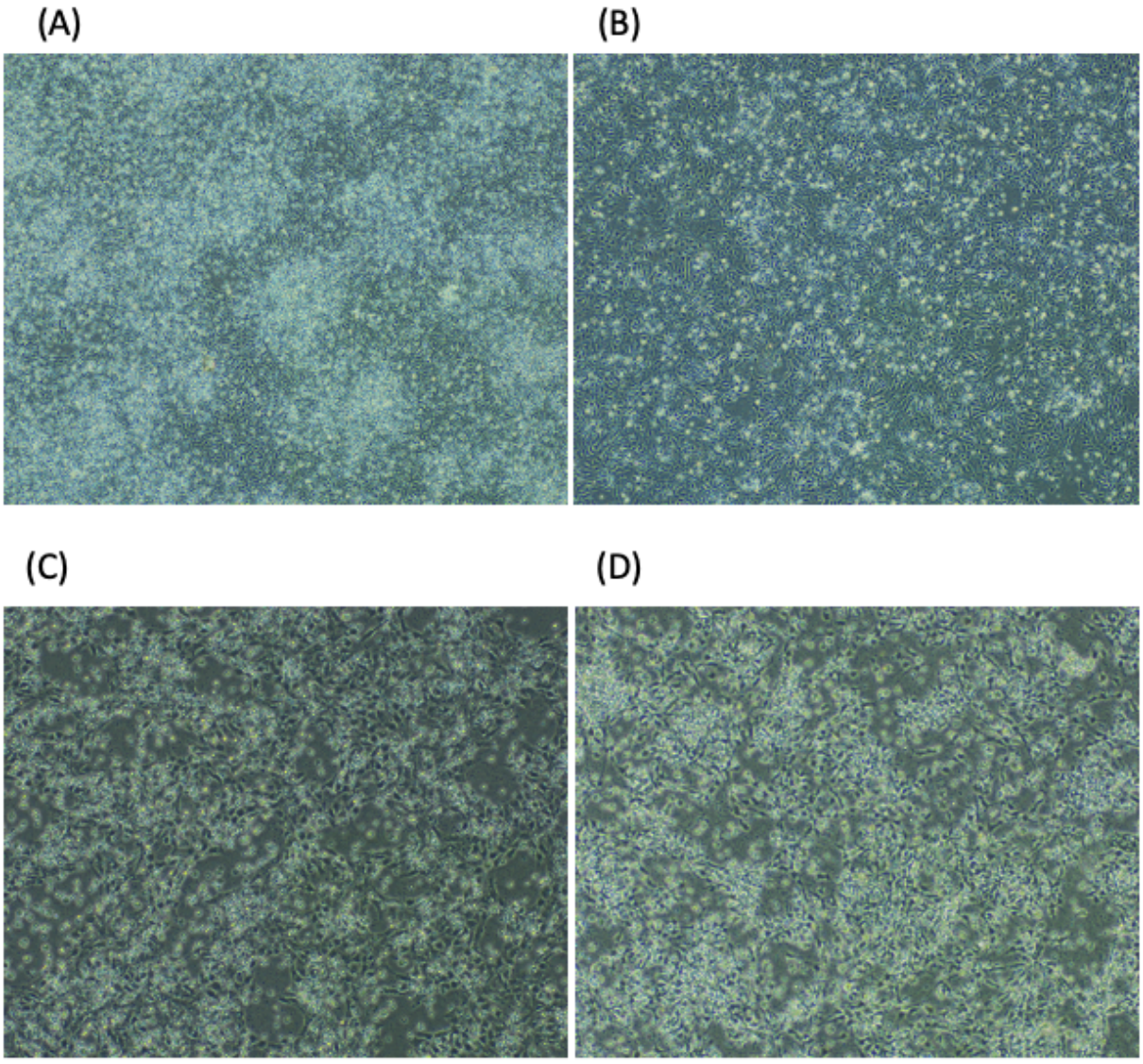

Figure 20: Morphology of NPC cells obtained from culture using the monolayer culture protocol from Stemcell Technologies. NPC derived from (A) control ATc2 at passage 0, day 3 and (B) patient Bc4 at passage 0, day 3, as well as dying NPC derived from (C) control ATc2 at passage 1, day 3 and (D) patient Bc4 at passage 1, day 5, are illustrated.

Figure 20 (A and B) displays the morphology of both control and patient cells at passage 0. Although a high number of dead cells was observed in the control, a confluent monolayer of healthy cells was observed underneath the dead cells. Bc4 cells showed improved survival compared to control and typical NPC morphology at passage 0. At passage 1, however, a rapid increase in the number of dead cells was observed (figure 20, C and D). Several approaches were conducted to improve the culturing conditions aiming at reducing the cell death rate, based on the troubleshooting guide provided by Stemcell Technologies. According to Stemcell Technologies, the first step would be to perform quality control experiments of the iPSC, such as checking for common genetic abnormalities using karyotyping, as well as their ability to differentiate into the three germ layers. Both quality control experiments were executed (figure 16, 17 and 18) and did not reveal any signs of abnormalities or poor iPSC quality.

Since the monolayer appeared as overcrowded, the next suggestion was to decrease the number of cells seeded onto the 6-well plates, as well as changing the length of the cultivation. However, none of the modifications overcame the high rate of cell death observed at early time-points. In addition to trying different cell densities for each of the three NPC protocols, we explored different plate coatings, including Geltrex^{TM} and Poly-L-Ornithine/Laminin coating, as well as Matrigel® for the monolayer protocol developed by Stemcell Technologies. However, differences in coating had a minor impact in cell growth and is most likely not the cause of the cell death. It was also ensured that we used 10 μM ROCK inhibitor for the first 24 hours as the troubleshooting guide stated if cell death in passage 1 was observed. With this protocol, NPCs did not survive further than passage 1. Similar features displayed in figure 20 were observed for all the other clones.

As the second trial of generating NPC failed, yet a third protocol was conducted with the same clones described for Protocol 2. Here, an EB-based protocol developed by Stemcell Technologies was attempted (figure 11). This procedure was suggested to be more robust than the monolayer protocol, improving the likelihood of generating healthy NPC cultures.

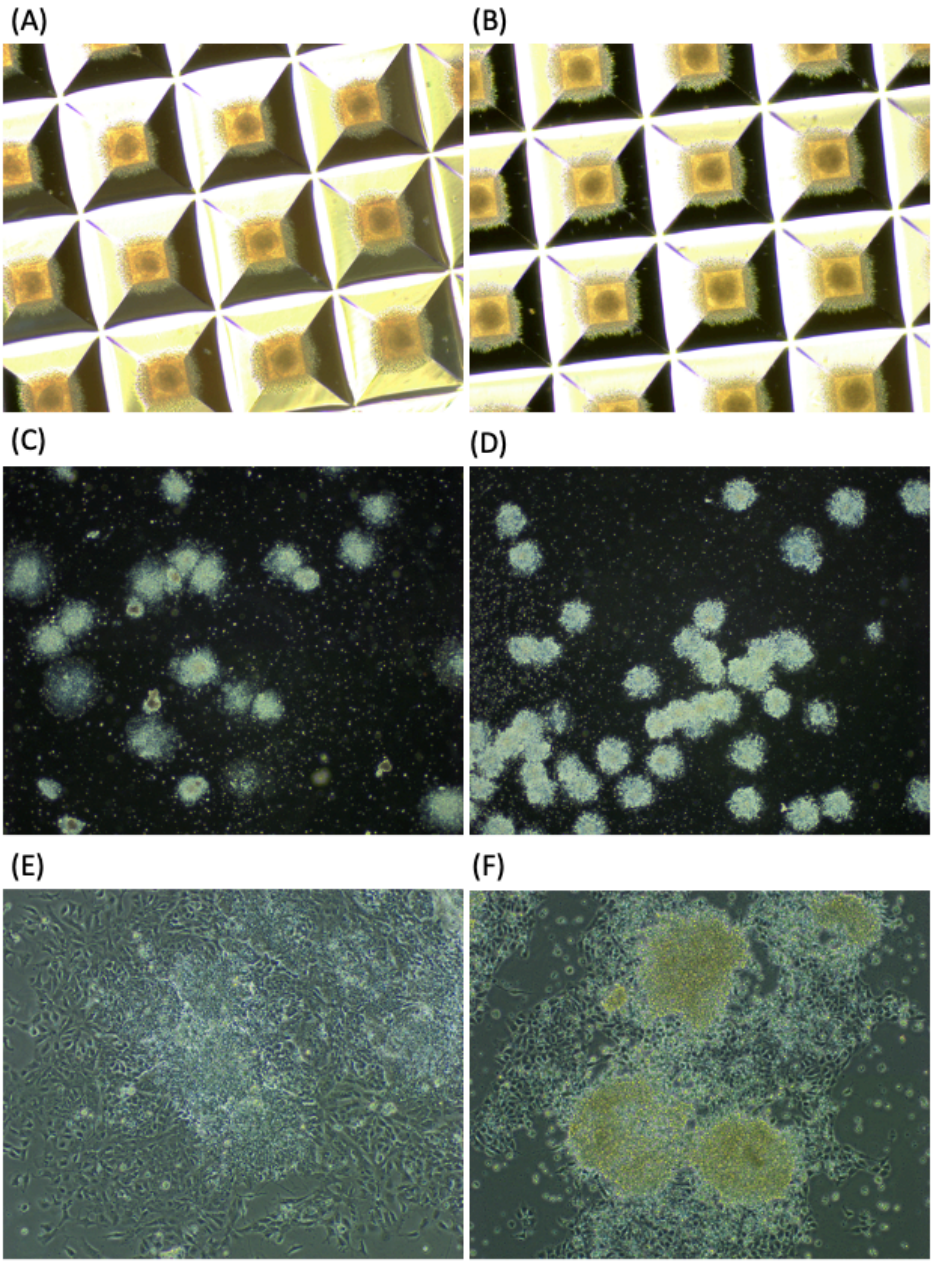

Figure 21: Early stages of iPSC differentiation to NPC using the embryoid body culture protocol from Stemcell Technologies. Cells were derived from: (A) Control ATc2 on day 1 cultured in Aggrewell^{TM}800. (B) Patient Tc18 on day 1 cultured in Aggrewell^{TM}800. (C) Control ATc2 on day 6 after transfer of EBs to 6-well plates. (D) Patient Tc18 on day 6 after transfer of EBs to 6-well plates. (E) Control ATc2 on day 8 in the 6-well plates. (F) Patient Tc18 on day 8 in the 6-well plates.

Figure 21 displays critical time points for differentiation of iPSC to NPC using the embryoid protocol. Figure 21 (A and B) shows one embryoid body in each Aggrewell^{TM} on day 1 after the iPSC passage. The EBs look healthy with a clear, defined border. However, after replating the cells onto the 6-well plates (figure 21, C and D) the required number of neural rosettes of $\geq$ 75% was not obtained. Control clone ATc2 had a successful generation of a few neural rosettes (figure 21, E) but not a sufficient number of NPCs after rosette selection. Similar results were obtained with other clones. Hence, the generation of NPC via the EB protocol also failed.

As the NPCs generated by Protocol 1 survived up to passage 5, they were employed as models to investigate biological processes at NPC level. The following sections will provide data on further characterization and functional assays performed with these cells.

4.2.2 qPCR for Characterization of NPC

Quantitative PCR was conducted to detect the gene expression of the neural progenitor markers Nestin, Pax6, DcX and Sox1 in NPCs at passage 4 obtained following the protocol by Li *et al.* (72). The pluripotent marker Nanog was also tested to confirm that the cells have differentiated from the pluripotent state.

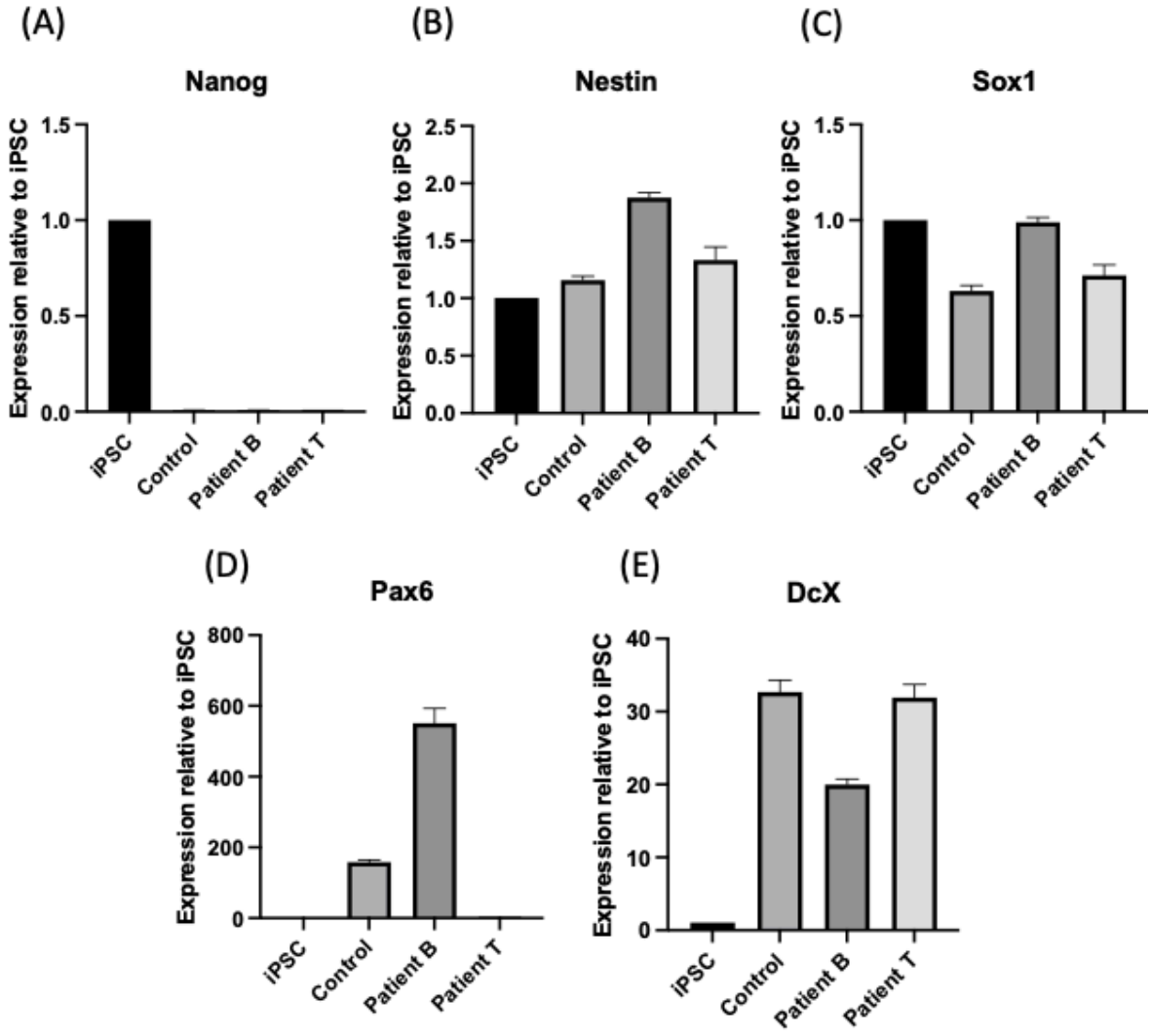

Figure 22: Expression levels of pluripotent marker gene (A) Nanog and the neural markers (B) Nestin (C) Sox1 (D) Pax6 (E) DcX for characterization of NPCs. The samples were iPSC, one control clone, an average of patient B and patient T.

As illustrated in figure 22 (A), the pluripotent marker Nanog, highly expressed in iPSC, was not detected in NPCs, indicating that the generated NPC no longer carry features from the pluripotent state. A similar expression of Nestin and Sox1 was detected for iPSC and NPC.

Both are markers for neural identity (47), so it is possible that the iPSCs used in this experiment have started to spontaneously differentiate in some degree in an ectodermal/neural direction. Notably, a 3-fold higher expression of the neural progenitor marker Pax6 was observed in patient B compared to iPSC, while lower levels or nearly no Pax6 expression were detected for control and Patient T, respectively. There are several stages to the generation of NPC and different markers are more apparent at the early or late stages of NPC differentiation. Moreover, different clones may undergo differentiation at different paces, leading to a mixed population of early, intermediate and more mature NPC, explaining the differences in levels of markers in different NPC clones (82). Importantly, like Pax6, the marker for intermediate progenitor cells DcX (83) was highly expressed only in NPC samples suggesting that iPSC was successfully differentiated to NPC.

4.2.3 Immunocytochemical Staining of NPC

Although transcription data is a useful indication of gene expression, mRNA levels may not directly correlate to protein expression levels, as mRNA can be modified and degraded prior to translation. So, to further confirm the expression of NPC markers at the protein level, ICC experiment was performed.

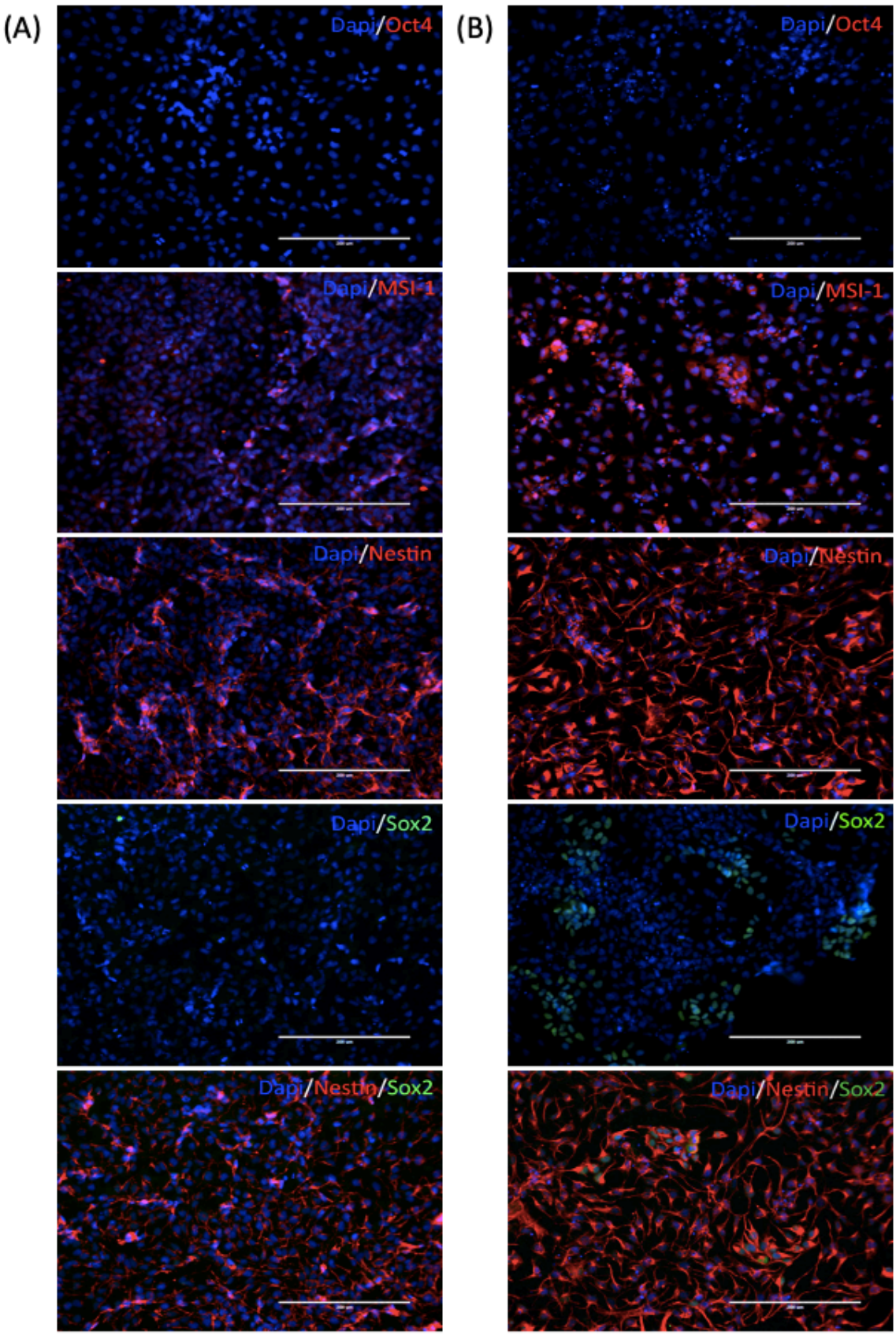

Figure 23: ICC results from the characterization of NPCs at passage 4. Cell nuclei are visualized by DAPI staining (blue). Scale bar: 200 µm. (A) Control AGc6. (B) Patient Bc4. First row: visualization of Oct4 (red). Second row: visualization of MSI-1 (green). Third row: visualization of Nestin (red). Fourth row: visualization of Sox2. Fifth row: double staining of Nestin (red) and Sox2 (green).

The lack of protein expression for the pluripotent marker Oct4, further confirms that the cells are not in a pluripotent state (figure 23). The cells also express the neural progenitor markers Nestin and Musashi-1, confirming that the cells have differentiated to the neural state. Sox2 is a master regulator for both pluripotent iPSCs and proliferative NPCs (84). It is partially expressed in the patient clone Bc4, and not expressed in control clone AGc1. The partial expression of Sox2 in patient Bc4 confirms the heterogeneity of NPCs. Based on the morphology of the NPCs and the qPCR expression, it is likely that Sox2 expression indicates proliferative NPCs, and not pluripotent iPSC, in patient Bc4 NPCs, at this stage. Apparently, the control NPCs are not proliferative yet, but not iPSCs anymore, at this stage. If control NPCs were cultured further to later passages, it is likely that they would express Sox2. As the NPC monolayer is heterogenous, determining at which stage the NPCs are at the point of characterization is challenging. Nevertheless, this data confirms that the generated cells are no longer iPSC and have progressed to a neural identity.

4.3 Viability Assay and Proliferation Assay using Proteasome Inhibitors

To verify whether ALP-related intracellular stress induces different responses in UCHL1-mutated NPCs compared to control NPCs, viability assays and proliferation assays were performed using UPS inhibitors. As previously mentioned, the UPS and ALP pathways are closely related, and inhibition of UPS induces ALP (85). The strategy was to first, perform survival assays using the live cell viability indicator PrestoBlue™ to delineate appropriate drug concentrations, i.e., doses that affect cell growth without leading to immediate cell death of all cells. To accomplish that, cells were exposed to several concentrations of MG132, Bortezomib and Epoxomicin and the number of living cells were measured after 24 hours of treatment. Once a suitable concentration was determined for each drug, cells were exposed to the selected drug doses and their impact on cell survival was monitored in a time-course experiment (0, 24, 48 and 72 h). The goal of the time-course experiment was to validate whether the long-term response after treatment was different between control and patient NPCs. Finally, as the differentiation of iPSC to NPC is a dynamic process, it is likely that the NPCs are a mix of different subpopulations of early, intermediate, and more mature NPCs, and each clone may have different distributions of such subpopulations. As cells in different states may respond to drug treatment in distinct ways, the final goal was to evaluate the impact of UPS inhibitors in the survival of control and patient cells by flow cytometry.

This methodology is highly sensitive and enables accurate quantification of live/dead cells in distinct cell populations, which is not possible to discern using the PrestoBlue™-plate reading assay.

4.3.1 Viability Assay

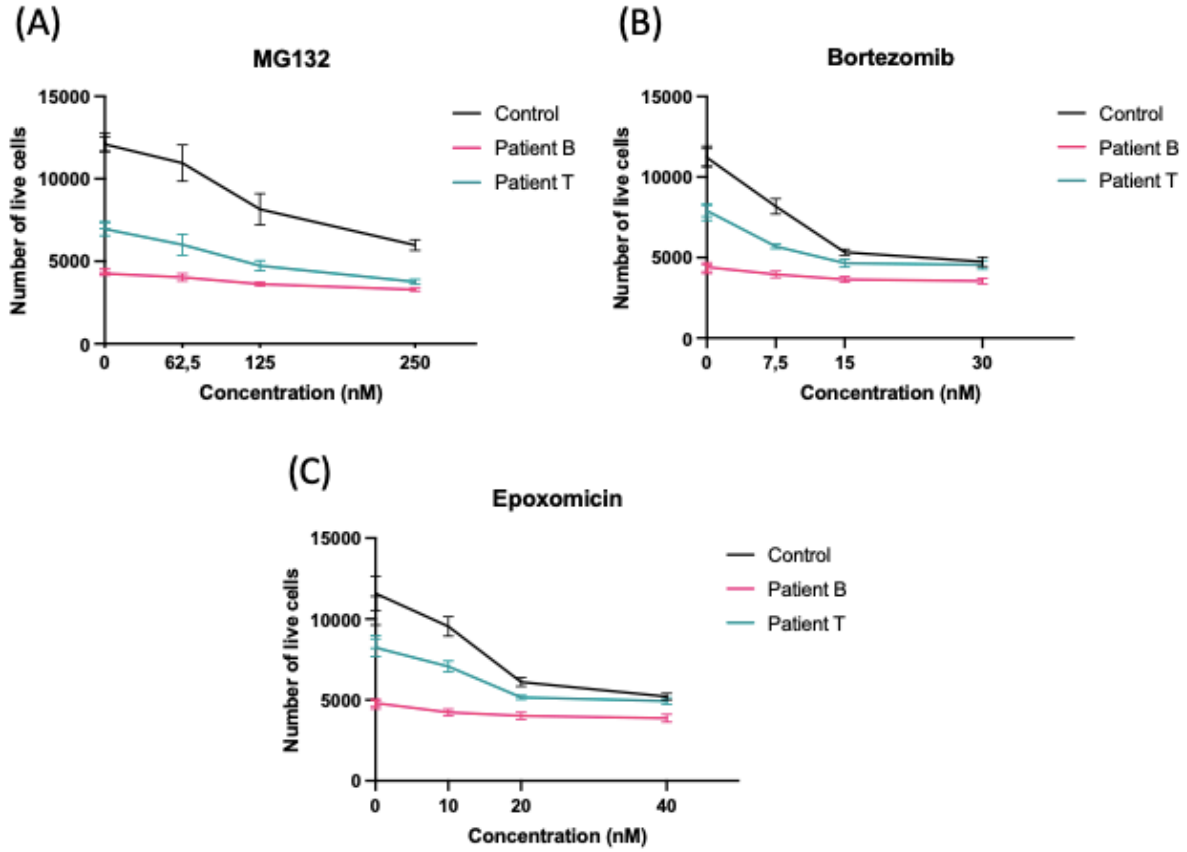

Figure 24: NPC survival upon exposure to different concentrations of (A) MG132, (B) Bortezomib (C) Epoxomicin. Relative measurements indicate number of live cells relative to DMSO control. NPCs used in this experiment are at passage 4. Error bars represent the standard deviation of 6 replicates.

Due to the paucity of literature on human NPC and proteasome inhibition using the described drugs, several assays were performed to determine drug doses that were not toxic to these cells. Figure 24 illustrates the last steps of this fine-tuning process. Here, NPCs were treated for 24 h with increased drug concentrations. According to the data, NPC from patient B were dead, even without any addition of drugs, as their fluorescence correspond to the baseline fluorescence of dead cells in culture medium with PrestoBlue™ (figure 37, appendix 3). It might be that these cells died during transference to the 96-well plate, or during the overnight incubation prior to drug treatment. Notably, fluorescence signals for Bc4 and Tc3 revealed that the initial cell number for these samples was lower than the standard values, observed for samples AGc1 and AGc6. As AGc1 and AGc6 are control cells, they were considered as references. Therefore,

drug doses that affected the survival of control clones without triggering immediate cell death were selected for the proliferation assay. For MG132, an appropriated dose would be between 62.5 nM and 125 nM, therefore, 100 nM was selected. For Bortezomib and Epoxomicin, 7.5 nM, and 10 nM were considered optimal concentrations to assess long-term drug exposure effects.

Obtaining the same initial cell number for all clones in cell survival assays has also been a challenge during this study. Cell concentrations were carefully measured with several replicates prior to plating. Still, the initial number of cells still varied at 24 hours after seeding. We believe that such variations could be a result of differences in adaptation after splitting and transferring cells to the assay plates, or due to initiation of cell death, which was often triggered at passage 4-5, but also occurred at earlier passages. These factors would decrease the number of living cells at variable rates, leading to the repeated variations observed in fluorescence 24 hours after plating cells. Notably, experiments where cells were platted and measured on the same day (day 0), showed the same initial cell number for all clones, suggesting that the differences observed in the initial cell number among the clones at 24 hours after plating was not due to poor counting of the cells.

4.3.2 Proliferation Assay

The main aims of the proliferation assay were to (i) confirm that the selected drug doses are appropriated; (ii) investigate whether control and patient NPCs respond differently to alterations in protein degradation systems in long term, and (ii) determine a feasible time point for further accurate quantification of cell death, on potential distinct cell populations, by flow cytometry.

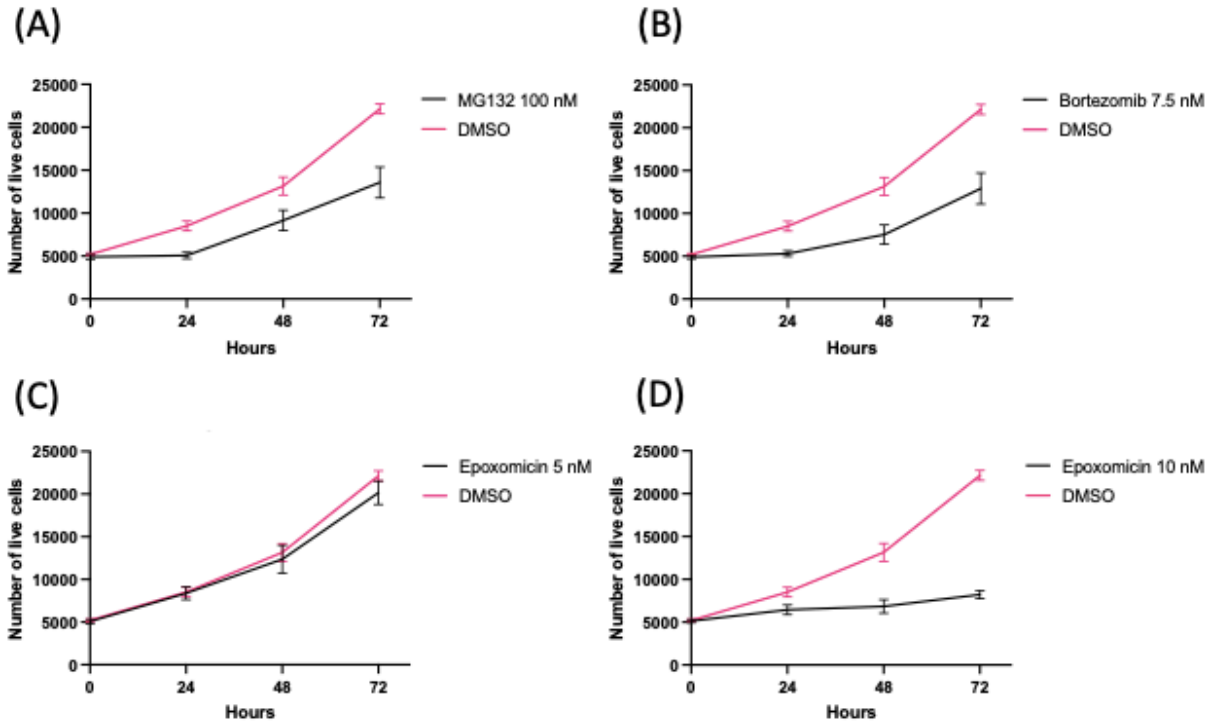

Figure 25: Proliferation of NPCs at passage 3 after exposure to selected doses of proteasome inhibitors: (A) 100 nM MG132. (B) 7,5 nM Bortezomib. (C) 5 nM Epoxomicin. (D) 10 nM Epoxomicin. A mean of the control clones AGc1 and AGc6 are presented in the graphs. Cells treated with vehicle control (DMSO) are shown as pink lines. Error bars represent the standard deviation of 6 replicates.

Once again, poor survival of patient clones hindered the second aim described above, therefore, only the viability patterns of control clones are shown in figure 25. As the final goal was to assess cell survival by flow cytometry and one should always compare the effect of a treatment on patient/mutated/diseased sample to what is observed in control samples, the results presented in figure 25 were used to accomplish the last aim described above. According to the data, the selected MG132 and Bortezomib doses are suitable for the next experiment. For Epoxomicin, 5 nM exerted little toxicity on the cells, while 10 nM killed the majority of cells already at 24 hours after treatment. Thus, 7,5 nM Epoxomicin was chosen as a candidate dose for the flow cytometry experiment.

Moreover, 48 hours was chosen as an ideal time point for further cell death measurements by flow cytometry. This choice was based on the fact that the drug impact in viability is more evident at 48 hours than at 24 hours. Although drug effects are yet more prominent at 72 hours, we have observed cell death at 72 hours in previous experiments (data not shown). Although we are not certain what caused the sudden cell death at 72 hours, we hypothesize that incubating NPCs for several days in the same medium might have been a contributing factor, as the NPC medium is changed on a daily basis during normal cell culture conditions.

Nevertheless, control- and patient-derived NPCs were then treated for 48 hours with MG132 (100 nM), Bortezomib (7.5 nM) or Epoxomicin (7.5 nM), stained with a cell death marker named 7-AAD (7-aminoactinomycin D) and submitted to flow cytometry analysis, which was performed by Nina Liabakk, Senior engineer at IKOM, NTNU. However, the analysis showed that at least 90% of the cells for all clones were dead when the experiment was performed, including untreated cells. Thus, no conclusions could be drawn regarding potential differences in response to UPS inhibitors between patient and control derived NPCs. Due to time constraints, this experiment could not be repeated.

It has been shown that UPS inhibition induces ALP activity and that ALP can compensate for impaired UPS function, i.e., ALP is able to degrade proteins that are commonly degraded by the UPS when the proteasome is impaired (85). If the UCHL1 mutations affect ubiquitin processing in a way to promote cargo degradation via ALP, therefore, improving basal level ALP activities compared to control cells, then, UPS inhibition would hinder the survival of control cells to a greater extent than patient cells. On the contrary, if UCHL1 mutations impact ubiquitin processing leading to a decrease in the cell ability to degrade cellular waste, then, UPS inhibition would lead to an increased number of dead patient cells compared to control cells. Due to issues in cell number observed for the viability assays and because the patient-derived NPCs died while conducting the proliferation assays, it was not possible to determine differences in toxicity or recovery between control and patient cells upon UPS inhibition. Nevertheless, optimal drug concentrations and suitable time points for NPC treatment with these drugs have been determined for further validations by flow cytometry.

4.4 Detecting Autophagic Flux by Western Blot

The main goal of this experiment was to evaluate the autophagic activity in control and patient-derived NPCs. Autophagic flux was evaluated by comparing the levels of the autophagic markers LC3 and p62 in untreated and Bafilomycin A1 treated cells.

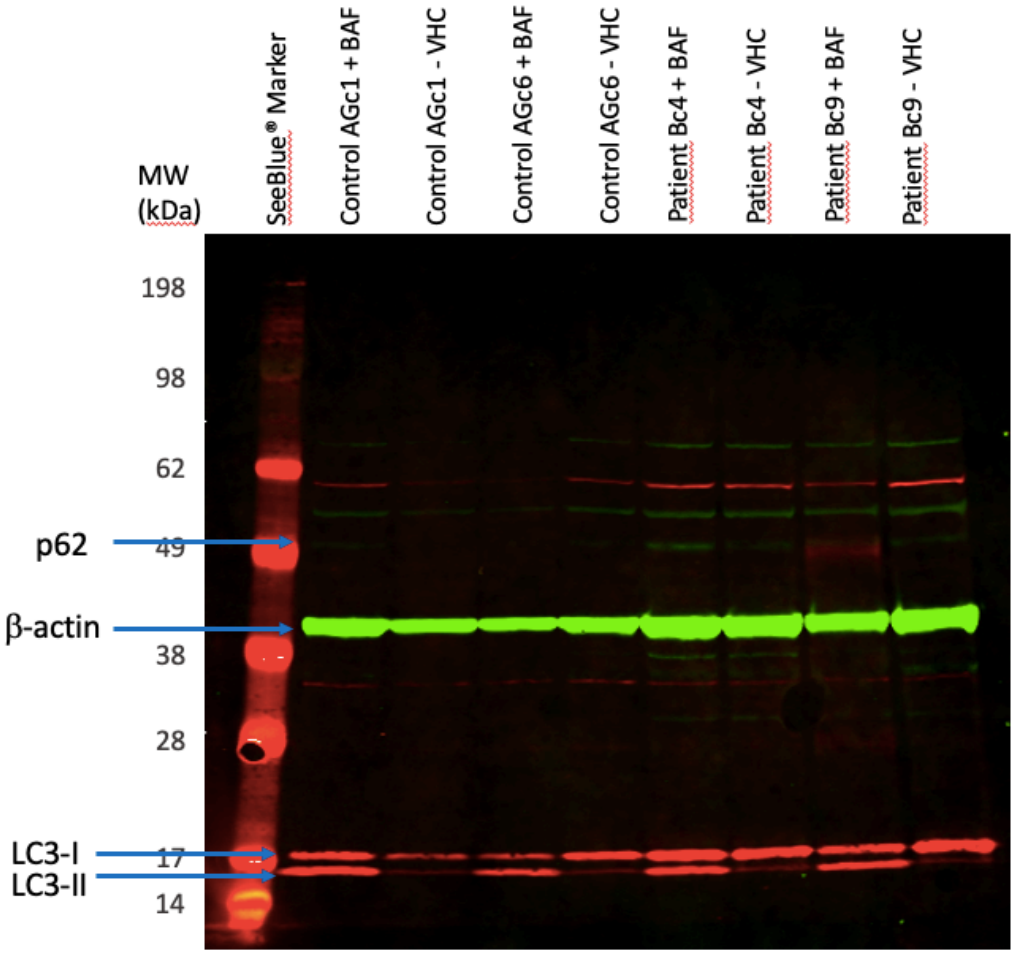

Figure 26: Detection of LC3-I/II and p62 in NPCs at passage 2. Beta-actin is used as loading control. AGc1 and AGc6 are control NPCs, Bc4 and Bc9 are patient-derived NPCs. VHC: Vehicle control (Ethanol); BAF: Bafilomycin A1. Patient T was not included in the experiment as the cells were not viable at this point.

Figure 26 shows that the levels of LC3-II increased in all samples upon Bafilomycin A1 treatment. Notably, the accumulation of LC3-II in treated samples are not due to protein loading, as verified by the levels of the internal control β-actin. This data indicates that autophagy activity is not impaired in control or patient-derived NPCs. To support these findings, the membrane was also probed with antibodies that recognize p62. As the signals detected on the 60 kDa region were quite weak, a figure with increased contrast was generated, along with the band intensities of β-actin, for reference of protein loading (figure 27).

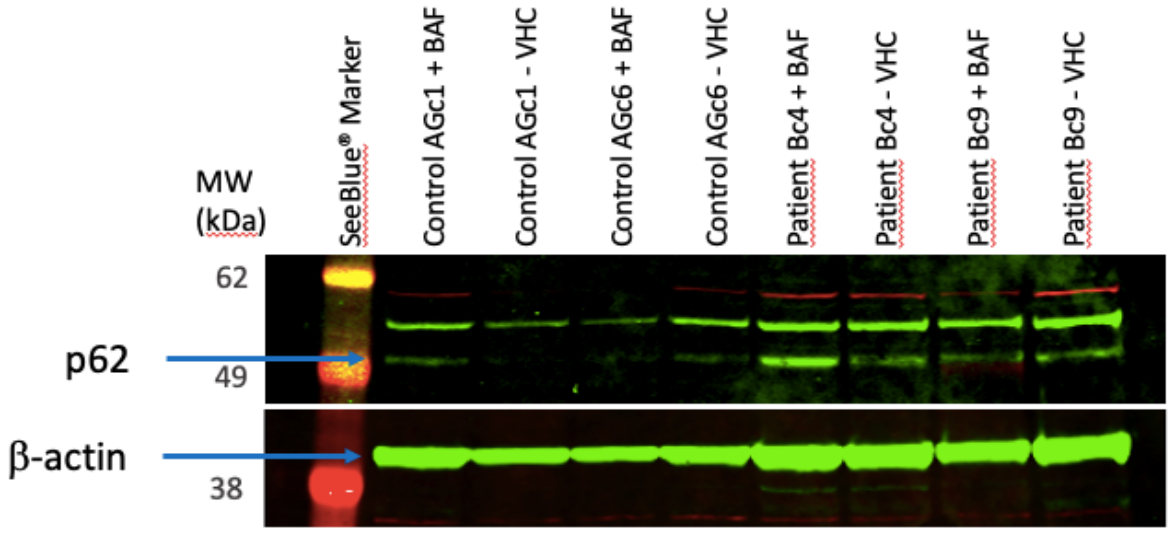

Figure 27: Enhanced contrast of the region where p62 was detected in the WB presented in figure 26. The green color was enhanced by using "levels" in photoshop. VHC: Vehicle control (Ethanol); BAF: Bafilomycin A1.

As shown in figure 27, sets of bands were detected in the region where p62 is expected to be detected. According to the detection of p62 in other cell lines in WBs developed in our lab, the band closer to the 49 kDa seems to be the one corresponding to p62. The upper band, which was weakly detected in other cell lines, such as fibroblasts (data not shown), seems to be the major target recognized by the p62 antibody in NPC. Whether the upper band is a post-translational form of p62 or a protein that is nonspecifically detected in this region, remains to be elucidated. In addition, fluorescence background in the region along with PVDF membrane quality issues where the lower band was detected, hindered proper analysis of p62 levels in all samples. By correlating to the β-actin levels, it seems that p62 levels could be either slightly increased or unchanged after treatment, with no clear differences in trend when comparing control and patient-derived NPCs.

Bafilomycin A1 inhibits the fusion between the autophagosome and lysosome during the ALP (12). As LC3-II and p62 are bound to the autophagosome membrane and degraded after fusion with the lysosome, inhibition by Bafilomycin A1 is expected to increase the levels of both markers (17). If the levels of LC3-II and p62 remain unaltered after treatment, it is most likely that the cells harbor a deficiency in the autophagic activity, such as a block of the autophagosome-lysosome formation (12). As discussed, the LC3-II pattern after Bafilomycin A1 treatment clearly shows that all tested clones are not deficient in ALP. Importantly, p62 is also involved in autophagy-independent molecular mechanisms, which could also impact its levels (86).

4.5 Detection of Autophagic Markers in NPCs

To investigate the involvement of ALP in neurodevelopment and neurodegeneration in UCHL1 dysfunctional cells, basal expression of autophagy-related genes, lysosomal markers, and associated proteins were monitored by qPCR. The panel of targets includes BECN, p62, LAMP1, CTSD, LC3A- and B as well as mTOR.

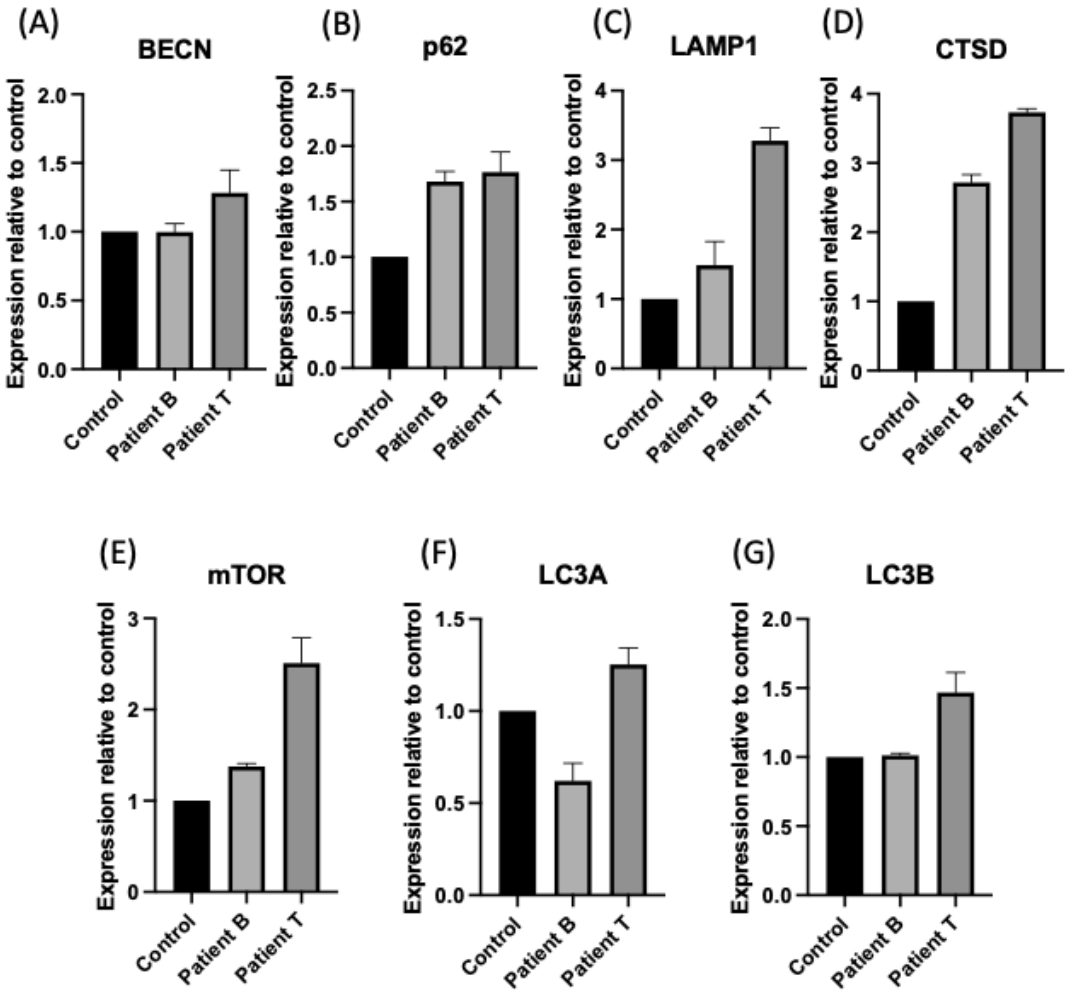

Figure 28: Expression levels of autophagic marker genes. The samples presented in the figures are a mean of two control clones, a mean of two patient B clones, and one patient T clone. Error bars represent the standard deviation of four replicates for control and patient B, and two replicates for patient T. Expression levels of (A) BECN. (B) p62 (C) LAMP1 (D) CTSD. (E) mTOR (F) LC3A (G) LC3B. Data is represented as relative to the expression levels of autophagic markers in control AGc1 NPC.

According to figure 28, the fold-change differences between control and patients NPCs are around 1.5 for Beclin 1 (BECN), p62 and the LC3 isoforms A and B. Thus, these markers are not considered differentially expressed between the samples. BECN plays a key role in autophagy during the initiation stage when the isolation membrane is formed. Although, there is at least a 2-fold increase in the expression levels of the lysosomal membrane protein LAMP1

when comparing Patient T with control NPCs, these findings are not corroborated by LAMP1 expression levels in Patient B, which are similar to control NPCs. Interestingly, the levels of Cathepsin D (CTSD), an enzyme ubiquitously distributed in lysosomes, increased almost 3- and 4-fold in patient B and T, respectively. This could indicate enhanced lysosomal activity in patient derived NPCs. Similar to LAMP1 levels, mTOR (mechanistic target of rapamycin) expression increased over 2-fold in Patient T while remained unchanged when comparing Patient B to control NPCs. mTOR regulates fundamental downstream targets directly associated with autophagy activation/inhibition (19). It is found in two distinct protein complexes, referred as mammalian target of rapamycin complexes 1 and 2 (mTORC1 and mTORC2). However, only mTORC1 directly regulates autophagy (87). Upon nutrient rich conditions, mTORC1 is activated via phosphorylation at Ser2448 and triggers phosphorylation of the ULK-ATG13-FIP200 kinase complex (88, 89). The phosphorylation of this complex will in turn result in inhibition of autophagy. Upon nutrient deprivation, mTOR is repressed leading to activation of FIP200 and ATG13, which together with ULK1/2, promotes the formation of the phagophore and thereby activation of autophagy (90, 91).

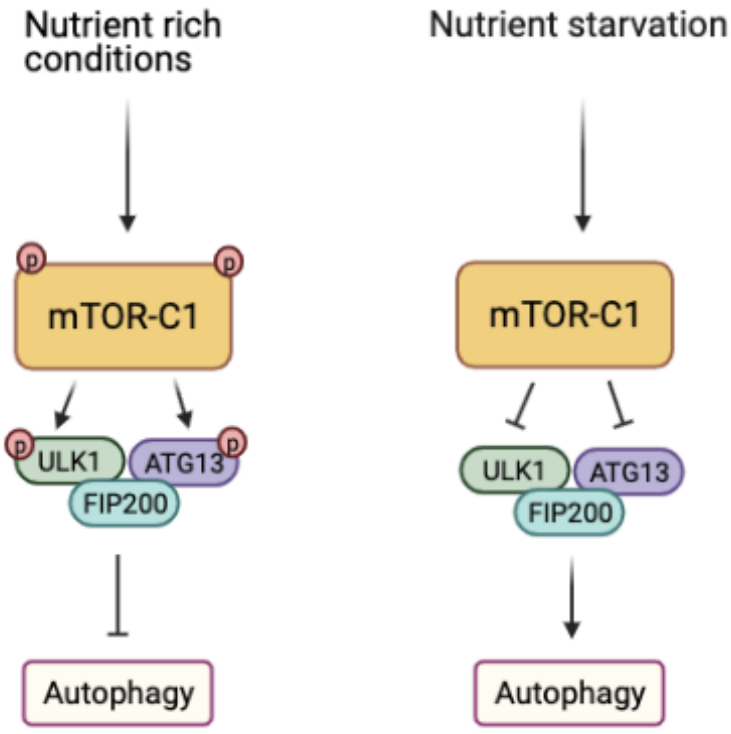

Figure 29: The functional role of mTOR-C1 in autophagy. mTOR-C1 is phosphorylated and activated at Ser2448 upon nutrient rich conditions. The activated mTOR-C1 phosphorylates the protein complex ULK-ATG13-FIP200 leading in inhibition of autophagy. mTOR-C1 is not phosphorylated during starvation, and autophagy will thus not be inhibited. Figure created using Biorender.com.

In our data, increased mTOR expression could perhaps be related to down-regulation of autophagy in Patient T cells. However, it is important to point out that transcription levels cannot be directly associated with mTOR activation, which is accomplished via post-translational modifications, as illustrated in figure 29.

Notably, this assay was performed only once and using only one control clone as reference for normalization. To validate these results, experiments with more replicates and including more targets should be performed. Another fundamental aspect already mentioned for mTOR is that mRNA levels do not necessarily correlate to protein levels, and several autophagic markers are activated or inhibited via post-translational modifications, affecting downstream targets and thereby entire biological pathways. Thus, a thorough screening on total protein amounts and their post-translational modified forms would provide a better overview on potential alterations in ALP in these cells.

4.6 Characterization of Cerebral Organoids

4.6.1 Cell Morphology of Cerebral Organoids

To examine the role of the UCHL1 mutation in human brain development, cerebral organoids were generated using control cells as well as patient cells harboring the UCHL1 mutation. As brain function is dependent on complex interactions between several cell types across several brain regions, the generation of cerebral organoids can provide valuable information that is important for the understanding of brain development. Figure 30 displays representative pictures in the process of generating cerebral organoids. Seven sets of cerebral organoids were generated in total, and the figure below displays set four which is a good representative.

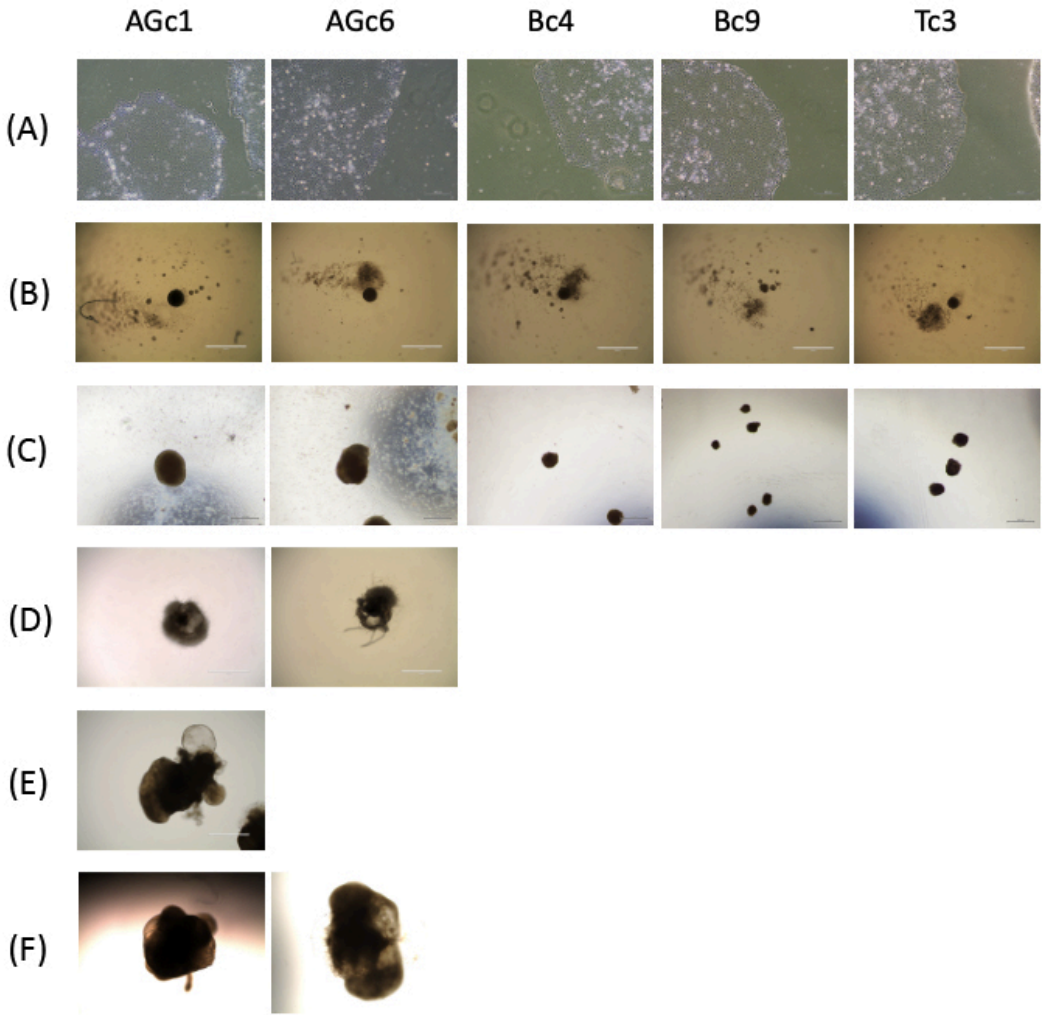

Figure 30: Phase-contrast pictures taken throughout cerebral organoid culture. (A) hiPSC ready for passage at day 5 for control clones Agc1 and Agc6 and patient clones Bc4, Bc9 and Tc3. (B) Embryoid bodies of control clones Agc1 and Agc6 and patient clones Bc4, Bc9 and Tc3 in 96-wells on day 3 after iPSC passage. Scale bar: 1000 µm. (C) Neuroectodermal tissues of control clones Agc1 and Agc6, and failed neuroectodermal tissues of patient clones Bc4, Bc9 and Tc3 grown in 24-well plates on day 11 after iPSC passage. Scale bar: 500 µm. (D) Neuroectodermal tissue of control clones Agc1 and Agc6 embedded in Matrigel on day 15 after iPSC passage. Scale bar: 1000 µm. (E) Cerebral organoid of control clones Agc1 in orbital shaker on day 29 after iPSC passage. No pictures were taken of control clone Agc6. Scale bar: 1000 µm. (F) Cerebral organoid of control clones Agc1 and Agc6 in orbital shaker on day 57 after iPSC passage. Scale bar: 1000 µm.

Figure 30 A displays parts of compact colonies of iPSC with distinct borders and well-defined edges both for control and patient cells. This was the starting point for the generation of organoids. Thus, iPSCs were carefully examined to ensure typical morphology without any signs of differentiation before proceeding to the generation of embryoid bodies in 96-well plates. Figure 30 displays newly generated embryoid bodies on day 3 after the iPSC passage. Dead cells are decorated around the area, this does not affect the formation of the EBs at the center, according to Lancaster *et al.* (66). All of the clones generated embryoid bodies, however, the patient EBs were smaller than the control EBs and lacked a clear edge. The control EBs had a diameter of approximately 300 μm and the patient EBs approximately 100-200 μm. However, all of the EBs were transferred on day 7 to the 24-well plates with a neural induction medium for further growth.

Figure 30 (C) displays EBs at day 11, grown in neural induction medium for 4 days. The control EBs have a diameter of approximately 5-600 μm, while the patients are about 1-200 μm. The control neuroectodermal tissues show smooth edges with bright optically translucent surfaces, a sign of healthy formation. The patient cells have no translucent surfaces and show no signs of neuroectodermal formation. Based on these results, we chose to discard the failed patient EBs and continue with the control neuroectodermal tissues. Figure 30 (D) shows the control organoids embedded in Matrigel® with buds of neuroepithelial cells growing into the Matrigel®. Figure 30 (E and F) are pictures taken in the orbital shaker showing further budding of the cerebral organoids.

Apart from the clonal variations between control and patient derived cells, variations between the control clones also occurred. Irregularities amongst control clones between the sets, as well as between the organoids in the same set, were also observed. Organoids deriving from control cells died at different time points or failed to induce neuroectodermal tissue. Such variations were also stated in the Lancaster protocol and is a common obstacle in organoid generation all over the scientific community (66).

Many of the generated organoids were too large to be properly examined under a standard tissue culture microscope. To visualize the gross morphology and to characterize the organoids, cryosectioning and immunohistostaining were performed.

4.6.2 Immunohistochemical Staining of Cerebral Organoids

The organoids were collected after 14 days, 1 month and 2 months in a bioreactor or orbital shaker and were characterized using neuronal markers, as illustrated in figure 31 and 32.

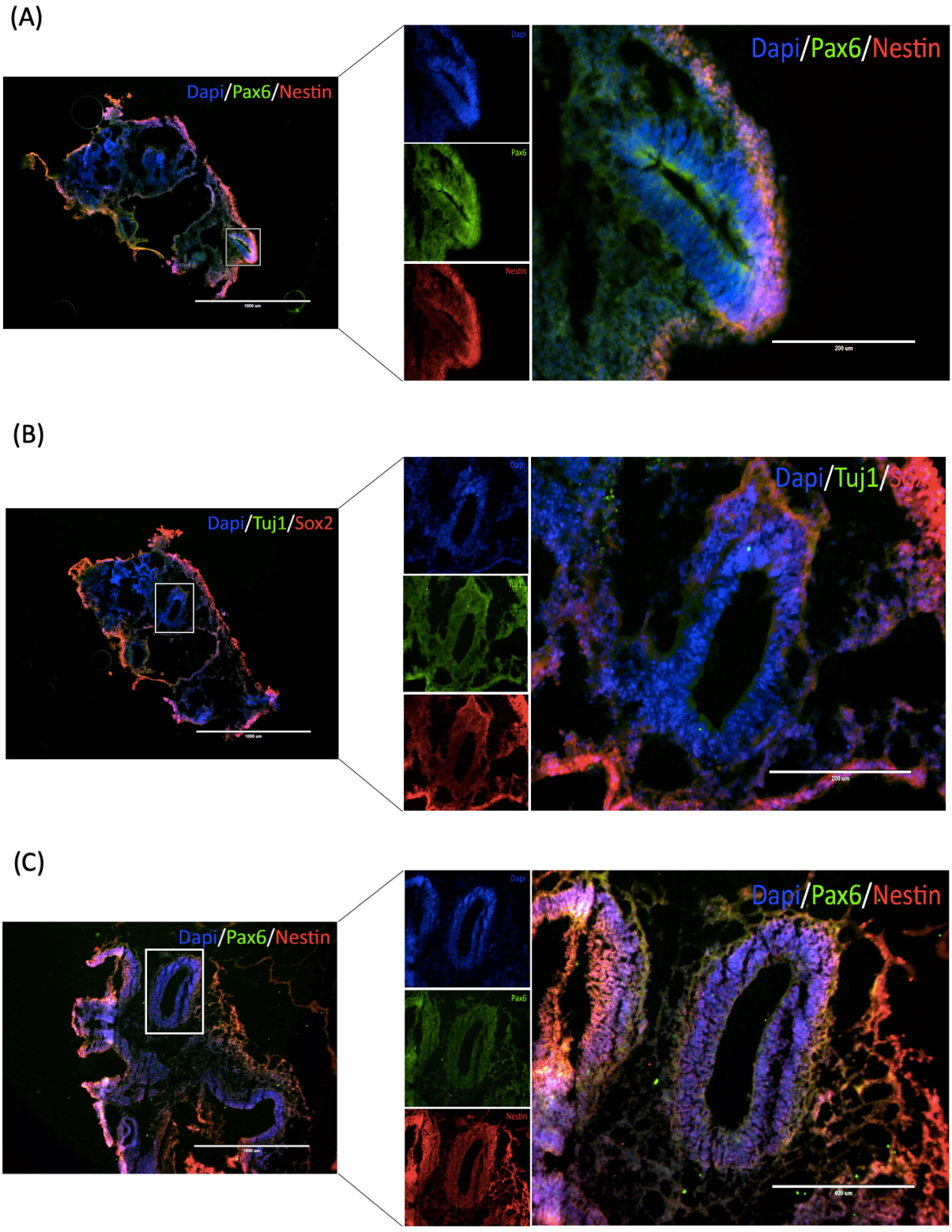

Figure 31: Immunohistochemical staining of neuronal markers in cerebral organoids derived from control clones Agc1 and Agc6 at early developmental stages. (A) neural progenitor markers Nestin and Pax6 after 14 days of culture in bioreactor or orbital shaker. (B) neural progenitor markers Tuj1 and Sox2 after 14 days of culture in bioreactor or orbital shaker. (C) neural progenitor markers Nestin and Pax6 after 30 days of culture in bioreactor or orbital shaker. To all pictures: Scale left: 1000 µm, right: 200 µm.

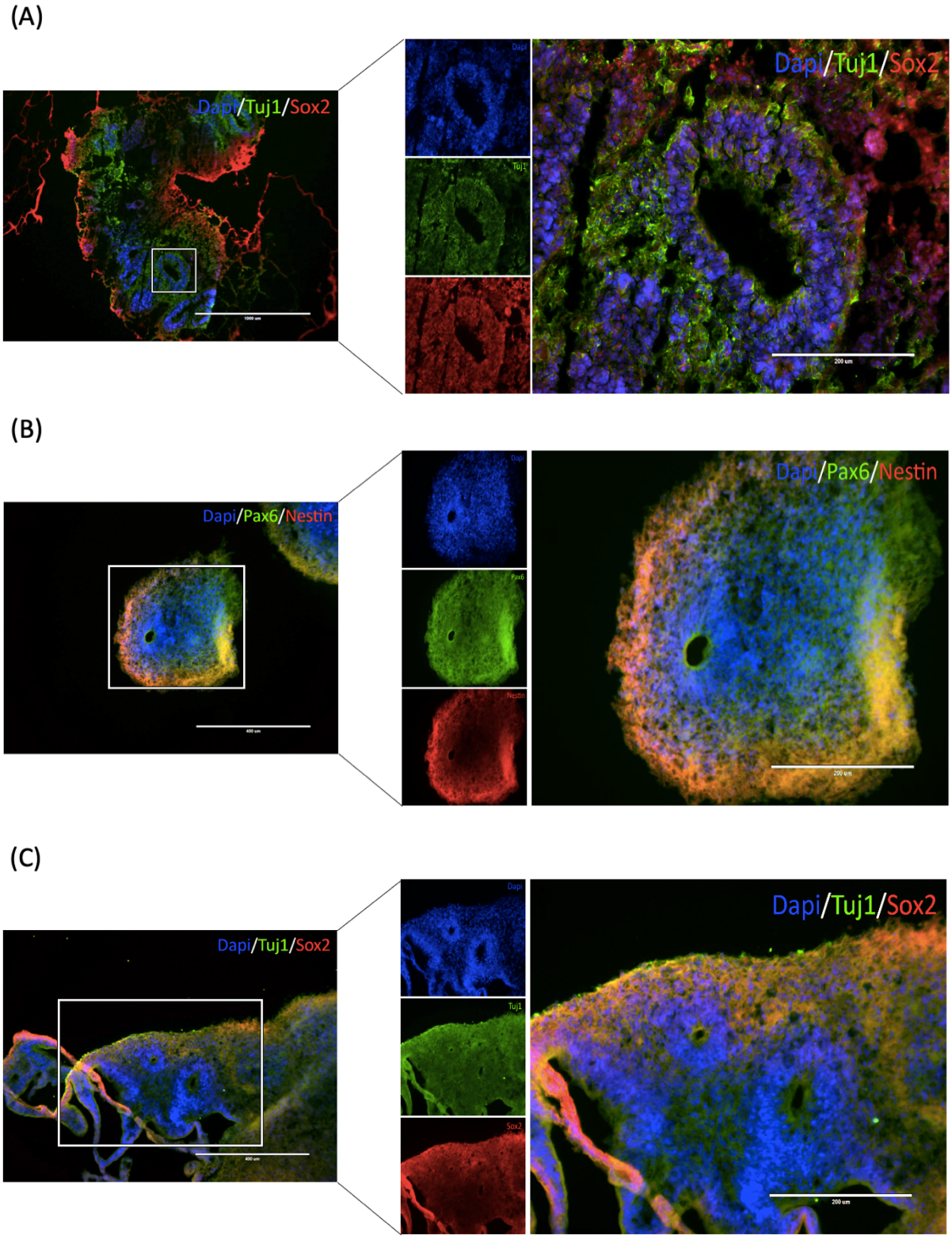

Figure 32: Immunohistochemical staining of neuronal markers in cerebral organoids derived from control clones Agc1 and Agc6 at late developmental stages. (A) neural progenitor markers Tuj1 and Sox2 after 30 days of culture in bioreactor or orbital shaker. Scale left: 1000 µm, right: 200 µm. (B) neural progenitor markers Nestin and Pax6 after 60 days of culture in bioreactor or orbital shaker. Scale left: 400 µm, right: 200 µm. (C) neural progenitor markers Tuj1 and Sox2 after 60 days of culture in bioreactor or orbital shaker. Scale left: 400 µm, right: 200 µm.

Figure 31 (A and B) shows cryosectioned organoids grown in the bioreactor or orbital shaker for 14 days and stained using Pax6 and Nestin and Sox2 and Tuj1, respectively. The immunohistochemical staining shows that the organoid tissues are positive for all markers. However, the expression of neuronal marker Tuj1 is not as prominent as the progenitor markers Sox2, Pax6 and Nestin around the ventricle-like cavities at this time point. In figure 32 (A), the marker Tuj1 is more prominent as the cerebral organoids have grown for 1 month in the bioreactor and orbital shaker. Tuj1 is also prominent in the organoids grown for 2 months (figure 32, C).

Immunohistochemical staining was performed on healthy control-derived organoids grown in the bioreactor or orbital shaker for 2 weeks, 1 month and 2 months. Lancaster *et al.* describe in their protocol that the organoids grown from 12 – 20 days express Sox2 and Pax6 from expanding neuroepithelium (66). However, we found that Sox2 and Pax6 was expressed in organoids grown for up to 2 months, revealing that the neuroepithelium is still expanding in the generated organoids (66). The organoids should start to exhibit neuronal differentiation after 1 month, this is marked with the neuronal marker Tuj1. The results display a higher expression of Tuj1 in cerebral organoids grown for 1 and 2 months compared to 2 weeks, indicating neuronal differentiation progress in brain organoids. This data also confirms the neuronal differentiation in our organoids. Due to time limitations, it was not possible to stain the organoids for different regions of the brain.

Cerebral organoids offer the opportunity to study interactions between cells in a 3D manner which provides the physiological relevance of the cellular environment in the brain (63). There have not been any reports on the generation of cerebral organoids with cells harboring this type of mutation in the UCHL1 gene. We attempted to generate cerebral organoids from patient iPSC harboring this mutation without any success. EBs of good quality were generated in the 96-well plates, however, the EBs did not have a distinct border, nor a sufficient size. Several sets were generated and neither of them generated proper cerebral organoids from the patient cells. As this was a 1-year project, we did not have enough time to develop specific protocols that might have generated successful organoids from patient cells. Importantly, we managed to generate cerebral organoids from the control cells, confirmed by immunohistochemical staining. The protocol employed was therefore proven to be sufficient for the generation of cerebral organoids. The phenotypic pattern displayed by patient cells indicates that these cells might have special requirements to successfully generate cerebral organoids.

Cerebral organoids provide a novel model of the human brain. The use of mouse models has not been sufficient in unraveling neurodevelopmental disease mechanisms as mouse lack many of the features of the human brain (65, 92). There is substantial evidence that cerebral organoids have the ability to model key aspects of the early development of the cerebral cortex in a species-specific manner, and from there, provide evidence of the basis of neurodevelopmental diseases (92). However, cerebral organoids are an *in vitro* model that does not have the typical patterning and environmental cues typically found in embryos, i.e., it lacks the crosstalk between the neural tissues and non-neural tissues as the surrounding embryonic tissue is not engaged (66). Also, the lack of vascularization by blood vessels is a limitation, as the blood vessels are important in gas exchange, nutrient supply and waste removal (80, 92). As organoids lack the meninges and vasculature, their growth is severely limited (66). It impacts growth patterns depending on the availability of nutrients and lack of body axes to pattern the neural tissues. Consequently, organoids have a tendency to display high variation in success rate (66). In our experiments, reproducibility was a major challenge, and this is known for all 3D models (93). Although the poor reproducibly described in organoid generation protocols could have greatly contributed to the failure in generating patient-derived organoids, one cannot rule out that lack of development could be the phenotype resulting from the UCHL1 mutations.

With the continued and rapid development of cerebral organoid technology, the challenges of maturity and reliability of cerebral organoid generation are largely improving. For instance, protocols for the generation of vascularized organoid models are now being established (94). Although a number of challenges still exist, including generation of less organized structures, human cerebral organoids are very good models to unravel disease mechanisms and for personalized treatment of brain diseases (64, 70).

5. Concluding Remarks and Future Perspectives

Despite its rare appearance in society, an understanding of the molecular basis of such an early-onset neurodegenerative syndrome can provide a unique insight into CNS maintenance. Further work to unravel the molecular mechanism underlying the clearance of protein aggregation and degradation of proteins in neurodevelopment and neurodegenerative diseases can potentially provide new prognostic markers and treatment modalities for neurodegenerative disorders linked to imbalance in ubiquitin processing as well as impairment of cellular degradation systems, such as the autophagy lysosomal pathway.

In this project iPSCs and NPCs were successfully characterized, and state-of-the-art stem cell technology was employed to generate cerebral organoids. However, due to the complications faced during differentiation and culturing of NPCs, it was not possible to find answers to if UCHL1 dysfunction affects ALP activities in the brain impacting neurodevelopment and neurodegeneration. The difficulties also restricted the possibility to further differentiate the NPCs to forebrain neurons and conduct experiments at this level of differentiation, which would certainly be the most relevant developmental stage. As there was nearly no information on the topic of NPC death in cell culture in the literature, finding the potential causes to overcome the described survival issues was a major challenge. Importantly, as producing FB neurons was the ultimate goal, a great deal of time was dedicated in finding a way to produce and culture healthy NPCs. Our experience from the NPC culture is that it is highly clone dependent. The different clones died at different time-points and thrived in different conditions. The establishment of a NPC culture protocol for each clone is not feasible within the timeframe of this project and would also lead to not comparable data, as all clones are not cultured in the same conditions. This emphasizes the importance to further work on the development of more reliable and robust differentiation protocols for the generation of neural progenitor cells.

Despite the NPC differentiation issues, we were able to delineate suitable proteasome inhibitors doses, as well as time-points after drug exposure, for future validation of cell viability by flow cytometry. Moreover, we conducted western blotting targeting the levels of LC3 and p62 to investigate the autophagic flux in NPC as well as qPCR targeting several autophagic markers. Neither of the experiments indicated clear differences in autophagic activity or levels of most autophagic markers at the NPC stage. Although the mRNA levels of the lysosomal endoprotease CTSD are increased in patient NPCs, which indicates enhanced lysosomal

function, this experiment was performed only once, with one set of clones and only one control clone. Hence, more biological replicates are necessary to confirm this data. In addition, expression of autophagy markers must be confirmed at protein level as well as their regulatory status via post-translational modifications. In future projects, these experiments must be repeated in NPC and performed in forebrain neurons and mature motor neurons, as neural stem cells themselves are not sufficient to recapitulate the disease.

We also aimed to develop cerebral organoids harboring the mutations R178Q and A216D to evaluate the role of UCHL1 in early brain development. However, we were only able to generate cerebral organoids deriving from healthy controls, thus being unable to conduct any experiments to investigate the role of the UCHL1 mutations in brain development. Variability during the generation of any organoids is a common drawback known in many laboratories. Further work on the development of a protocol of higher success rate for the generation of organoids is necessary.

6. References

1. Rydning SL, Backe PH, Sousa MML, Iqbal Z, ÿye A-M, Sheng Y, et al. Novel UCHL1 mutations reveal new insights into ubiquitin processing. Human Molecular Genetics. 2017;26(6):1217-8.
2. Bingol B. Autophagy and lysosomal pathways in nervous system disorders. Mol Cell Neurosci. 2018;91:167-208.
3. Chen R-H, Chen Y-H, Huang T-Y, SpringerLink. Ubiquitin-mediated regulation of autophagy. 2019.
4. Kenney DL, Benarroch EE. The autophagy-lysosomal pathway. General concepts and clinical implications. 2015;85(7):634-45.
5. Khandia R, Dadar M, Munjal A, Dhama K, Karthik K, Tiwari R, et al. A Comprehensive Review of Autophagy and Its Various Roles in Infectious, Non-Infectious, and Lifestyle Diseases: Current Knowledge and Prospects for Disease Prevention, Novel Drug Design, and Therapy. Cells. 2019;8(7).
6. Saha S, Panigrahi DP, Patil S, Bhutia SK. Autophagy in health and disease: A comprehensive review. Biomed Pharmacother. 2018;104:485-95.
7. Dikic I, Elazar Z. Mechanism and medical implications of mammalian autophagy. Nat Rev Mol Cell Biol. 2018;19(6):349-64.
8. Bhutia SK, Mukhopadhyay S, Sinha N, Das DN, Panda PK, Patra SK, et al. Autophagy: cancer's friend or foe? Adv Cancer Res. 2013;118:61-95.
9. Yun CW, Lee SH. The Roles of Autophagy in Cancer. Int J Mol Sci. 2018;19(11).
10. Seranova E, Connolly Kyle J, Zatyka M, Rosenstock Tatiana R, Barrett T, Tuxworth Richard I, et al. Dysregulation of autophagy as a common mechanism in lysosomal storage diseases. Essays in Biochemistry. 2017;61(6):733-49.
11. Martini-Stoica H, Xu Y, Ballabio A, Zheng H. The Autophagy-Lysosomal Pathway in Neurodegeneration: A TFEB Perspective. Trends in neurosciences. 2016;39(4):221-34.
12. Mizushima N, Yoshimori T. How to Interpret LC3 Immunoblotting. AUTOPHAGY. 2007;3(6):542-5.
13. Ichimura Y, Kirisako T, Takao T, Satomi Y, Shimonishi Y, Ishihara N, et al. A ubiquitin-like system mediates protein lipidation. Nature Nature. 2000;408(6811):488-92.
14. Yu L, Chen Y, Tooze SA. Autophagy pathway: Cellular and molecular mechanisms. Autophagy. 2018;14(2):207-15.
15. Bj¯rk¯y G, Lamark T, Pankiv S, ÿvervatn A, Brech A, Johansen T. Monitoring autophagic degradation of p62/SQSTM1. Methods in enzymology. 2009;452:181-97.
16. Pankiv S, Clausen TH, Lamark T, Brech A, Bruun JA, Outzen H, et al. p62/SQSTM1 Binds Directly to Atg8/LC3 to Facilitate Degradation of Ubiquitinated Protein Aggregates by Autophagy. JOURNAL OF BIOLOGICAL CHEMISTRY. 2007;282(33):24131.
17. Grasso D. Autophagy in Cell Fate and Diseases. 2015.
18. Jaber FA, Khan NM, Ansari MY, Al-Adlaan AA, Hussein NJ, Safadi FF. Autophagy plays an essential role in bone homeostasis. Journal of cellular physiology. 2019;234(8):12105-15.
19. Kocaturk NM, Gozuacik D. Crosstalk Between Mammalian Autophagy and the Ubiquitin-Proteasome System. Frontiers in cell and developmental biology. 2018;6.
20. Kisselev AF, van der Linden WA, Overkleeft HS. Proteasome inhibitors: an expanding army attacking a unique target. Chem Biol. 2012;19(1):99-115.
21. Ge P-f, Zhang J-z, Wang X-f, Meng F-k, Li W-c, Luan Y-x, et al. Inhibition of autophagy induced by proteasome inhibition increases cell death in human SHG-44 glioma cells. Acta Pharmacol Sin Acta Pharmacologica Sinica. 2009;30(7):1046-52.

22. Day INM, Thompson RJ. UCHL1 (PGP 9.5): Neuronal biomarker and ubiquitin system protein. PRONEU Progress in Neurobiology. 2010;90(3):327-62.
23. Rape M. Ubiquitylation at the crossroads of development and disease. Nature Reviews Molecular Cell Biology. 2018;19(1):59-70.
24. Bishop P, Rocca D, Henley JM. Ubiquitin C-terminal hydrolase L1 (UCH-L1): structure, distribution and roles in brain function and dysfunction. Biochemical Journal. 2016;473(16):2453-62.
25. Cohen-Kaplan V, Livneh I, Avni N, Fabre B, Ziv T, Kwon YT, et al. p62- and ubiquitin-dependent stress-induced autophagy of the mammalian 26S proteasome. Proceedings of the National Academy of Sciences. 2016;113(47):E7490-E9.
26. Fusco C, Mandriani B, Micale L, Malerba N, Cocciadiferro D, Augello B, et al. TRIM50 regulates Beclin 1 proautophagic activity. Biochim Biophys Acta Mol Cell Res Biochimica et Biophysica Acta - Molecular Cell Research. 2018;1865(6):908-19.
27. Bilguvar K, Tyagi NK, Ozkara C, Tuysuz B, Bakircioglu M, Choi M, et al. Recessive loss of function of the neuronal ubiquitin hydrolase UCHL1 leads to early-onset progressive neurodegeneration. procnatiacadscie Proceedings of the National Academy of Sciences of the United States of America. 2013;110(9):3489-94.
28. Costes S, Gurlo T, Rivera JF, Butler PC. UCHL1 deficiency exacerbates human islet amyloid polypeptide toxicity in beta -cells Evidence of interplay between the ubiquitin/proteasome system and autophagy. AUTOPHAGY. 2014;10(6):1004-14.
29. Liu Y, Fallon L, Lashuel HA, Liu Z, Lansbury PT. The UCH-L1 Gene Encodes Two Opposing Enzymatic Activities that Affect a-Synuclein Degradation and Parkinson's Disease Susceptibility. Cell Cell. 2002;111(2):209-18.
30. It Is All about (U)biquitin: Role of Altered Ubiquitin-Proteasome System and UCHL1 in Alzheimer Disease. 2016.
31. Liu H, Povysheva N, Rose ME, Mi Z, Banton JS, Li W, et al. Role of UCHL1 in axonal injury and functional recovery after cerebral ischemia. Proceedings of the National Academy of Sciences of the United States of America. 2019;116(10):4643-50.
32. Zhang D, Han S, Wang S, Luo Y, Zhao L, Li J. cPKCg-mediated down-regulation of UCHL1 alleviates ischaemic neuronal injuries by decreasing autophagy via ERK-mTOR pathway. JCMM Journal of Cellular and Molecular Medicine. 2017;21(12):3641-57.
33. Uddin MS, Al Mamun A, Stachowiak A, Tzvetkov NT, Takeda S, Atanasov AG, et al. Autophagy and Alzheimer's disease: From molecular mechanisms to therapeutic implications. Front Aging Neurosci Frontiers in Aging Neuroscience. 2018;10(JAN).
34. Xie M, Han Y, Yu Q, Wang X, Wang S, Liao X, et al. UCH-L1 Inhibition Decreases the Microtubule-Binding Function of Tau Protein. JAD Journal of Alzheimer's Disease. 2015;49(2):353-63.
35. Das Bhowmik A, Patil SJ, Deshpande DV, Bhat V, Dalal A, SpringerLink. Novel splice-site variant of UCHL1 in an Indian family with autosomal recessive spastic paraplegia-79. 2018.
36. Ichida JK, Kiskinis E. Probing disorders of the nervous system using reprogramming approaches. EMBO J The EMBO Journal. 2015;34(11):1456-77.
37. Takahashi K, Tanabe K, Ohnuki M, Narita M, Ichisaka T, Tomoda K, et al. Induction of Pluripotent Stem Cells from Adult Human Fibroblasts by Defined Factors. CELL - CAMBRIDGE MA-. 2007;131(5):861-72.
38. Rubin LL. Stem Cells and Drug Discovery: The Beginning of a New Era? Cell Cell. 2008;132(4):549-52.
39. Yu J, Vodyanik MA, Smuga-Otto K, Antosiewicz-Bourget J, Frane JL, Tian S, et al. Induced Pluripotent Stem Cell Lines Derived from Human Somatic Cells. Science Science. 2007;318(5858):1917-20.

40. Park IH, Arora N, Huo H, Lensch MW, Daley GQ, Maherali N, et al. Disease-Specific Induced Pluripotent Stem Cells. Cell Cell. 2008;134(5):877-86.
41. Williams EC, Zhong X, Mohamed A, Li R, Liu Y, Dong Q, et al. Mutant astrocytes differentiated from Rett syndrome patients-specific iPSCs have adverse effects on wild-type neurons. Human Molecular Genetics. 2014;23(11):2968-80.
42. Chen KG, Mallon BS, Park K, Robey PG, McKay RDG, Gottesman MM, et al. Pluripotent Stem Cell Platforms for Drug Discovery. Trends Mol Med. 2018;24(9):805-20.
43. Kurreck J, Stein CA, Wiley VCH. Molecular medicine an introduction2016.
44. Nagasaka R, Matsumoto M, Okada M, Sasaki H, Kanie K, Kii H, et al. Visualization of morphological categories of colonies for monitoring of effect on induced pluripotent stem cell culture status. RETH Regenerative Therapy. 2017;6:41-51.
45. Heurtier V, Owens N, Gonzalez I, Mueller F, Proux C, Mornico D, et al. The molecular logic of Nanog-induced self-renewal in mouse embryonic stem cells. Nat Commun Nature Communications. 2019;10(1).
46. Niwa H, Miyazaki J-i, Smith AG. Quantitative expression of Oct-3/4 defines differentiation, dedifferentiation or self-renewal of ES cells. Nat Genet Nature Genetics. 2000;24(4):372-6.
47. MartÌnez-CerdeÒo V. Neural Progenitor Cell Terminology. 2018.
48. Liem Jr KF, Tremml G, Roelink H, Jessell TM. Dorsal Differentiation of Neural Plate Cells Induced by BMP-Mediated Signals from Epidermal Ectoderm. Cell. 1995;82(6):969.
49. Tao Y, Zhang S-C. Neural Subtype Specification from Human Pluripotent Stem Cells. STEM Cell Stem Cell. 2016;19(5):573-86.
50. Riemens RJM, Esteller M, Delgado-Morales R, Riemens RJM, Riemens RJM, van den Hove DLA, et al. Directing neuronal cell fate in vitro: Achievements and challenges. Prog Neurobiol Progress in Neurobiology. 2018;168:42-68.
51. Pasca SP, Panagiotakos G, Dolmetsch RE. Generating Human Neurons In Vitro and Using Them to Understand Neuropsychiatric Disease. Annual Review of Neuroscience. 2014;37:479-501.
52. Bell S, Maussion G, Jefri M, Peng H, Theroux J-F, Silveira H, et al. Disruption of GRIN2B Impairs Differentiation in Human Neurons. Stem Cell Reports Stem Cell Reports. 2018;11(1):183-96.
53. Kanemura Y, Yamasaki M, Kanemura Y, Mori K, Fujikawa H, Hayashi H, et al. Musashi1, an evolutionarily conserved neural RNA-binding protein, is a versatile marker of human glioma cells in determining their cellular origin, malignancy, and proliferative activity. DIF Differentiation. 2001;68(2-3):141-52.
54. Suzuki S, Shibata S, Mastuzaki Y, Okano H, Namiki J. The neural stem/progenitor cell marker nestin is expressed in proliferative endothelial cells, but not in mature vasculature. J Histochem Cytochem Journal of Histochemistry and Cytochemistry. 2010;58(8):721-30.
55. Gerrard L, Rodgers L, Cui W. Differentiation of Human Embryonic Stem Cells to Neural Lineages in Adherent Culture by Blocking Bone Morphogenetic Protein Signaling. Stem cells. 2005;23(9):1234.
56. Yuan F, Fang K-H, Cao S-Y, Qu Z-Y, Li Q, Krencik R, et al. Efficient generation of region-specific forebrain neurons from human pluripotent stem cells under highly defined condition. Sci Rep Scientific Reports. 2016;5(1).
57. Kondo T, Asai M, Tsukita K, Kutoku Y, Ohsawa Y, Sunada Y, et al. Modeling Alzheimer's disease with iPSCs reveals stress phenotypes associated with intracellular Aβ and differential drug responsiveness. Cell Stem Cell. 2013;12(4):487-96.
58. Brennand KJ, Simone A, Jou J, Gelboin-Burkhart C, Tran N, Sangar S, et al. Modelling schizophrenia using human induced pluripotent stem cells. Nature. 2011;473(7346):221-5.

59. Induced pluripotent stem cells from patients with Huntington's disease show CAG-repeat-expansion-associated phenotypes. Cell Stem Cell. 2012;11(2):264-78.
60. Bell S, Hettige NC, Silveira H, Peng H, Wu H, Jefri M, et al. Differentiation of Human Induced Pluripotent Stem Cells (iPSCs) into an Effective Model of Forebrain Neural Progenitor Cells and Mature Neurons. Bio Protoc. 2019;9(5):e3188.
61. Duan L, Bhattacharyya BJ, Belmadani A, Pan L, Miller RJ, Kessler JA. Stem cell derived basal forebrain cholinergic neurons from Alzheimer's disease patients are more susceptible to cell death. Molecular Neurodegeneration. 2014;9(1):3.
62. Lancaster MA, Knoblich JA. Organogenesis in a dish: Modeling development and disease using organoid technologies. science Science. 2014;345(6194):283.
63. Marton RM, Pasca SP. Organoid and Assembloid Technologies for Investigating Cellular Crosstalk in Human Brain Development and Disease. TICB Trends in Cell Biology. 2020;30(2):133-43.
64. Lancaster MA, Renner M, Martin C-A, Wenzel D, Bicknell LS, Hurles ME, et al. Cerebral organoids model human brain development and microcephaly. Nature. 2013;501(7467).
65. Marshall JJ, Mason JO. Mouse vs man: Organoid models of brain development & disease. Brain Research. 2019;1724:146427.
66. Lancaster MA, Knoblich JA. Generation of cerebral organoids from human pluripotent stem cells. Nat Protoc Nature Protocols. 2014;9(10):2329-40.
67. Kadoshima T, Sakaguchi H, Nakano T, Soen M, Ando S, Eiraku M, et al. Self-organization of axial polarity, inside-out layer pattern, and species-specific progenitor dynamics in human ES cell-derived neocortex. procnatiacadscie Proceedings of the National Academy of Sciences of the United States of America. 2013;110(50):20284-9.
68. Shevde NK, Mael AA. Techniques in Embryoid Body Formation from Human Pluripotent Stem Cells. 2013.
69. Eiraku M, Watanabe K, Matsuo-Takasaki M, Kawada M, Yonemura S, Matsumura M, et al. Self-Organized Formation of Polarized Cortical Tissues from ESCs and Its Active Manipulation by Extrinsic†Signals. Cell Stem Cell Cell Stem Cell. 2008;3(5):519-32.
70. Koo B, Choi B, Park H, Yoon KJ. Past, Present, and Future of Brain Organoid Technology. Molecules and cells. 2019;42(9):617-27.
71. Cooke MJ, Phillips SR, Shah DSH, Athey D, Lakey JH, Przyborski SA. Enhanced cell attachment using a novel cell culture surface presenting functional domains from extracellular matrix proteins. Cytotechnology. 2008;56(2):71-9.
72. Li W, Sun W, Zhang Y, Wei W, Ambasudhan R, Xia P, et al. Rapid induction and long-term self-renewal of primitive neural precursors from human embryonic stem cells by small molecule inhibitors. Proceedings of the National Academy of Sciences of the United States of America. 2011;108(20):8299-304.
73. Rocha AJ. Guidelines for Successful Quantitative Gene Expression in Real- Time qPCR Assays. 2016.
74. Burry RW. Controls for Immunocytochemistry An Update. J Histochem Cytochem Journal of Histochemistry & Cytochemistry. 2011;59(1):6-12.
75. Andrews PW, Ben-David U, Benvenisty N, Coffey P, Eggan K, Knowles BB, et al. Assessing the Safety of Human Pluripotent Stem Cells and Their Derivatives for Clinical Applications. Stem cell reports. 2017;9(1):1-4.
76. Andrews PW. The selfish stem cell. NATURE BIOTECHNOLOGY. 2006;24(3):325-6.
77. Hilz H, Wiegers U, Adamietz P. Stimulation of Proteinase K Action by Denaturing Agents: Application to the Isolation of Nucleic Acids and the Degradation of Masked Proteins. FEBS European Journal of Biochemistry. 1975;56(1):103-8.

78. Borra RC, Lotufo MA, Gagioti SM, Barros Fde M, Andrade PM. A simple method to measure cell viability in proliferation and cytotoxicity assays. Brazilian oral research. 2009;23(3).
79. Mariani J, Coppola G, Zhang P, Abyzov A, Provini L, Tomasini L, et al. FOXG1-Dependent Dysregulation of GABA/Glutamate Neuron Differentiation in Autism Spectrum Disorders. Cell. 2015;162(2):375-90.
80. Qian X, Jacob F, Song MM, Nguyen HN, Song H, Ming G-L. Generation of human brain region-specific organoids using a miniaturized spinning bioreactor. Nat Protoc. 2018;13(3):565-80.
81. Topol A, Tran NN, Brennand KJ. A guide to generating and using hiPSC derived NPCs for the study of neurological diseases. J Vis Exp. 2015(96):e52495-e.
82. Pan X, Li X-J, Liu X-J, Yuan H, Li J-F, Duan Y-L, et al. Later Passage Neural Progenitor Cells from Neonatal Brain Are More Permissive for Human Cytomegalovirus Infection. Journal of virology. 2013;87.
83. Boldrini M, Fulmore CA, Tartt AN, Simeon LR, Pavlova I, Poposka V, et al. Human Hippocampal Neurogenesis Persists throughout Aging. Cell Stem Cell. 2018;22(4):589-99.e5.
84. Lodato MA, Ng CW, Wamstad JA, Cheng AW, Thai KK, Fraenkel E, et al. SOX2 co-occupies distal enhancer elements with distinct POU factors in ESCs and NPCs to specify cell state. PLoS Genet. 2013;9(2):e1003288-e.
85. Nedelsky NB, Todd PK, Taylor JP. Autophagy and the ubiquitin-proteasome system: Collaborators in neuroprotection. Biochimica et Biophysica Acta (BBA) - Molecular Basis of Disease Biochimica et Biophysica Acta (BBA) - Molecular Basis of Disease. 2008;1782(12):691-9.
86. Galluzzi L, Galluzzi L, Galluzzi L, Galluzzi L, Green DR. Autophagy-Independent Functions of the Autophagy Machinery. Cell Cell. 2019;177(7):1682-99.
87. Kim YC, Guan K-L. mTOR: a pharmacologic target for autophagy regulation. The Journal of Clinical Investigation. 2015;125(1):25-32.
88. NavÈ BT, Ouwens M, Withers DJ, Alessi DR, Shepherd PR. Mammalian target of rapamycin is a direct target for protein kinase B: identification of a convergence point for opposing effects of insulin and amino-acid deficiency on protein translation. Biochemical Journal. 1999;344(Pt 2):427-31.
89. Peterson RT, Beal PA, Comb MJ, Schreiber SL. FKBP12-Rapamycin-associated Protein (FRAP) Autophosphorylates at Serine 2481 under Translationally Repressive Conditions. JBC Journal of Biological Chemistry. 2000;275(10):7416-23.
90. Faes S, Demartines N, Dormond O. Resistance to mTORC1 Inhibitors in Cancer Therapy: From Kinase Mutations to Intratumoral Heterogeneity of Kinase Activity. Oxidative Medicine and Cellular Longevity. 2017;2017:1726078.
91. Ganley IG, Lam DH, Wang J, Ding X, Chen S, Jiang X. ULK1.ATG13.FIP200 complex mediates mTOR signaling and is essential for autophagy. J Biol Chem. 2009;284(18):12297-305.
92. Mason JO, Price DJ. Building brains in a dish: Prospects for growing cerebral organoids from stem cells. Neuroscience. 2016;334:105-18.
93. Quadrato G, Brown J, Arlotta P. The promises and challenges of human brain organoids as models of neuropsychiatric disease. Nat Med. 2016;22(11):1220-8.
94. Shi Y, Sun L, Wang M, Liu J, Zhong S, Li R, et al. Vascularized human cortical organoids (vOrganoids) model cortical development in vivo. PLoS biology. 2020;18(5).
95. Tarnowski BI, Spinale FG, Nicholson JH. DAPI as a Useful Stain for Nuclear Quantitation. Biotechnic & Histochemistry Biotechnic & Histochemistry. 1991;66(6):296-302.

1. Appendix 1: Materials

1.1 Coating of Cultureware

Table 2: Volumes of Geltrex™, Matrigel® and Poly-L-Ornithine/Laminin used for various cultureware.

Cultureware	Volume	Supplier	Catalog number
96-well plate	50 µL	Sarstedt & Co.	83.3924
48-well plate	150 µL	Sarstedt & Co.	83.3923
24-well plate	300 µL	Sarstedt & Co.	83.3922
12-well plate	500 µL	Sarstedt & Co.	83.3921
6-well plate	1 mL	Sarstedt & Co.	83.3920

Table 3: Reagents used for Geltrex™ and Matrigel® coating.

Reagents	Supplier	Catalog number
Geltrex™	Gibco, Thermo Fisher Scientific	A14133-02
Matrigel® Matrix	Corning	356234
DMEM/F12 (1X)	Gibco, Thermo Fisher Scientific	11330-032

Table 4: Reagents used for Poly-L-Ornithine/Laminin coating.

Reagents	Supplier	Catalog number
Poly-L-Ornithine	Sigma-Aldrich	P4957
PBS (1X)	Thermo Fisher Scientific	BR0014G
Cultrex 3D Laminin I	R&D Systems	3446-005-01
DMEM/F12 (1X)	Gibco, Thermo Fisher Scientific	11330-032

1.2 Cell Culture iPSC

The medium used for iPSC culture was partly self-made. 0.271g of $NaHCO_3$ was added to 0.5 L of DMEM/F12 under stirring. The pH was adjusted to 7.4 using 100 Mm NaOH and filtered before adding the rest of the reagents. The reagents are listed in table 5. To make the complete E8 medium (E8 (+) medium) to use for the iPSC culture, essential 8 supplement and basal E8 medium from Thermo Fisher Scientific were added to the self- made E8 medium. See table 6 for reagents and volumes.

Table 5: Reagents and amounts used to make the self-made E8 medium, a component for the final E8 (+) medium.

Reagents	Amount	Supplier	Catalog number
DMEM/F12	1,0 L	Gibco, Thermo Fisher Scientific	11330-032
Pen Strep	10 mL	Gibco, Thermo Fisher Scientific	15140-122
Ascorbic acid 2-phosphate	64 mg/L	Sigma-Aldrich	A8960
Sodium selenite	14 µg/L	Sigma-Aldrich	S5261
$NaHCO_3$	534 mg/L	Sigma-Aldrich	S6014
Insulin	20 mg/L	Sigma-Aldrich	I9278
Human recombinant transferrin	10,7 mg/L	Sigma-Aldrich	T3705
FGF-2	100 µg/L	Peprotech	100-18B
TGF-β1	2,0 µg/L	Peprotech	100-21C

Table 6: List of reagents needed to make the complete E8 (+) medium to use for iPSC culture.

Reagents	Amount	Supplier	Catalog number
Homemade E8 medium	250 mL	Self-made	
Essential 8 supplement (50X)	2,0 mL	Gibco, Thermo Fisher Scientific	A2858501
Basal E8 medium	100 mL	Gibco, Thermo Fisher Scientific	A2858501

Table 7: Reagents used for iPSC culture and passage.

Reagents	Supplier	Catalog number
E8 (+) Medium	Partly self-made (see table 6)	
D-PBS (1X)	Thermo Fisher Scientific	14190-144
6-well standard plate	Sarstedt & Co	83.3920
UltraPure™ 0.5M EDTA	Thermo Fisher Scientific	15575020

Table 8: Reagents used to store iPSCs in -80°C.

Reagents	Supplier	Catalog number
D-PBS (1X)	Thermo Fisher Scientific	14190-144
Cell scraper	Sarstedt & Co.	83.3952
PBS (1X)	Thermo Fisher Scientific	BR0014G

Table 9: Reagents used for NPC passage.

Reagents	Supplier	Catalog Number
6-well standard plate	Sarstedt & Co.	83.3920
D-PBS (1X)	Thermo Fisher Scientific	14190-144
Accutase	Stemcell Technologies	07920
DMEM/F12 (1X)	Gibco, Thermo Fisher Scientific	11330-032
Trypan Blue Stain 0,4%	Invitrogen by Thermo Fisher Scientific	T10282
10 µM Y-27632 (Rock inhibitor)	Stemcell Technologies	72304
Countess™ Counting Chamber Slides	Invitrogen by Thermo Fisher Scientific	C10228

Table 10: Reagents and volumes used to make the neural stem cell (NSC) medium used for NPCs in passage 0 following monolayer protocol 1.

Reagents	Volume	Supplier	Catalog number
DMEM/F12 (1X)	25 mL	Gibco, Thermo Fisher Scientific	11330-032
Pen Strep	0.5 mL	Gibco, Thermo Fisher Scientific	15140-122
Neurobasal-A medium (1X)	25 mL	Gibco, Thermo Fisher Scientific	10888-022
Glutamax (100X)	0.25 mL	Thermo Fisher Scientific	35050061
50 µg/mL BSA	100 µL	Sigma Aldrich	05470-1g
N2 supplement (100X)	0.5 mL	Gibco, Thermo Fisher Scientific	17502-001
B-27® Supplement (50X)	1.0 mL	Gibco, Thermo Fisher Scientific	12587-001
10 ng/mL Human Lif	5 µL	Peprotech	300-05
4 µM CHIR99021	20 µL	Tocris/Biotechne	4423
3 µM SB431542	7.5 µL	Stemcell Technologies	72234
0.1 µM Compound E	2.5 µL	Tocris/Biotechne	6476
10 µM Y-27632	50 µL	Stemcell Technologies	72304

Table 11: Reagents and volumes used to make the neural progenitor medium (NEM) used for NPCs in passage 1 to 5 following monolayer protocol 1, a modification of Li *et al.*

Reagents	Volume	Supplier	Catalog number
DMEM/F12 (1X)	25 mL	Gibco, Thermo Fisher Scientific	11330-032
Pen Strep	0.5 mL	Gibco, Thermo Fisher Scientific	15140-122
Neurobasal-A medium (1X)	25 mL	Gibco Thermo Fisher Scientific	10888-022
Glutamax (100X)	0.25 mL	Thermo Fisher Scientific	35050061
N2 supplement (100X)	0.5 mL	Gibco, Thermo Fisher Scientific	17502-001
B-27® Supplement (50X)	1 mL	Gibco, Thermo Fisher Scientific	12587-001
1 µg/mL Laminin	50 µL	Sigma Aldrich	L2020

10 ng/mL FGF-2	5 µL	Peprotech	100-18B
10 ng/mL human EGF	5 µL	R&D Systems	236-EG-200
20 ng/mL BDNF	10 µL	Peprotech	450-02

Table 12: Specific reagents used for the monolayer culture by Stemcell Technologies.

Reagents	Supplier	Catalog number
STEMdiff™ SMADi Neural Induction Kit	Stemcell Technologies	08580
STEMdiff™ Neural Progenitor Medium	Stemcell Technologies	05833

Table 13: Specific reagents used for the embryoid body protocol by Stemcell Technologies.

Reagents	Supplier	Catalog Number
AggreWell™ 800 24-well Plate	Stemcell Technologies	34811
Anti-Adherence Rising Solution	Stemcell Technologies	07010
STEMdiff™ SMADi Neural Induction Kit	Stemcell Technologies	08580
40 µm Cell Strainer	Corning	431750
STEMdiff™ Neural Rosette Selection Reagent	Stemcell Technologies	05832

Table 14: Reagents used to store live NPCs in the nitrogen tank.

Reagents	Supplier	Catalog number
Dimethyl sulfoxide (DMSO)	Sigma Aldrich	472301-500ML-D

Table 15: Reagents used to store cell pellets of NPCs at -80ºC.

Reagents	Supplier	Catalog number
PBS (1X)	Thermo Fisher Scientific	BR0014G

1.3 qPCR

Table 16: Reagents used for RNA isolation.

Reagents	Supplier	Catalog number
RNeasy® Mini Kit (250)	Qiagen	74106
b-mercaptoethanol	Sigma-Aldrich	M6250
EtOH 70%	VWR Chemicals	64-17-5
Nuclease-Free Water	Ambion	AM9938
RNAse-Free DNAse Set (50)	Qiagen	79254

Table 17: Amount of RNA obtained from RNA isolation of iPSC.

Sample	Amount of RNA (ng/µL)	Volume 1000ng RNA (µL)	Volume H_2O (µL)
AGc1	241,8	4,1	5,9
AGc6	694,1	1,4	8,6
Bc4	666,4	1,5	8,5
Bc9	745,9	1,3	8,7
Tc3	310,6	3,2	6,8

Table 18: Amount of RNA obtained from RNA isolation of NPC.

Sample	Amount of RNA (ng/µL)	Volume 1000ng RNA (µL)	Volume H_2O (µL)
AGc1	338,9	3,0	7,1
AGc6	115,7	8,6	1,4
Bc4	124,1	8,1	2,0
Bc9	120,1	8,3	1,7
Tc3	126,0	7,9	2,1

Table 19: Reagents used for the cDNA synthesis.

Reagents	Supplier	Catalog number
High-Capacity cDNA Reverse Transcription Kit	Thermo Fisher Scientific	4368814
Nuclease-Free Water	Ambion	AM9938

Table 20: Volume of reagents in the DNase mastermix.

Reagents	Volume (µL)
Buffer	2,0
dNTPs	0,8
Random Primer	2,0
MMLV	1,0
H_2O	4.2

Table 21: Running program used for the DNA synthesis using the Bio-Rad T100 Thermal Cycler.

Temperature (ºC)	Time (minutes)
25	10
37	120
85	5
4	∞

Table 22: Reagents used for the qPCR set-up.

Reagents	Supplier	Catalog number
Power SYBR® Green PCR master mix (2X)	Thermo Fisher Scientific	4368577
Nuclease-Free Water	Ambion	AM9938

Table 23: Reagents and volumes to make the qPCR reaction mix with a final volume of 20 µL.

Reagents	Volume (µL)
2x buffer	10
Forward primer	1
Reverse primer	1
H_2O	5

Table 24: List of primers used for iPSC and NPC characterization.

Gene	Forward primer	Reverse primer
b-actin	GTTACAGGAAGTCCCTTGCCATCC	CACCTCCCCTGTGTGGACTTGGG
Nanog	TGCGTCACACCATTGCTATTTTC	AATACCTCAGCCTCCAGCAATG
Oct4	GTACTCCTCGGTCCCTTTCC	CAAAAACCCTGGCACAAACT
Sox2	GCCGAGTGGAAACTTTTGTCG	GGCAGCGTGTACTTATCCTTCT
Nestin	GGCGCACCTCAAGATGTCC	CTTGGGGTCCTGAAAGCTG
DcX	TCAGGGAGTGCGTTACATTTAC	GTTGGGATTGACATTCTTGGTG
Sox1	TACAGCCCCATCTCCAACTC	GCTCCGACTTCACCAGAGAG

Table 25: List of primers detecting autophagic markers.

Gene	Forward primer	Reverse primer
b-actin	GTTACAGGAAGTCCCTTGCCATCC	CACCTCCCCTGTGTGGACTTGGG
BECN1	AAGAGGTTGAGAAAGGCGAG	TGGGTTTTGATGGAATAGGAGC
p62	AGGACAAATTGCGCCCATTT	TCTCTTTCAGGGACAGGCTG
LAMP1	GGGCCTCTGTTCCTTTCTCT	GTCCTCGTCTTTCTCCTGCT
LC3A	GTTGGTCAAGATCATCCGGC	TGAGGACTTTGGGTGTGGTT
LC3B	AACGGGCTGTGTGAGAAAAC	CCCACTGACCTAAACCCCAT
mTOR	GCAGTGCTGTGAAAAGTGGA	CCCCTCCAAATCCCTTCACT
CTSD	AACTGCTGGACATCGCTTGCT	CATTCTTCACGTAGGTGCTGGA

1.4 Immunocytochemistry iPSC and NPC

Table 26: Reagents used for immunocytochemistry.

Reagents	Supplier	Catalog number
Paraformaldehyde	Merck	30525-89-4
PBS (1X)	Thermo Fisher Scientific	BR0014G
Triton-X	Sigma Aldrich	9002-93-1

Blocking buffer – BSA – Triton-X – Normal goat serum	 Sigma Aldrich Sigma Aldrich Thermo Fisher Scientific	 05470-1g 9002-93-1 10000C

Table 27: Primary antibodies used for characterization of iPSC by immunocytochemistry.

Name	Host	Dilution	Supplier	Catalog number
Nanog	Rabbit	1:200	Cell Signaling Technology	4903
SSEA4	Mouse	1:200	Cell Signaling Technology	4755
Oct4	Rabbit	1:200	Cell Signaling Technology	2840

Table 28: Primary antibodies used for characterization of NPCs by immunocytochemistry.

Name	Host	Dilution	Supplier	Catalog number
Oct4	Rabbit	1:200	Cell Signaling Technology	2840
MSI-1	Rabbit	1:200	Merck	AB5977
Nestin	Rabbit	1:200	Merck	ABD69
Sox2	Mouse	1:200	Thermo Fisher Scientific	MA1-014

Table 29: Secondary Antibodies used for immunocytochemistry of iPSC and NPC. Dapi is a compound which binds to the AT-regions of the DNA and emits blue, fluorescent light in both live and fixed cells. This compound can therefore show the nuclei of the cell and assess the cell morphology (95).

Name	Host	Target	Dilution	Supplier	Catalog number
A488	Goat	Mouse	1:500	Thermo Fisher Scientific	A32723
A594	Goat	Rabbit	1:500	Thermo Fisher Scientific	A32740
Dapi			1:1000	Thermo Fisher Scientific	62248

1.5 Germ Layer Differentiation

Table 30: Reagents used for cell culture to the three germ layers, ectoderm, mesoderm and endoderm.

Reagents	Supplier	Catalog number
STEMdiff Trilineage Differentiation Kit	Stemcell Technologies	05230
E8 (+) Medium	Partly self-made (see table 6) Thermo Fisher Scientific	
24-well plate	Sarstedt & Co.	83.3922

Table 31: Plating densities for differentiation to ectoderm, mesoderm and endoderm in 24-well plates.

Lineage	Cell Density (cells/cm^2)	Total number of cells in 24-well plate
Ectoderm	200 000	400 000
Mesoderm	50 000	100 000
Endoderm	200 000	400 000

Table 32: Primary antibodies used for immunocytochemistry after germ layer differentiation.

Name	Host	Dilution	Supplier	Catalog number
Oct4	Rabbit	1:400	Cell Signaling Technology	2840
Brachyury	Goat	1:500	R&D Systems	AF2085
Sox17	Goat	1:200	R&D Systems	AF1924
Nestin	Rabbit	1:250	Sigma-Aldrich	ABD69
Pax6	Mouse	1:500	Sigma-Aldrich	MAB5552

Table 33: Secondary Antibodies used for immunocytochemistry after germ layer differentiation.

Name	Host	Target	Dilution	Supplier	Catalog number
Goat anti-mouse A488	Goat	Mouse	1:500	Thermo Fisher Scientific	A32723
Goat anti-rabbit A594	Goat	Rabbit	1:500	Thermo Fisher Scientific	A32740
Goat anti-rabbit A488	Goat	Rabbit	1:500	Thermo Fisher Scientific	A11008
Donkey anti-goat A594	Donkey	Goat	1:500	Thermo Fisher Scientific	A11058

1.6 Karyotyping

Table 34: Reagents used for karyotyping.

Reagents	Supplier	Catalog number
hPSC Genetic Analysis Kit	Stemcell Technologies	07550
DNeasy® Blood and Tissue Kit	Qiagen	69506
Nuclease-Free Water	Ambion	AM9938
MicroAmp® Fast 96-Well Reaction Plate	Applied Biosystems, Thermo Fisher Scientific	4346907
MicroAmp® Optical adhesive film	Applied Biosystems, Thermo Fisher Scientific	4311971
Multiply® mStrip Pro 8-Strip	Sarstedt & Co.	72.991.002

Table 35: Amount of DNA obtained from the DNA isolation, volumes of sample and H_2O used for each sample.

Sample	Amount of DNA (ng/ µL)	300 ng DNA (µL)	H_2O (µL)
Control AGc1	44,5	6,7	83,3
Control ATc2	65,4	4,6	85,4
Patient Bc4	56,1	5,3	84,7
Patient Bc6	62,3	4,8	85,2
Patient Bc9	65,6	4,6	85,4
Patient Tc3	74,2	4,0	86,0
Patient Tc9	71,9	4,2	85,8
Patient Tc18	83,5	3,6	86,4

Calculations used for finding the volumes of primer-probe mix and nuclease-free water:
Number of reactions per primer probe = (number of genomic DNA samples (including control) to be analyzed * 3) + n

– Where 6 – 10 samples, n = 3

The number of samples for this experiment was 9, including control.
Number of reactions per primer probe = 9*3 + 3
Number of reactions per primer probe = 30

Volume of nuclease-free water = number of reactions per primer-probe X 1,5 µL.
Volume of nuclease-free water = 30 * 1,5 µL
Volume of nuclease-free water = 45 µL

Volume of primer-probe stock solution = number of reactions per primer-probe x 0,5 µL.
Volume of primer-probe stock solution = 30 x 0,5 µL
Volume of primer-probe stock solution = 15 µL

The total volume for each sample: 45 µL + 15 µL = 60 µL.

1.7 Cell Viability Assay and Proliferation Assay

Table 36: Reagents used for viability assay and proliferation assay

Reagent	Supplier	Catalog number
Bortezomib	MedChemExpress	HY-10227
Epoxomicin	MedChemExpress	HY-13821
MG132	Sigma Aldrich	M7449
Dimethyl sulfoxide (DMSO)	Sigma Aldrich	472301-500ML-D
PrestoBlue™ Cell Viability Reagent	Invitrogen by Thermo Fisher Scientific	A13262

1.8 Western Blot

Table 37: Reagents used for treatment with Bafilomycin A1 and collection of cells.

Reagents	Supplier	Catalog number
Bafilomycin A1	Santa Cruz Biotechnology	SC-201550A
Ethanol	VWR Chemicals	20821.310
PBS	Thermo Fisher Scientific	BR0014G
Accutase	Stemcell Technologies	07920

Table 38: Reagents used for protein extraction and measurement.

Reagents	Volume	Supplier	Catalog number
Master mix used for protein extraction			
RIPA buffer – 50 mM Tris (7,4 pH) – 15 mM NaCl – 1% NP40 – 0,5% Na-Deoxycholate – 1% SDS – 10 mM EGTA – 10% $MgCl_2$	500 µL	 Merck Merck Merck Merck Thermo Fisher Scientific Merck Merck	 10708976001 106404 492018 D6750 28312 E3889 105833
Phosphatase inhibitor cocktail 2	5 µL	Sigma Aldrich	P5726
Phosphatase inhibitor cocktail 3	5 µL	Sigma Aldrich	P0044
Complete	10 µL	Roche	11697498001
DTT	0,5 µL	Thermo Fisher Scientific	P2325
Micrococcal nuclease	0,5 µL	Thermo Fisher Scientific	88216
Benzonase	0,5 µL	EMD Millipore	E1014
RNase A	0,5 µL	Sigma Aldrich	12091021
Omni Cleave	0,5 µL	Epicentre Technologies	OC7850K
Reagent used for measurement of protein concentration			
Bio-Rad Protein Assay Dye Reagent Concentrate	Bio-Rad	5000006	

When measuring the protein concentrations for the cells collected after treatment with bafilomycin and ethanol, all of the concentrations were low. The volume of sample loaded in the gels are higher than recommended to ensure a positive result on the membrane later on.

Table 39: Protein Concentrations used for Western blot for measuring autophagic flux. The protein concentration is calculated using the K-factor = 22,02 for quantification of protein samples. Cells treated with Bafilomycin is indicated with "Baf1" while the vehicle controls are indicated with "VC". 8-10 µL of LDS and 4 µL of DTT was added to each sample to reach a total volume of approximately 32 µL.

Sample	**Average absorbance (AU)**	**Concentration (µg/ µL)**	**Volume 50 ng (µL)**	**Volume H_2O (µL)**	**Total Volume (µL)**
Control AGc1 (BAF)	56,5	2,66	19,5	0	32
Control AGc1 (VHC)	62,0	2,8	17,8	0,2	32
Control AGc6 (BAF)	-14,0	-0,6	-78,7	0	32
Control AGc6 (VHC)	-20,5	-0,9	-53,8	0	32
Patient Bc4 (BAF)	97,0	4,4	11,4	6,6	32
Patient Bc4 (VHC)	36,0	1,6	18,7	0	32
Patient Bc9 (BAF)	60,5	2,7	18,2	0	32
Patient Bc9 (VHC)	-16,5	-0,7	29,0	0	32

Table 40: Reagents used for application of gel and western blot.

Reagents	**Supplier**	**Catalog number**
LDS Sample Buffer (4X)	Thermo Fisher Scientific	1771790
DTT	Thermo Fisher Scientific	P2325
NuPAGE™ MOPS SDS Running buffer (20X)	Thermo Fisher Scientific	NP0001
MES Running buffer (pH 7,3) – 50 mM MES – 50 mM Tris – 1 mM EDTA – 0,1% SDS	 Merck Merck Thermo Fisher Scientific Thermo Fisher Scientific	 1.06126.1000 10708976001 15575020 28312
NuPAGE™ Transfer buffer (20X)	Thermo Fisher Scientific	NP0006
Trans-Blot Mini 0,2 µm PVDF Transfer Pack	Bio-Rad	1704156
Methanol	Thermo Fisher Scientific	M/4056/PB17
PBS-T – Tween® 20 – PBS – dH_2O	 VWR Chemicals Thermo Fisher Scientific	 28829.296 BR0014G
PBS	Thermo Fisher Scientific	BR0014G
Milk powder (1% fat)	Normilk Levanger	

Table 41: Primary antibodies used for western blot measuring autophagic flux by LC3 and p62.

Name	Host	Dilution	Supplier	Catalog Number
LC3	Rabbit	1:1000	Cell Signaling Technology	3868S
p62	Guineapig	1:2000	Progen	GP62-C

Table 42: Secondary antibodies used for western blot measuring autophagic flux by LC3 and p62.

Name	Host	Target	Dilution	Supplier	Catalog Number
IRDye® 680 RD	Goat	Rabbit	1:25000	Li-Cor	926-68071
IRDye® 800 RD	Donkey	Guineapig	1:25000	Li-Cor	926-32411

1.9 Cerebral Organoids

Table 43: Reagents and volumes used for to make 50 mL the EB medium. This medium was used from day 1 after passage on the EBs grown in the 96-well plate.

Reagents	Volume	Supplier	Catalog number
DMEM/F12 (1X)	40 mL	Gibco, Thermo Fisher Scientific	11330-032
Pen Strep	0.4 mL	Gibco, Thermo Fisher Scientific	15140-122
Knockout Serum Replacement	10 mL	Thermo Fisher Scientific	10828028
Fetal Bovine Serum (FBS)	1.5 mL	Thermo Fisher Scientific	A3160802
MEM NEAA	0.5 mL	Thermo Fisher Scientific	11140050
2-mercaptoethanol	1.0 µL	Merck	8057400005
bFGF (15 ng/µL)	10 µL	Thermo Fisher Scientific	13256029

Table 44: Reagents and volumes used to make 50 mL of the Neural Differentiation Medium (NDM) modified from Mariani J (79). This medium was used from the start of the iPSC passage and until day 7 of EB culture.

Reagents	Volume	Supplier	Catalog number
DMEM/F12 (1X)	50 mL	Gibco, Thermo Fisher Scientific	11330-032
Pen Strep	0.5 mL	Gibco, Thermo Fisher Scientific	15140-122
N2 Supplement	0.5 mL	Thermo Fisher Scientific	17502048
B-27 without Vit-A	1.0 mL	Thermo Fisher Scientific	12587010

2-mercaptoethanol (50 µM)	50 µL	Thermo Fisher Scientific	31350010
Noggin (100 ng/mL)	10 µL	R&D Systems	1967-NG-025

Table 45: Reagents and volumes used to make 50 mL for the Neural Induction Medium (NIM) used to culture the EBs in the 24-well plate.

Reagents	**Volume**	**Supplier**	**Catalog number**
DMEM/F12 (1X)	50 mL	Gibco, Thermo Fisher Scientific	11330-032
Pen Strep	0.5 mL	Gibco, Thermo Fisher Scientific	15140-122
N2 Supplement	0.5 mL	Thermo Fisher Scientific	17502048
MEM NEAA	0.5 mL	Thermo Fisher Scientific	11140050
Heparin (5 mg/ml)	50 µL	Sigma Aldrich	H3149

Table 46: Reagents and volumes used to make 50 mL the Differentiation Medium for culture in Matrigel® and in bioreactor/orbital shaker.

Reagents	**Volume**	**Supplier**	**Catalog number**
DMEM/F12 (1X)	25 mL	Gibco, Thermo Fisher Scientific	11330-032
Neurobasal-A medium (1X)	25 mL	Gibco, Thermo Fisher Scientific	10888-022
Pen Strep	0.5 mL	Gibco, Thermo Fisher Scientific	15140-122
Glutamax (100X)	0.25 mL	Thermo Fisher Scientific	35050061
N2 Supplement	0.25 mL	Thermo Fisher Scientific	17502048
MEM NEAA	0.25 mL	Thermo Fisher Scientific	11140050
Insulin	12.5 µL	Sigma Aldrich	I9278
2-mercaptoethanol (50 µM)	17.5 µL	Thermo Fisher Scientific	31350010
B-27 without Vit-A*	0.5 mL	Thermo Fisher Scientific	12587010
B-27 with Vit-A**	0.5 mL	Thermo Fisher Scientific	17504044

*For the culture in Matrigel® B-27 without vitamin A was used.
**For the culture in the bioreactor/orbital shaker B-27 with vitamin A was used.

Table 47: Reagents used for the preparation of cerebral organoids for cryosectioning and immunohistochemistry.

Reagents	**Supplier**	**Catalog number**
PBS (1X)	Thermo Fisher Scientific	BR0014G
Paraformaldehyde	Merck	30525-89-4

Sucrose (saccharose)	Merck	1.07687
Erythrosine 239	Ral Diagnostics	45430
Tissue OCT	VWR	00411243

Table 48: Reagents used for immunohistochemistry of cerebral organoid tissue.

Reagents	**Supplier**	**Catalog number**
PBS-T – Tween® 20 – PBS – dH_2O	 VWR Chemicals Thermo Fisher Scientific	 28829.296 BR0014G
Blocking buffer – BSA – Triton-X – Normal goat serum	 Sigma Aldrich Sigma Aldrich Thermo Fisher Scientific	 05470-1g 9002-93-1 10000C
PBS	Thermo Fisher Scientific	BR0014G
Dapi	Thermo Fisher Scientific	62248
Ultra-pure water	Millipore	SYNSVHFWW
Prolong Gold antifade reagent with DAPI	Thermo fisher Scientific	P36935

Table 49: Primary antibodies used for immunohistochemistry of cerebral organoid tissue. The dilutions vary from 1:200 – 1:1000.

Name	**Host**	**Dilution**	**Supplier**	**Catalog Number**
Sox2	Rabbit	1:200 – 1:1000	Cell Signaling Technology	3579
Tuj1	Mouse	1:200 – 1:1000	R&D Systems	MAB1196
Nestin	Rabbit	1:200 – 1:1000	Sigma-Aldrich	ABD69
Pax6	Mouse	1:200 – 1:1000	BioLegend	862002

Table 50: Secondary antibodies used for immunohistochemistry of cerebral organoid tissue. The dilutions vary from 1:500 – 1:2000. The dilutions used for each result is indicated in the figure text of the result part.

Name	**Host**	**Target**	**Dilution**	**Supplier**	**Catalog Number**
A488 Goat anti-mouse	Goat	Mouse	1:500 – 1:2000	Thermo Fisher Scientific	A32723
A594 Goat anti-rabbit	Goat	Rabbit	1:500 – 1:2000	Thermo Fisher Scientific	A11008
A647 Goat anti- rabbit	Goat	Rabbit	1:500 – 1:2000	Thermo Fisher Scientific	A21244

2. Appendix 2: Plate Layout

2.1 qPCR

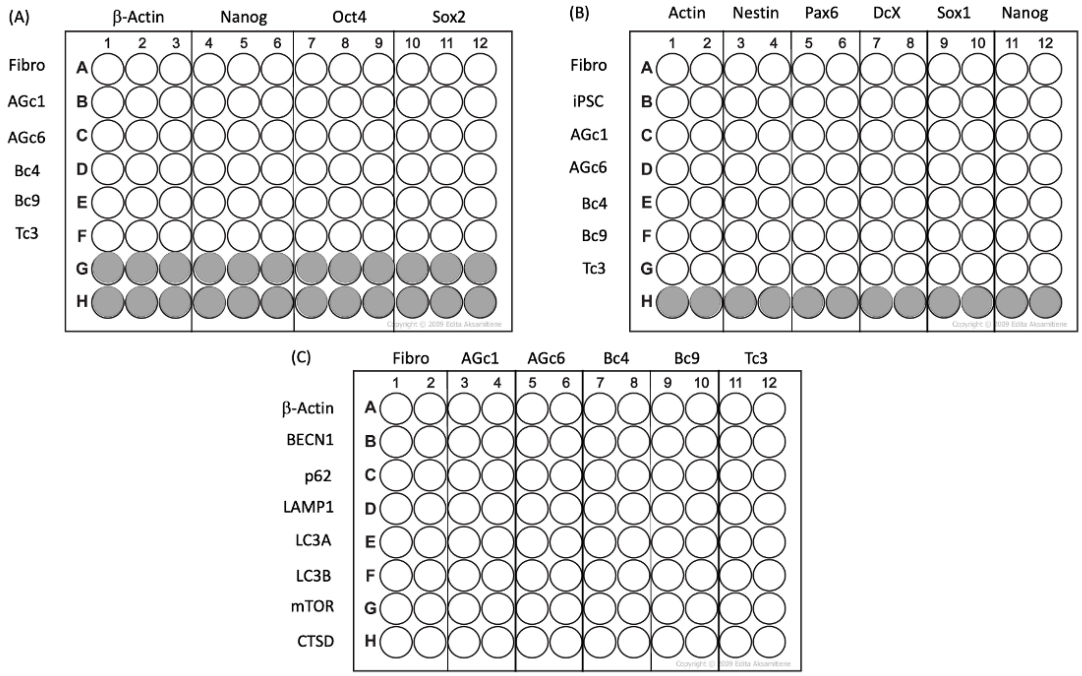

Figure 33: qPCR lay-out using the 96-well qPCR plate. (A) iPSC characterization. (B) NPC characterization. (C) Detecting autophagic markers in NPCs. The grey wells were not in use.

2.2 Karyotyping

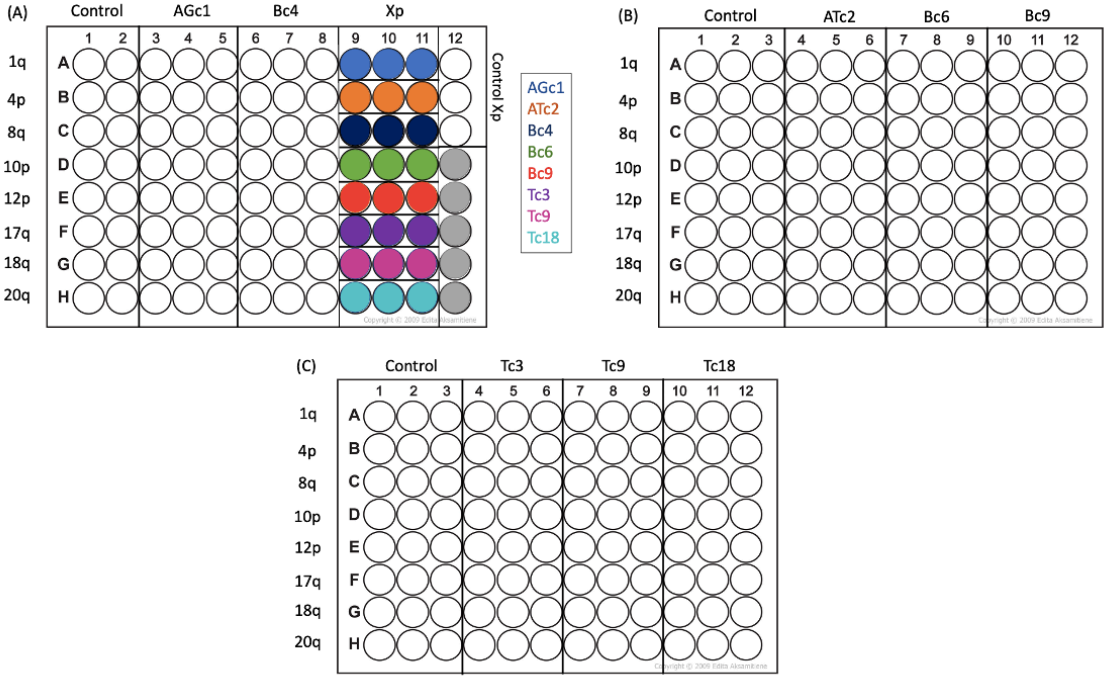

Figure 34: qPCR lay-out for Karyotyping. Lay-out for (A) Plate 1. (B) Plate 2. (C) Plate 3. The grey wells were not in use.

2.3 Viability Assay

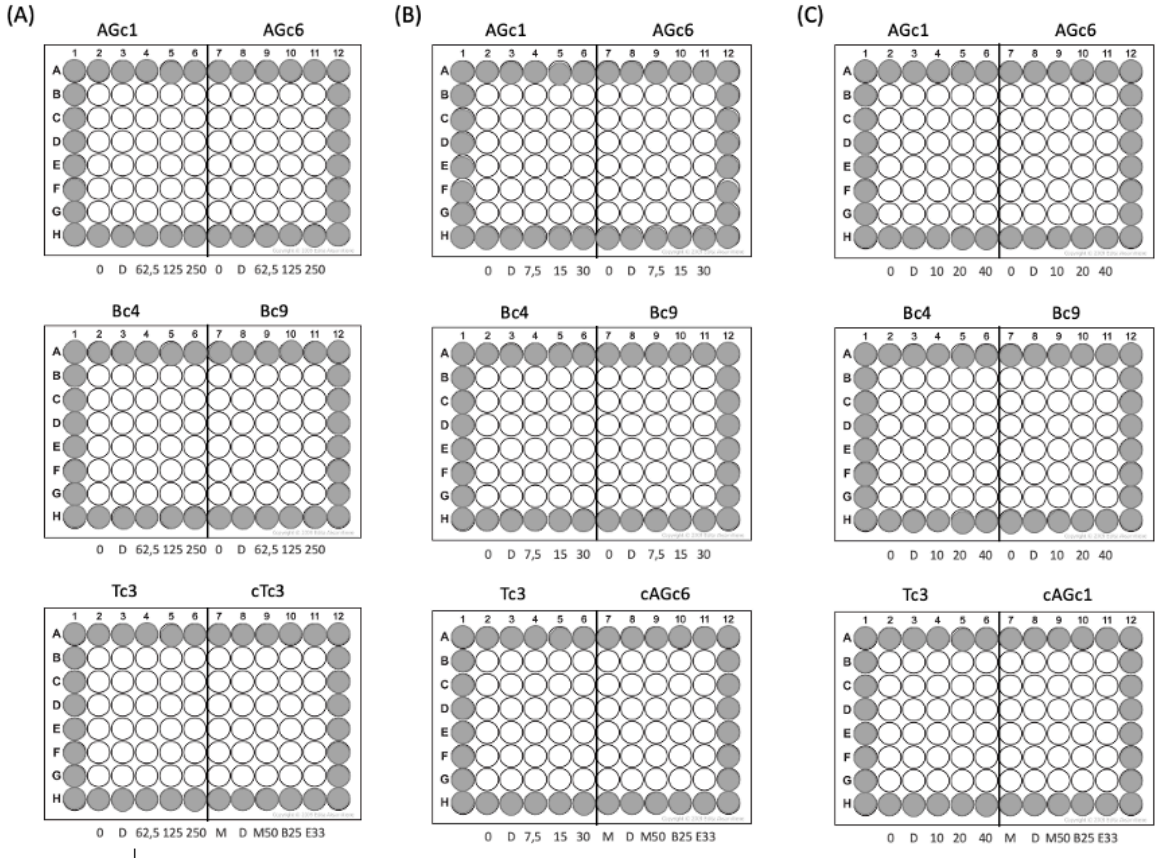

Figure 35: Set-up for viability assay. (A) MG132. (B) Bortezomib. (C) Epoxomicin. The grey wells were not in use.

2.4 Proliferation Assay

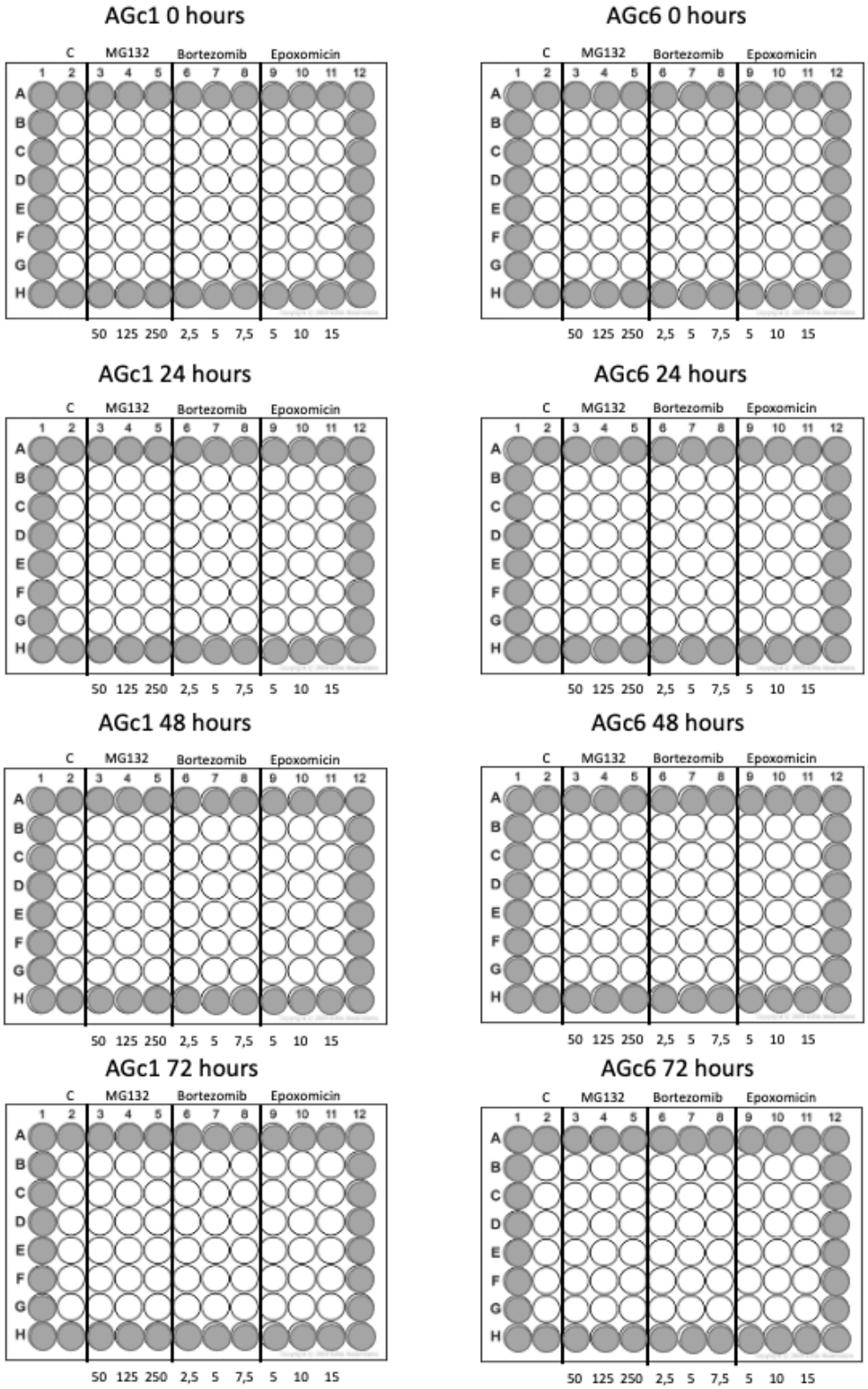

Figure 36: Set-up for proliferation assay. C is designated control for the plate where the DMSO were added. The grey wells were not in use.

3. Appendix 3: Supplementary Results

3.1 Loading Controls for Viability Assay

As the results show a baseline fluorescence correlating to approximately 4000 cells, a loading control experiment was conducted to verify where the baseline fluorescence originated from. We wanted to check the baseline fluorescence for PrestoBlue™ plus: (i) only medium; (ii) medium plus DMSO, and (iii) cells treated with high amounts of UPS inhibitors to check the fluorescence emitted from dead cells incubated with the drugs.

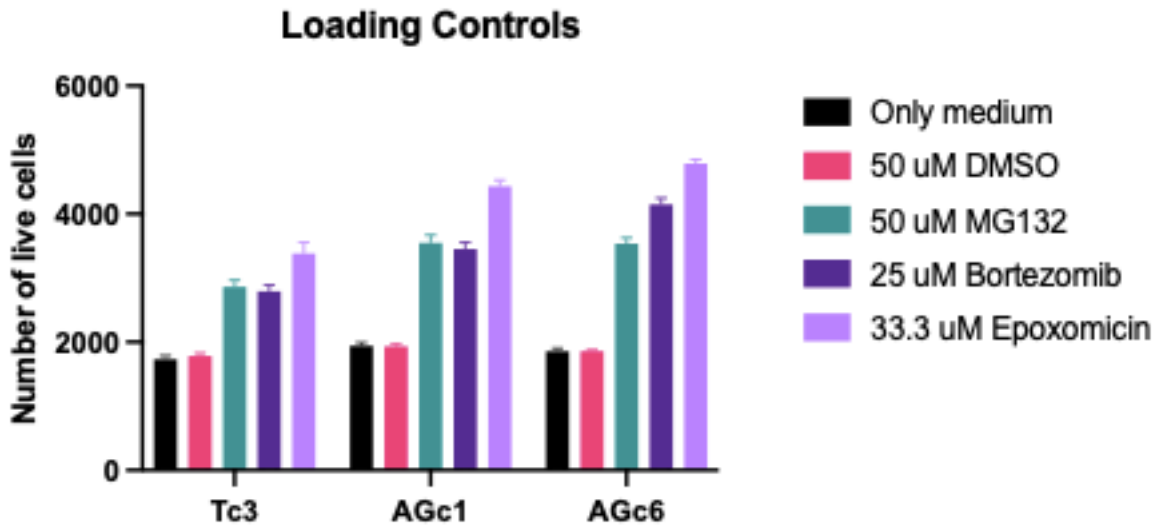

Figure 37: Control experiment used to evaluate the background fluorescence in different conditions. Medium = Only medium and no cells. DMSO = Medium with 50 µM of DMSO and no cells. For the three next conditions, a high concentration of the drugs was used to see how much fluorescence the drug plus dead cells emit. MG132 (50 µM) = Cells treated with 50 µM of MG132. Bortezomib (25 µM) = Cells treated with 25 µM of Bortezomib. Epoxomicin (33.3 µM) = Cells treated with 33.3 µM Epoxomicin.

The loading controls reveal a baseline fluorescence of approximately 2000 cells only from the medium or medium with DMSO together with the PrestoBlue™ solution. The dead cells together with the drugs emit a fluorescence correlating to approximately 3000 to 4500 cells. This explains the high baseline fluorescence of the viability and proliferation assays and shows that the signal for dead cells correspond to about 4000 live cells for the assays.

Another loading control experiment was conducted using only drugs without any cells, measured after 24, 48 and 72 hours. All of the measurements displayed a fluorescence between 80 and 100.

NTNU

Norwegian University of
Science and Technology